ABSTRACT

INTERACTION OF METHOXYETHYL METHYL IMIDAZOLIUM-BASED IONIC LIQUIDS WITH URANIUM AND ITS EFFECT ON BIOREDUCTION OF URANIUM

by
Hao Wang

Ionic liquids (ILs) are new materials with unique properties such as non-measurable vapor pressure, low melting point below 100°C and tunable physical-chemical properties. These liquids demonstrate tremendous potential applications in many fields, including nuclear waste treatment.

In this study, new MOEMIM (methoxyethyl methyl imidazolium)-based ionic liquids were synthesized. Their properties were characterized by UV-Vis spectroscopy (UV-vis), Fourier transform infrared spectroscopy (FTIR), mass spectroscopy (MS) and NMR (Nuclear magnetic resonance). The interaction between ILs and uranium has been explored by various analysis techniques, including pH, potentiometric titration, UV-vis, MS and EXAFS (extended x-ray absorption fine structure). Among all the ILs studied here, $MOEMIMBF_4$ demonstrated a strong complexation with uranium, while others showed weak interaction.

Next, the effect of ILs on the bioreduction of uranium by *clostridium* sp. was explored. The result revealed that, in presence of $MOEMIMBF_4$, most of the U(VI) and reduced U(IV) can be maintained in the aqueous phase for long time, while most of uranium precipitates out very quickly in presence of other ILs. This could be explained by the formation of uranium complex associated with $MOEMIMBF_4$. However, the complexation reduced bioavailability of uranium, resulting in the decreased bioreduction efficiency. The effect of different concentration of $MOEMIMBF_4$ was also investigated

in this study. The results disclosed that the elevated concentration could diminish the bioredution percentage, which may result from the raised toxicity.

In addition, toxicity of a variety of ILs on *clostridium* sp. was also examined here. Optical density (OD), pH and gas production were determined. The result revealed that the anion plays a very important role on toxicity. The more fluorine atoms the anion contains, the more toxic the IL is. Furthermore, the $EC_{50\text{-}48hour}$ of each IL on *clostridium* sp. was determined, and the partition coefficient (*Kow*) between octanol and water was measured, and also the E_{LUMO} was calculated by Sparton'02. Based on these data, a series of QSAR models were developed to predict the toxicity of ILs.

Besides, the biodegradation of pyridium-based ILs by urealyticum bacteria in presence of low concentration uranium was explored in this study. The bacteria growth was monitored by OD, pH, UV-vis, and the biodegradation products were determined by HPLC (high performance liquid chromatography) and MS, and the concentration of uranium in the solution was measured by KPA (kinetic phosphorescence analyzer). The result revealed that uranium under low concentration doesn't exert much inhibition on bacterium growth, but it formed complex with the biodegradation intermediate, leading to the elevated uranium concentration in the solution. After the intermediate was further consumed by bacterium, uranium was released again and precipitated out of the solution. Later, with the pH decrease because of the acids produced from biodegradation, uranium came back to solution again. The biodegradation pathway is similar to that in absence of uranium examined in previous work by Zhang (2006).

INTERACTION OF METHOXYETHYL METHYL IMIDAZOLIUM-BASED IONIC LIQUIDS WITH URANIUM AND ITS EFFECT ON BIOREDUCTION OF URANIUM

by
Hao Wang

A Dissertation
Submitted to the Faculty of
New Jersey Institute of Technology and Rutgers,
The State University of New Jersey - Newark
in Partial Fulfillment of the Requirements for the Degree of
Doctor of Philosophy in Environmental Science

Department of Chemistry and Environmental Science

August 2007

APPROVAL PAGE

INTERACTION OF METHOXYETHYL METHYL IMIDAZOLIUM-BASED IONIC LIQUIDS WITH URANIUM AND ITS EFFECT ON BIOREDUCTION OF URANIUM

Hao Wang

Dr. Sanjay V. Malhotra, Dissertation Advisor — Date
Assistant Professor of Chemistry and Environmental Science, NJIT

Dr. Arokiasamy J. Francis, Committee Member — Date
Group Leader of Molecular Environmental Science at Brookhaven National Laboratory, Associate Director of Center for Environmental Molecular Science at Stony Brook University / Brookhaven National Laboratory

---

Dr. Tamara Gund, Committee Member — Date
Professor of Chemistry and Environmental Science, NJIT

Dr. Norman Loney, Committee Member — Date
Associate Professor of Chemical Engineering, NJIT

Dr. Daniel J. Watts, Committee Member — Date
Executive Director of Otto H. York Center for Environmental Engineering and Science, Panasonic Professor of Sustainability, NJIT

Dr. Somenath Mitra, Committee Member — Date
Professor of Chemistry and Environmental Science, NJIT

BIOGRAPHICAL SKETCH

Author: Hao Wang

Degree: Doctor of Philosophy

Date: August 2007

Undergraduate and Graduate Education:

- Doctor of Philosophy in Environmental Science,
  New Jersey Institute of Technology, Newark, NJ, 2007

- Master of Environmental Science,
  Beijing Normal University, Beijing, P.R.China, 2003

- Bachelor of Environmental Engineering,
  Beijing Industry and Business University, Beijing, P.R.China, 1999

Major: Environmental Science

Presentations and Publications:

Hao Wang, Cleve J. Dodge, Arokiasamy J. Francis and Sanjay V. Malhotra,
"Interaction of methoxyethyl methyl imidazolium tetrafluoroborate with uranium and its application on uranium bioreduction,"
231th ACS National Meeting, Chicago, March 2007

Hao Wang, Vineet Kumar, Arokiasamy J. Francis and Sanjay V. Malhotra,
"Toxicity study of methoxyethyl methyl imidazolium-based ionic liquids,"
231th ACS National Meeting, Chicago, March 2007

Chengdong Zhang, Hao Wang and Sanjay V. Malhotra,
"Enzymatic synthesis of dipeptides in ionic liquids," (Submitted to Advanced Synthesis and Catalysis).

Hao Wang, Cleve J. Dodge, Arokiasamy J. Francis and Sanjay V. Malhotra,
"Investigation of interaction between uranium and 1-methoxyethyl-3-methyl imidazolium based ionic liquids," (in preparation).

Hao Wang, Cleve J. Dodge, Arokiasamy J. Francis and Sanjay V. Malhotra, "Effects of ILs on bioreduction of U(VI) to U(IV) by Clostridium sp.," (in preparation).

Hao Wang, Arokiasamy J.Francis and Sanjay V. Malhotra, "Biodegradation of pyridium tetrafluoroborate in presence of uranium," (in preparation).

To those who care about me and those I am concerned about

ACKNOWLEDGMENT

First of all, I would like to give my most sincere appreciation to my advisor, Dr. Sanjay V. Malhotra. He not only directed my research, but also always stood by and supported me. He gave me encouragement when I felt frustrated; he lent me a hand when I needed help; and he advised me when I was in a dilemma.

I would also express my greatest gratitude to Dr. Arokiasamy J. Francis for his directing my research and countless help. Most of my experiment was done in his lab at Brookhaven National Laboratory (BNL). He was always very kind and gave me plenty of important suggestions. His valuable insight and knowledge will benefit my whole life.

I am also really grateful to Dr. Tamara Gund, Dr. Norman Loney and Dr. Daniel Watts for serving as committee members and actively participating in my research.

I also want to give special thanks to Dr. Cleveland J. Dodge and Dr. Chengdong Zhang for helping in my experiment, to Dr. Vineet Kumar for the synthesis of ILs, and to Dr. Jeff B. Gillow, Dr. Weimin Gao for their help when I stayed in BNL.

I am obliged to the following individuals for their help in these years: Gayle Katz (secretary of the department), Ying Xiao, Bin Wang, Ornthida Saekhow, Da Jeong Shim and Yuhong Chen (fellow graduate students).

Also, I appreciate the help from Dr. Ronald S. Kane and Ms. Clarisa Gonzalez-Lenahan for thesis review, as well as help from Mr. Jeffrey W. Grundy in the International Students and Faculty Office.

Finally, particularly thanks to my family. Without their endless support, I could have done nothing.

TABLE OF CONTENTS

TABLE OF CONTENTS
(Continued)

TABLE OF CONTENTS
(Continued)

Chapter **Page**

TABLE OF CONTENTS
(Continued)

Chapter **Page**

TABLE OF CONTENTS
(Continued)

LIST OF TABLES

LIST OF FIGURES

LIST OF FIGURES
(Continued)

LIST OF FIGURES
(Continued)

LIST OF FIGURES
(Continued)

LIST OF FIGURES
(Continued)

LIST OF FIGURES
(Continued)

CHAPTER 1

INTRODUCTION AND OBJECTIVES

1.1 Ionic Liquids

1.1.1 The Development of Ionic liquids (ILs)

Ionic liquid is liquid that contains only ions (*http://en.wikipedia.org/wiki/Ionic_liquid*). This term is used to refer to molten salts, such as liquid sodium chloride over 800°C. However, today, this term is defined as salts that melt below about 100°C. Particularly, the salts are called room-temperature ionic liquids if they are liquids at room temperature.

Room temperature ionic liquids are not new. Ethylammonium nitrate, which is liquid at room temperature, was first described in 1914 (Walden, 1914). In the late 1940s, *N*-alkylpyridinium chloroaluminates were studied as electrolytes for electroplating aluminium. These systems were reexamined by the groups of Hussey (1983), Robinson (1979) and Wilkes (1982) in the late 1970s. The first examples of ionic liquids based on dialkylimidazolium cations were reported in the 1980s by Wilkes and coworkers. They contained chloroaluminate anions ($AlCl_4^-$ or $Al_2Cl_7^-$) and proved to be useful catalysts/solvents for Friedel–Crafts acylations. However, the chloroaluminate anion's high reactivity to water was prohibitive to the wide scale use of these ionic liquids. In 1992, Wilkes and Zawarotko reported the preparation of ionic liquids with alternative anions like hexafluorophosphate ($[PF_6]^-$) and tetrafluoroborate ($[BF_4]^-$), which allowed for a greater range of ILs applications (Wilkes, et al. 1992). Since then, various, new, moisture- stable, neutral ionic liquids were developed, attracting significant interest from the scientific community.

Figure 1.1 shows some commonly used cations and anions of ionic liquids.

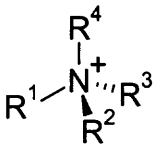

Ammomium

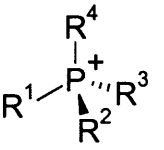

Phosphonium

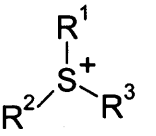

Sulfonium

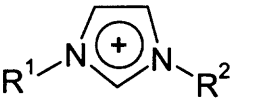

Imidazolium

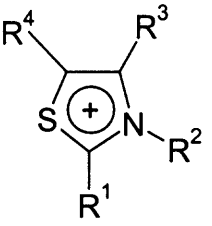

Thiazolium

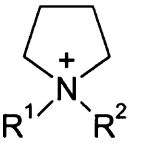

Pyrrolidium

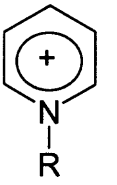

Pyridinium

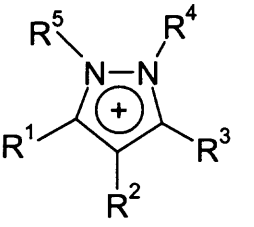

Pyrazolium

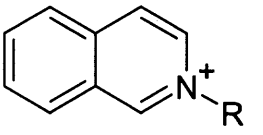

Isoquinolium

R, R^1, R^2, R^3 and R^4 = alkyl chains

Cations used in ionic liquids

$[BF_4]$, [Br], $[PF_6]$, [I],[CF_3SO_3], $[CF_3COO]$, $[CF_3SO_2)_2N]$,
$[SbF_6]$, $[NO_2]$, $[NO_3]$, $[HSO_4]$, $[CH_3COO]$, [Cl], $[(CN)_2N]$,
$[AlCl_4]$, [OTs], $[AuCl_4]$, Carborane anoins

Anions used in ionic liquids

Figure 1.1 Commonly used cations and anions in ionic liquids.

1.1.2 Properties of Ionic Liquids

Properties of ILs are summarized below.

- They have no measurable vapor pressure. Compared with traditional organic solvents that are highly volatile and toxic, ILs are non-volatile, can be used in high vacuum systems and are easily contained. In addition, they are environmentally friendly and, therefore, called 'green' solvents.

- They generally have reasonable thermal stability. While tetraalkylammonium salts have limited thermal stability, owing to decomposition via the Hoffmann elimination, [EMIM][BF_4] is reported to be stable up to 300 °C and [EMIM][$(CF_3SO_2)_2N$] up to 400 °C (Bonhote, et al., 1996). In other words, many ionic liquids have liquid ranges of more than 300 °C, compared to the 100 °C liquid range of water.

- Since ILs only consist of ions, they possess a large electrochemical window (up to 7ev).

- On the one hand, they are good solvents for many organic, inorganic and organometallic compounds. On the other hand, they are immiscible with some organic solvents (e.g. alkanes) and therefore can be used in two-phase systems. Similarly, lipophilic ionic liquids can be used in aqueous biphasic systems.

- They are tunable solvents. Different combinations of cations and anions can form different ionic liquids that possess various physical chemical properties. For example, a suitable choice of cation/anion cans readliy affect polarity and hydrophilicity/lipophilicity.

Due to their unique characteristics, ILs are considered to be one of the most promising green solvents anticipated to replace traditional toxic organic solvents.

1.1.3 Application of ILs in Industry

Separation and Extraction Due to their special properties such as non-volatility and good solvation for many inorganic and organic chemicals, ILs are considered an alternative to organic solvents in Liquid-Liquid extraction. Liquid –liquid extraction of heavy metal ions in ILs has become increasingly attractive. Visser et al. (2001) have reported the applications of functionized ILs as the extractant in a liquid/liquid extraction

of Hg^{2+} and Cd^{2+} and uranium. They explored the applications of PAN (1-(pyridylazo)-2-naphthol), TAN (1-thiazoly-lazo)-2-napthol), CN^-, OCN^-, SCN^- and halides extractants for the partition of a metal cation between an ionic liquid phase and an aqueous phase. Wei et al. (2003) used dithizone as a metal chelate to form neutral metal-dithizone complexes with heavy metal. They proposed that ionic liquids may be participating in a liquid ion exchange process in which $[PF_6]^-$ is replaced by a more hydrophobic metal-anion complex formed in the aqueous phase. Hirayama et al. (2005) reported the high extraction performance of [BMIM][PF_6], [HMIM][PF_6] and [OMIN][PF_6] for divalent metal cations with 4,4,4-trifluoro-1-(2-thienyl)-1,3-butanedione (Htta). In addition, ILs have been used as co-extract solvents for actinide extractions from radioactive waste.

Organic Synthesis in ILs Many synthesis reactions have been tested in ILs. Friedel-crafts acylation has been examined in pyridinium based ILs (Xiao, et al. 2005). The reactions were found to proceed under relatively mild conditions with excellent conversions, and ILs were recycled and reused effectively. A study of Diels-Alder reaction was carried out by Welton and co-workers (1999). They investigated the rate and selectivity between cyclopentadiene and methyl acrylate in a number of neutral ILs. It was found that the ratio of 'endo' and 'exo' decreased slightly as the reaction proceeded, and were dependent on reagent concentration and ILs. The first example of an electrophilic nitration in an ionic liquid was performed by Wilkes and co-workers (Wilkes et al. 1987). A number of aromatic compounds were nitrated with KNO_3 and dissolved in chloroaluminate (III) ionic liquids. Lee et al.(2001) have studied the Lewis acid-catalyzed three-component synthesis of α-amino phosphorate in [BMIM][PF_6], [BMIM][OTf], [BMIM][BF_4] and [BMIM][SbF_6], finding the reaction gave good yields

in ILs with Lewis acids. The reaction was also performed in [BMIM][PF_6] with $Sm(OTf)_3$ as the catalyst, which gave a yield of 99% (compared with 70% for the reaction in dichloromethane).

Transition Metal Catalysis in ILs ILs shows promising applications in transition metal catalysis. Many transition metal complexes dissolve readily in ionic liquids, enabling their use as solvents in transition metal catalysis. Depending on the coordinative properties of the anion, and on the degree of the cation's reactivity, the ILs can be classified into four types: (1) "innocent" solvent: ILs with weakly coordinating and inert cations and anions, can be looked on as innocent solvents in transition metal catalysis. In this case, ILs just provide a more or less 'polar medium' for feedstock and products; (2) solvent and co-catalyst: ILs formed by the treatment of a halide salt with a Lewis acid generally act both as solvent and as co-catalyst; (3) solvent and ligand/ligand precursor: both the cation and anion of ILs can act as a ligand or ligand-precursor for a transition metal complex dissolved in ILs; (4) solvent and transition metal catalyst: for example, acidic chloroalluminate ILs act as both solvent and catalyst for reactions conventionally catalyzed by $AlCl_3$, such as catalytic Friedel-Crafts alkylation (Wasserscheid, 2003). Suarez et al.(1995) firstly investigated the Rh-catalyzed hydrogenation of cyclohexene in [BMIM][BF_4]. They found the reaction rate in ILs was faster than for the comparable reaction in acetone. Moreover, that all ionic catalyst solutions tested could be reused repeatedly. Ley et al. (2001) reported on the oxidation of alcohols catalyzed by an ammonium perruthenate catalyst dissolved in [Net_4][Br] and [EMIM][PF_6]. Gaillion and Bedioui (2001) investigated the electro-assisted activation of molecular oxygen by Jacobsen's epoxidate catalysts dissolved in [BMIM][PF_6] and were able to provide

evidence for the formation of the highly reactive oxomanganese(V) intermediate which was not detectable in organic solvents.

Biocatalysis Biocatalysis represents the process in which a starting material is converted into the desired product in just one step. This can be achieved either by whole cells or purified enzymes. Biocatalysis in nature tends to perform optimally in aqueous environments such as pH 7 and temperatures below 40°C. Sometimes, however, the solubility of substrate or product is so low that it inhibits microorganism activity. This problem can be overcome by the addition of organic solvents or ILs, thus increasing the solubility of the substrate or product while maintaining the activity of the cell or enzyme. ILs have been recently studied as biocatalysts in enzymatic systems, wherein the ILs work as a pure or co-solvent in an aqueous phase, or as a two-phase system together with other solvents (Kragl et al., 2001). The merits of using ILs as biocatalysts include: 1) an increased solubility of hydrophobic substrates and/or products; 2) an inhibition of water-dependent side reactions; 3) an extension of enzyme activity in polar solvents; 4) an increase of enzyme stability and enantioselectivity; 5) the increase of recyclability without changing biocatalytical functions; 6) compared with conventional organic solvent, ILs have no measurable vapor pressure and are "greener".

Early in 1984, Magnuson et al. (1984) investigated the influence of ethylammonium/water mixtures on enzyme activity and stability. They observed an increased activity of alkaline phosphatase at low concentrations of $[H_3NEt][NO_3]$. Erbeldinger et al. (2000) reported the use of the protease thermolysin for the synthesis of the dipeptide Z-aspartame. The results demonstrated reaction rates comparable to those found in conventional organic solvents, and improved enzyme stability in ionic liquids.

The ILs were recycled several times. Laszlo and Compton (2001) used the protease α-chymotrypsin for transesterification reactions in [OMIM][PF_6] and [BMIM][PF_6], and compared the results with those in organic solvents (e.g. cetonitrile or hexane). They found that, for both ILs and organic solvents, the reaction rates were of the same order and magnitude. Iborra et al. (2001) examined the transesterification of N-acetyl-L-tyrosine ethyl ester in different ILs and compared their stabilizing effect relative to that found with 1-propanol as the solvent. Although the enzyme activity was inhibited to only 10 to 50% of the value in 1-propanl, the higher yield was obtained due to the increase in stability.

Lipases are the most studied enzymes as biocatalysts in ILs. Sheldon and co-workers (2000) were the first group to study the potential use of lipase in ILs. They investigated the reactivity of *Candida antarctica* lipase in ILs such as [BMIM][PF_6] and [BMIM][BF_4]. Their comparison of the reaction rate in ILs and in organic solvents confirmed the similarity for all of the reactions. The kinetic resolution of (R, S)-1-phenylethanol and of eight lipases and two esterases in ten ILs have been explored by Kragl et al. (2001). No reaction was observed for the esterase, but for the lipases from *Pseudomonas* sp. and *Alcaligenes* sp., an improved enantioselectivity was found in [BMIM][$(CF_3SO_2)_2$] as solvent, in comparison with MTBE.

However, there is still a long way to go before ILs can become commonly used in biocatalysis. This will require: 1) a demonstration of stability and recyclability over prolonged periods of time under the reaction conditions applied; 2) an investigation of mass transport limitations for biocatalysts immobilized on heterogeneous supports; 3) the development of suitable methods for product isolation if they are not volatile.

1.2 Radioactive Waste

The United States is the world's largest supplier of commercial nuclear power. In 2005, there were 104 U.S. commercial nuclear generating units that are fully licensed to operate. Together, they provide about 20% of the Nation's electricity (*Energy Information Administration, http://www.eia.doe.gov/fuelnuclear.html*). According to preliminary EIA data, in July 2006, nuclear generation rose to 72,186 billion kilowatt hours. The increase of nuclear power generation correspondingly requires more uranium production. Table 1.1 summarizes the production statistics of the U.S. Uranium Industry from 1993 to 2005.

Table 1.1 Summary Production Statistics of U.S. Uranium Industry from 1993 to 2005

Items	1993	1994	1995	1996	1997	1998	1999	2000	2001	2002	2003	2004	2005[E]
Exploration and Development													
Surface Drilling (million feet)	1.1	0.7	1.3	3.0	4.9	4.6	2.5	1.0	0.7	W	W	1.2	1.7
Drilling Expenditures [a] (million dollars)	5.7	1.1	2.6	7.2	20.0	18.1	7.9	5.6	2.7	W	W	10.6	16.4
Mine Production of Uranium													
(million pounds U_3O_8)	2.1	2.5	3.5	4.7	4.7	4.8	4.5	3.1	2.6	2.4	[E] 2.2	2.5	3.0
Uranium Concentrate Production													
(million pounds U_3O_8)	3.1	3.4	6.0	6.3	5.6	4.7	4.6	4.0	2.6	[E] 2.3	[E] 2.0	2.3	2.7
Uranium Concentrate Shipments													
(million pounds U_3O_8)	3.4	6.3	5.5	6.0	5.8	4.9	5.5	3.2	2.2	3.8	[E] 1.6	2.3	2.7
Employment													
(person-years)	871	980	1,107	1,118	1,097	1,120	848	627	423	426	321	420	638

[a] Expenditures are in nominal U.S. dollars.
W=Data withheld to avoid disclosure. E = Estimate - The 2003 annual amounts were estimated by rounding to the nearest 200,000 pounds to avoid disclosure of individual company data. The 2005 annual amounts contain limited imputation for missing data.

With the drastic increase of uranium production, there is increasing concern about contamination by uranium waste of the air, soil and groundwater. Uranium, its decay products, and associated trace elements create human health and environmental hazards due to their radioactivity. High levels of radon and uranium in domestic drinking water or indoor radon has been found to turn up in areas known to be uranium-enriched. How to safely and cost-effectively dispose of these radioactive wastes from mining sites and nuclear power plants is a great challenge for us.

1.3 Current Treatment Methods for Nuclear Waste

Various physical, chemical and biological technologies have been attempted to recover and remediate nuclear waste, including Ion-exchange (Gu, et al. 2005), electrosorption (Xu, et al., 2000), photodegradation (Dodge, et al. 2002), biosorption (Sar, et al., 2004), and chemical reduction (Jeon, et al., 2005). Here are some of the more prominent methods.

1.3.1 Plutonium and Uranium Recovery by Extraction (PUREX)

PUREX (www.w*ikipedia.com*) is the process for the reprocessing of spent nuclear fuel to separate uranium and plutonium from the fission products. Following the dissolution of the irradiated fuel in aqueous nitric acid, uranium and plutonium are transferred to an organic phase by vigorous mixing with an organic solvent extraction, 30 percent tributyl phosphate (TBP) in kerosene is used as organic solvent, while the fission products remain in the aqueous nitric phase. Further process steps enable the subsequent separation of uranium and plutonium from one another. The efficient actinide purification is based

upon a detailed understanding of the coordination chemistry, hydrolytic behavior, and the valence state control of f-element ions and complex dissolved in aqueous solutions.

However, the disadvantage is obvious. It needs a large amount of organic solvent for the extraction, which is hazardous and not environmentally friendly. As an alternative, ILs could replace the organic solvent in the liquid-liquid extraction to greatly reduce this risk since it is nonvolatile and shows good salvation for actinides.

1.3.2 Electrorefining of Metals

Electrorefining is the electrodeposition of metals from their ores that have been put in solution or liquefied. Most metal ore occurs in nature in an oxidized form and thus must be reduced to its metallic forms. The ore firstly is dissolved following some preprocessing in an aqueous electrolyte or in a molten salt and the resulting solution is electrolyzed. Then the metal is deposited on the cathode while the anodic reaction is usually an oxygen evolution (*www.wikipedia.com*). This process has also been used to process spent nuclear fuel as it has the capacity to separate heavy elements such as uranium, plutonium, and fission products such as cesium and strontium.

However, it also has some disadvantages. Cd is commonly used as the cathode, which is toxic. In addition, this process may be energy costly as it often requires high amounts of energy to obtain molten salt. ILs are a reasonable alternative to molten salt because they are liquid at room temperature, and contain high ion conductivity and high thermal stability.

1.3.3 Bioremediation

The actinides exist in various oxidation states, which play an important role on their solubility in aqueous phase. However, under appropriate conditions, the oxidation state can be changed by direct or indirect microbial action including: (i) oxidation-reduction reactions; (ii) changes in pH and redoxpotential; (iii) chelation or the production of specific sequestering agents; (iv) biosorption by biomass and biopolymers; (v) formation of stable minerals; (vi) biodegradation of actinide-organic complexes (Francis, 1998). Based on these mechanisms, some bioremediation methods have been developed: (1) Bioaccumulation: an active process in which metals are taken into living cells and sequestered intracellular by complexation with specific metal-binding components or by precipitation; (2) Biosorption: both living and dead microorganisms have abundant functional groups like carboxyl, hydroxyl and phosphate on their surface, upon which metals can bind.; (3) Bioprecipitation or biomineralization: the process in which metal precipitates and minerals by bacterial metabolism; (4) Bioreduction: as mentioned above, different oxidation states may affect the solubility of metals, resulting in dissolution or precipitation. For instance, U(VI) is highly soluble in water, while U(IV) is not. However, the reduction of soluble U(VI) by *Clostridium* s.p resulted in precipitation of U(IV); (5) Biodegradation: Metal-organic complex could also be degraded by microorganism, which may result in metal solubility changes.

Among these technologies, bioremediation is considered to be a simple, environmentally-friendly, cost-effective alternative for the cleanup of uranium contamination. Unlike PUREX and electro refining, it doesn't need an organic solvent and high energy. It is a promising method to deal with low-level radioactive waste.

1.4 Objectives

There is growing interest in the use of ionic liquids in actinide separation chemistry. Allen et al. (2002) screened a series of ILs, such as 1-butyl-3-methyl imidazolium nitrate, and 1-ethyl-3-methylimidazolium chloride, for their radiochemical stability towards alpha, beta and gamma irradiation. The results show ILs are comparable to benzene in terms of overall stability, and much better than mixtures of TBP and kerosene. Visser and Roger et al. (2001) reported that addition of $[C_{4\sim8}mim][PF_6]$ to the extractant like CMPO (octylphenyl-N,N-di-isobutyl carbamoylphosphine oxide)/TBP(tri-n-butyl phosphate) can significantly enhance the partitioning of actinides to these ILs. A patented process demonstrates the dissolution of nuclear fuel cladding with $[BMIM][NO_3]$ with additional PUREX processing to recover uranium and plutonium. Warrant et al. (2002) at Los Alamos National Lab have investigated the potential application of ILs containing cyclic quaternary ammonium cations with $[N(SO_2CF_3)_2]^-$ anion in actinide electro-processing. They were found to combine favorable viscosity and conductivity properties with excellent electrochemical stability. Visser et al (2001) have introduced task-specific ionic liquids incorporating specific extracting moieties linked to the imidazolium part of the IL, which exhibit very high distribution ratios for Hg^{2+} and Cd^{2+} when functionalized with sulfur containing moieties, and for Pu^{4+} and UO_2^{2+} when functionalized with carbamoylmethylphosphine oxide moieties.

These studies, however, have not provided any information about the mechanics of 'why' and 'how' ILs have the ability to enhance the partitioning of actinides and other metals. Also, understanding the interaction between ILs and actinides is critical as it can help in better designing of ILs and treatment of U and other actinides. In addition, there is

no report about the application of ILs in bioremediation of actinides in waste and contaminated soil. Can some ILs improve the bioremediation of nuclear waste, such as bioreduction of uranium? Furthermore, although ILs are regarded as "green" solvents, currently there is little information about the toxicity of ILs. What plays an important role in toxicity of ILs? How do the cation and anion influence the toxicity?

Due to the lack of critical information, I worked to seek some of the answers to these questions. The objectives of my work include:

- To Synthesize and characterize the new [MOEMIM] based ILs.
- To Study the interaction between Uranium and ILs.
- To Investigate the effect of interaction of U-ILs on bioreduction of U(VI) to U(IV) by *Clostridium* sp.
- To examine the toxicity of ILs.
- To Develop a Quantitative Structure-Activity Relationship (QSAR) model to predict toxicity of ILs.
- To explore the effect of uranium on biodegradation of ILs by new cultured bacterium.

CHAPTER 2

SYNTHESIS AND CHARACTERIZATION OF IONIC LIQUIDS

2.1 Introduction

Concern about the toxicity of ILs and the potential for large quantity industrial spills harmful to the environment, prompt the desire to design new ILs which are less toxic and easier to biodegrade in nature. Boethling (1996) identified three factors which are important in the design of biodegradable compounds: (1) the presence of potential sites of enzymatic hydrolysis, such as esters and amides; (2) the introduction of oxygen in the form of hydroxyl, aldehyde or carboxylic acid groups; (3) the presence of unsubstituted linear alkyl chains and phenyl rings, which represent possible sites for attack by oxygenases. Based on these principles, Gathergood *et al.* (2004) has reported the study on biodegradable ILs that was incorporated with the ester and amide functionality into the cation side chain. The introduction of a group susceptible to enzymatic hydrolysis greatly improved the biodegradation as compared with the commonly used dialkyimidazolium ILs.

Based on toxicity studies from this literature, a new series of functionized ILs have been synthesized in this study. These new ILs incorporate either an ether or a carboxylic group into the cation side chain, with various anions. They are expected to possess less toxicity to bacteria, and also to be more easily biodegraded by bacteria. The structures of these ILs are shown in Figure 2.1.

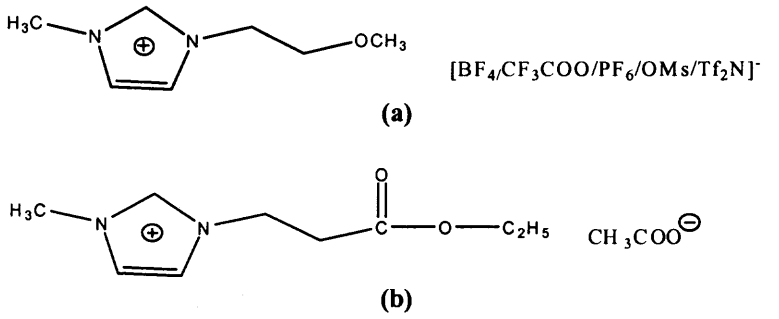

Figure 2.1 Ionic liquids used in this study: (a) 1-methoxyethyl-3-methyl imidazolium (MOEMIM)-based ILs; (b)3-methyl-1-(ethoxycarbonylmethyl) imidazolium (MECOOMIM)-based ILs.

2.2 Synthesis and Characterization of Ionic Liquids

2.2.1 1-methoxyethyl-3-methyl imidazolium tetrafluoroborate ([MOEMIM][BF_4])

2.2.1.1 Synthesis.

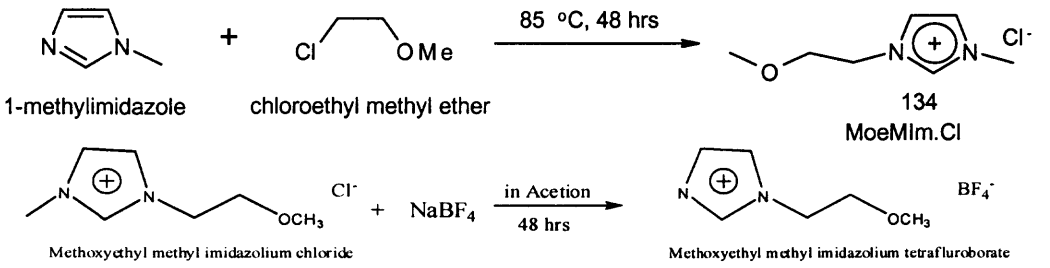

Figure 2.2 Two-step Synthesis of [MOEMIM][BF_4].

1-methylimidazole was first reacted with chloroethyl methyl ether for 48 hours at 85°C to get 1-methoxyethyl-3-methyl imidazolium chloride ([MOEMIM][Cl]). Then [MOEMIM][Cl] (0.243 mol, 43 g) was taken in acetone (200 ml) in a conical flask and added to $NaBF_4$ (0.319 mol, 35 g). The reaction mixture was stirred at room temperature for 48 hours and then the NaCl precipitate was filtered through celite and the filtrate was concentrated on rotavapor under vacuum. The product obtained was diluted with CH_2Cl_2

and passed through a silica gel column. The filtrate was concentrated, dried in vacuum oven to give the desired product (39.21 g, 70.6% yield).

2.2.1.2 Characterization.

UV-Vis Spectrometry [MOEMIM] based ILs have characteristic absorption at 211nm, which is due to the absorption of imidazolium ring. After 240nm it is transparent.

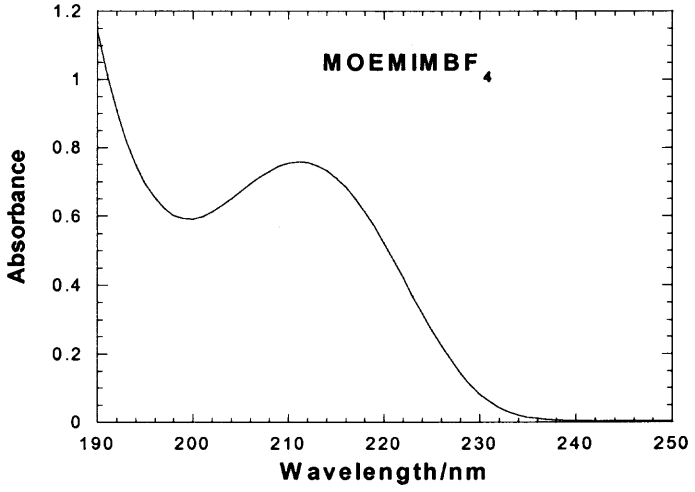

Figure 2.3 UV-vis spectrum of [MOEMIM][BF_4].

Fourier Transform Infrared Spectroscoy **(FTIR)** FTIR was shown in Figure2.4, and the absorption wavelength was listed below.

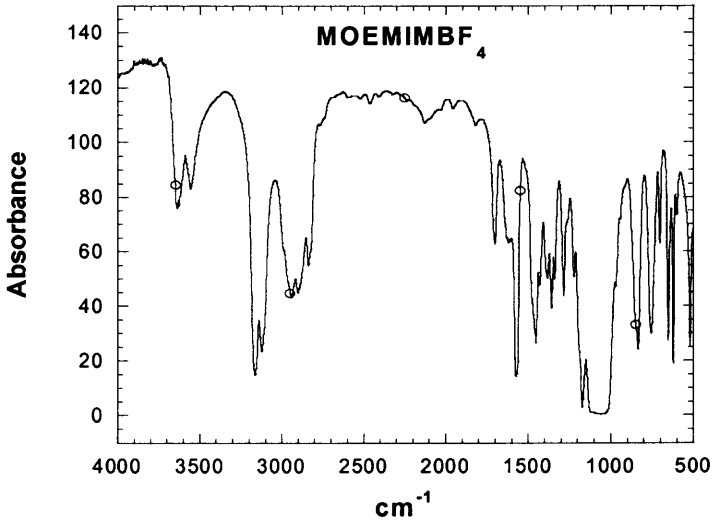

Figure 2.4 FTIR spectrum of [MOEMIM][BF_4].

IR (film, neat): 3164, 3123, 2941, 2902, 1576, 1455, 1356, 1287, 1172, 1059, 834, 756, 654, 624 cm^{-1}. The peaks at > 3100 cm^{-1} are attributed to the ring C-H stretch, while those around 3000 cm^{-1} resulted from C-H aliphatic stretches. The peak at around 1100 cm^{-1} is contributed to the C-O stretch from the ester group.

Mass Spectrometry **(MS)** Mass spectrum was displayed in Figure 2.5 below.

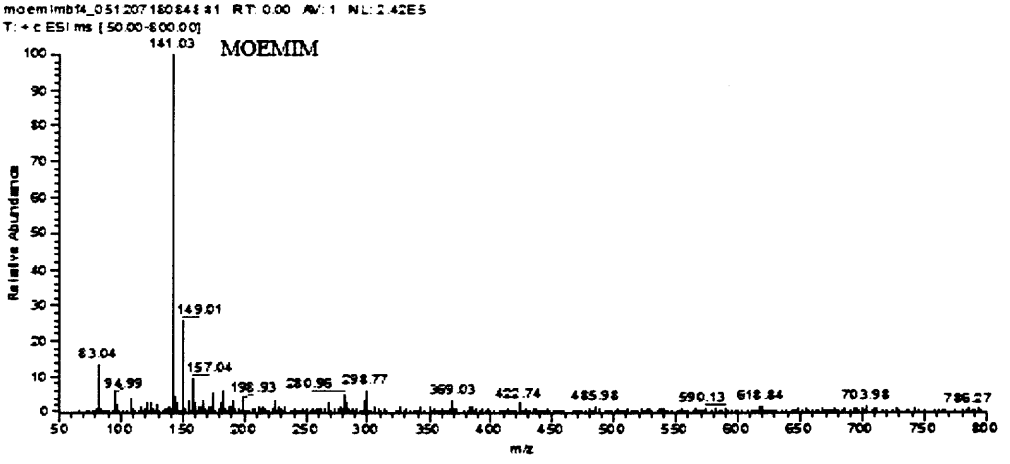

(a)

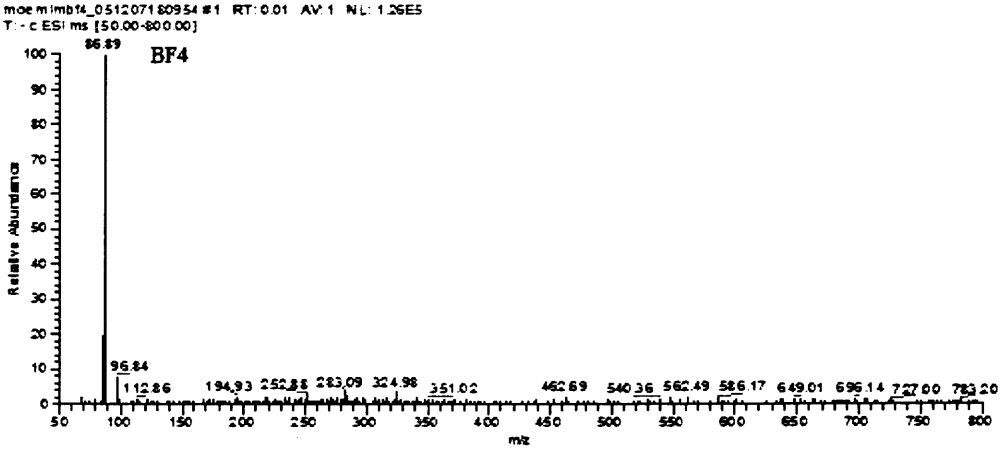

(b)

Figure 2.5 Mass spectra of MOEMIM][BF_4]: (a) positive mode; (b) negative mode.

141(m/e) in positive mode corresponds to [MOEMIM] cation, and 87(m/e) refers to [BF_4] anion, confirming this IL is [MOEMIM][BF_4].

Nuclear Magnetic Resonance (NMR) Structure of [MOEMIM][BF_4] was shown in Figure 2.6, and both ^1H and ^{13}C NMR data are also shown here.

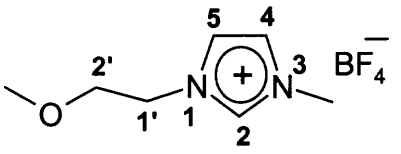

Figure 2.6 Structure of [MOEMIM][BF_4].

^1H NMR (300 MHz, Acetone-d_6): δ3.33 (3H, s, OCH_3), 3.79 (2H, t, J = 5.0Hz, C-2'Hs), 4.40 (3H, s, N^3-CH_3), 4.47 (2H, t, J = 4.9Hz, C-1'Hs), 7.64 (1H, t, J = 1.75Hz, C-4H), 7.67 (1H, t, J = 1.75Hz, C-5H), 8.85 (1H, s, C-2H).

^{13}C NMR (75.5 MHz, Acetone-d_6): δ36.37(OCH_3), 50.00 (C-2'), 58.69 (N^3-CH_3), 70.60 (C-1'), 123.64 (C-4), 124.27 (C-5), 137.72 (C-2).

2.2.2 1-methoxyethyl-3-methylimidazolium hexafluorophosphate([MOEMIM][PF_6])

2.2.2.1 Synthesis. [MOEMIM][Cl] (19.97 g, 0.113 mol) was taken in acetone (100 ml) in a conical flask and added to KPF_6 (25.09 g, 0.136 mol). The reaction mixture was stirred at room temperature for 48 hours and then the KCl precipitate was filtered through celite and the filtrate was concentrated on rotavapor under vacuum. The product obtained was diluted with CH_2Cl_2, washed three times with water, dried over $NaSO_4$, concentrated under vacuum and finally dried in a vacuum oven to give the desired product (27.82 g, 86% yield).

2.2.2.2 Characterization.

UV-Vis UV-vis spectrum was shown in Figure 2.7. As it can be seen, [MOEMIM][PF_6] has the same absorption as that of [MOEMIM][BF_4] because they have the same cation. The anion doesn't have an effect on UV absorption.

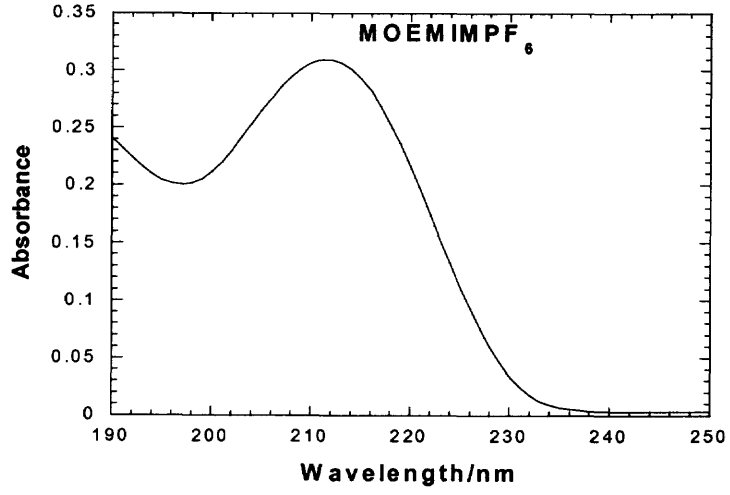

Figure 2.7 UV-vis spectrum of [MOEMIM][PF_6].

FTIR Figure 2.8 displays the FTIR of [MOEMIM][PF_6].

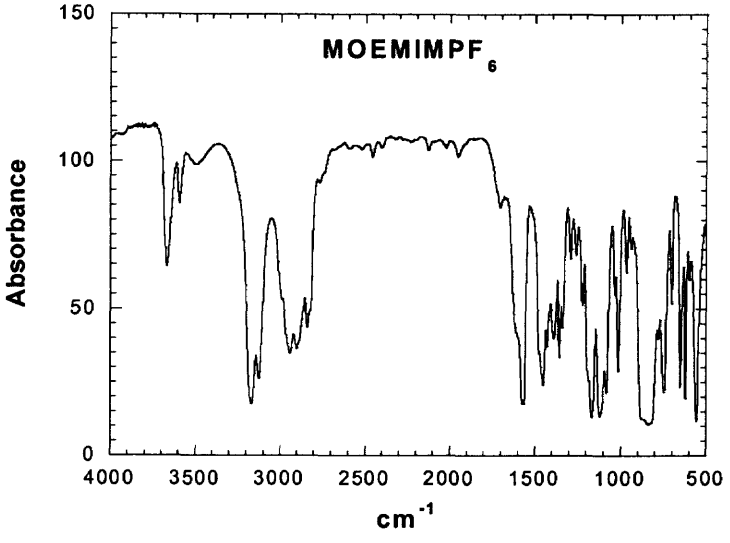

Figure 2.8 FTIR spectrum of [MOEMIM][PF_6].

IR (film, neat): 3700, 3171, 3126, 2943, 2903, 1577, 1568, 1454, 1171, 1123, 1084, 837, 741, 653, 624 cm^{-1}. It is similar to the spectrum of [MOEMIM][BF_4] in Figure 2.4.

Mass Spectrometry MS in both positive and negative mode as shown in Figure 2.9. 141(m/e) in positive mode is [MOEMIM] cation, and 145(m/e) in negative mode represents $[PF_6]$ anion; proving this IL is [MOEMIM]$[PF_6]$.

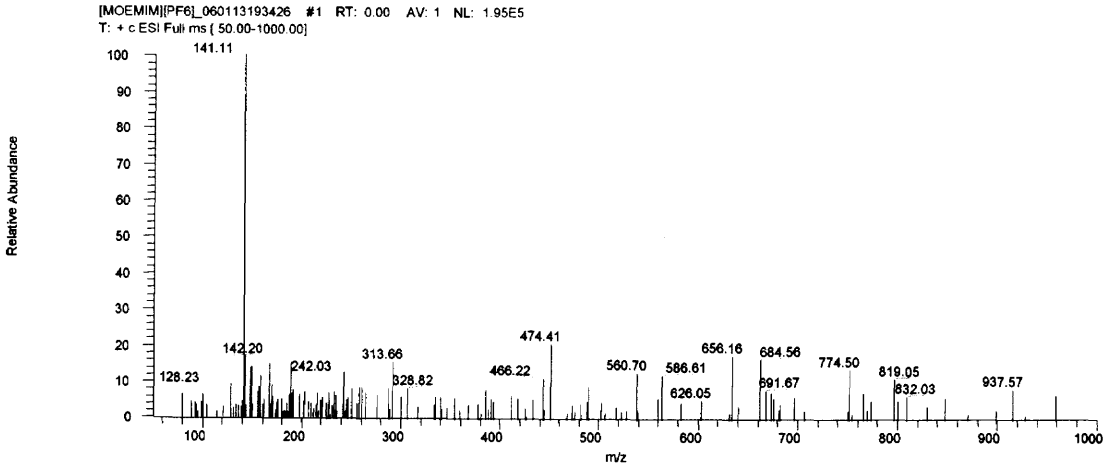

(a)

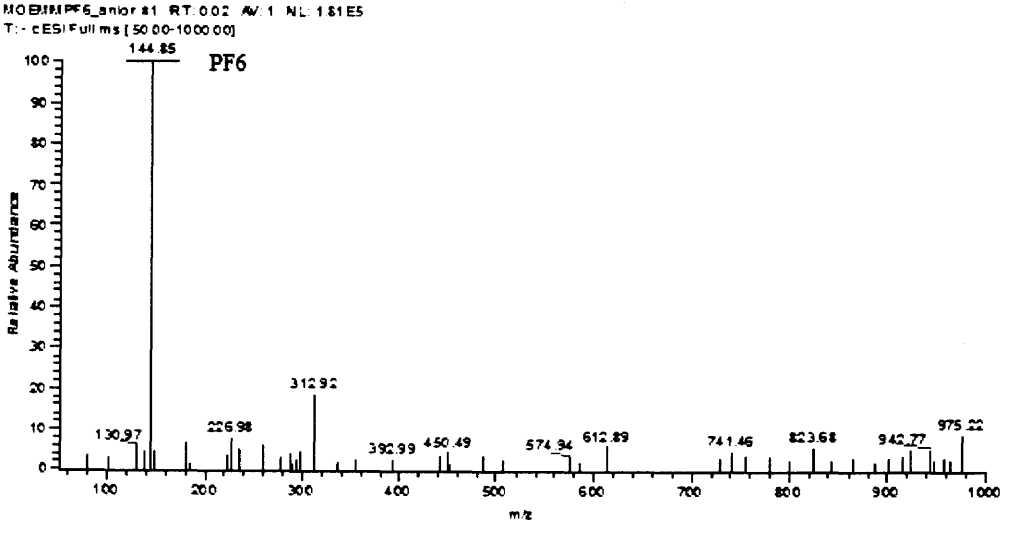

(b)

Figure 2.9 Mass spectra of $[MOEMIM][PF_6]$: (a) positive mode; (b) negative mode.

NMR ^{1}H NMR (300 MHz, Acetone-d_6): δ3.34 (3H, s, OCH_3), 3.79 (2H, t, J = 5.0Hz, C-2'Hs), 4.00 (3H, s, N^3-CH_3), 4.45 (2H, t, J = 4.9Hz, C-1'Hs), 7.57 (1H, t, J = 1.75Hz, C-4H), 7.62 (1H, t, J = 1.75Hz, C-5H), 8.76 (1H, s, C-2H).

^{13}C NMR (75.5 MHz, Acetone-d_6): δ36.41(OCH_3), 50.16 (C-2'), 58.73 (N^3-CH_3), 70.51 (C-1'), 123.67 (C-4), 124.22 (C-5), 137.52 (C-2).

2.2.3 1-methoxyethyl-3-methyl imidazolium trifluoro acetate-[MOEMIM][CF_3COO]

2.2.3.1 Synthesis. [MOEMIM][Cl] (0.113 mol, 20 g) was taken in acetone (150 ml) in a conical flask and added to CF_3COONa (0.181 mol, 24.63 g). The reaction mixture was stirred at room temperature for 48 hours and then the NaCl precipitate was filtered through celite and the filtrate was concentrated on rotavapor under vacuum. The product obtained was diluted with CH_2Cl_2 and passed through a silica gel column. The filtrate was concentrated, dried in a vacuum oven to give the desired product (25 g, 87% yield).

2.2.3.2 Characterization.

UV-Vis [MOEMIM][CF_3COO] also shows the same UV spectrum as [MOEMIM][BF_4] and [MOEMIM][PF_6].

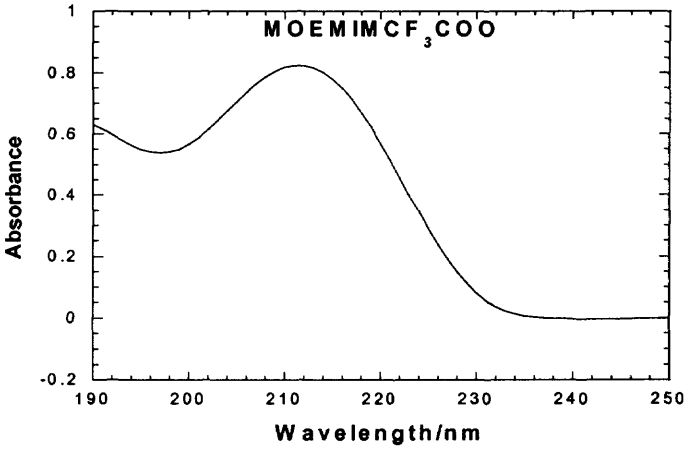

Figure 2.10 UV-vis spectrum of [MOEMIM][CF_3COO].

FTIR IR (film, neat): 3227, 3153, 3102, 2942, 2903, 1689, 1575, 1454, 1419, 1202, 1173, 1124, 828, 801, 719, 655, 625 cm^{-1}. This spectrum is different from those in Figure 2.4 and 2.8 because it displays a broad, intensive band centered around 3500 cm^{-1}, which is attributed to the O-H stretch. The broad shape is due to the hydrogen bonding interaction between the cation and aion.

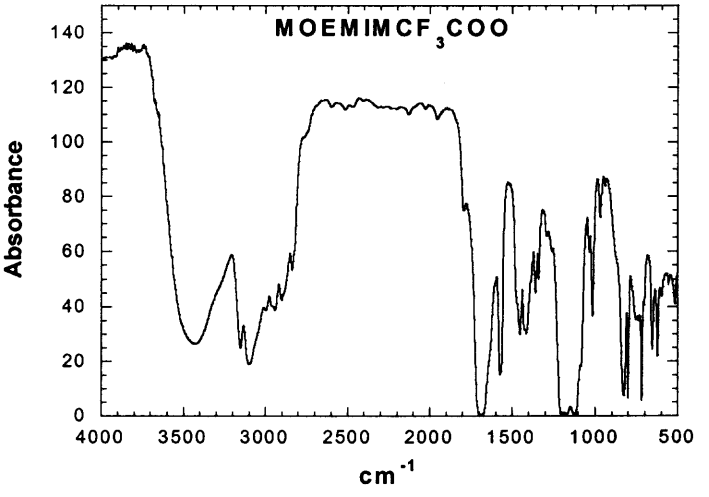

Figure 2.11 FTIR spectrum of [MOEMIM][CF_3COO].

MS MS is shown in Figure2.12. 141(m/e) in positive mode corresponds to MOEMIM cation. Although there are some other peaks present in negative mode, the base peak is 113(m/e) that represents the CF_3COO anion, indicating the IL is [MOEMIM][CF3COO].

NMR ^{1}H NMR (300 MHz, Acetone-d_6): δ3.30 (3H, s, OCH_3), 3.79 (2H, t, J = 5.0Hz, C-2'Hs), 4.03 (3H, s, N^3-CH_3), 4.54 (2H, t, J = 4.9Hz, C-1'Hs), 7.77-7.79 (2H, m, C-4H, C-5H), 9.46 (1H, s, C-2H).

^{13}C NMR (75.5 MHz, Acetone-d_6): δ36.39 (OCH_3), 50.00 (C-2'), 58.73 (N^3-CH_3), 70.95 (C-1'), 118.26 (q, J = 295.8Hz, CF_3COO) 123.82 (C-4), 124.45 (C-5), 138.53(C-2), 161.55 (q, J = 33.0Hz, CF_3COO).

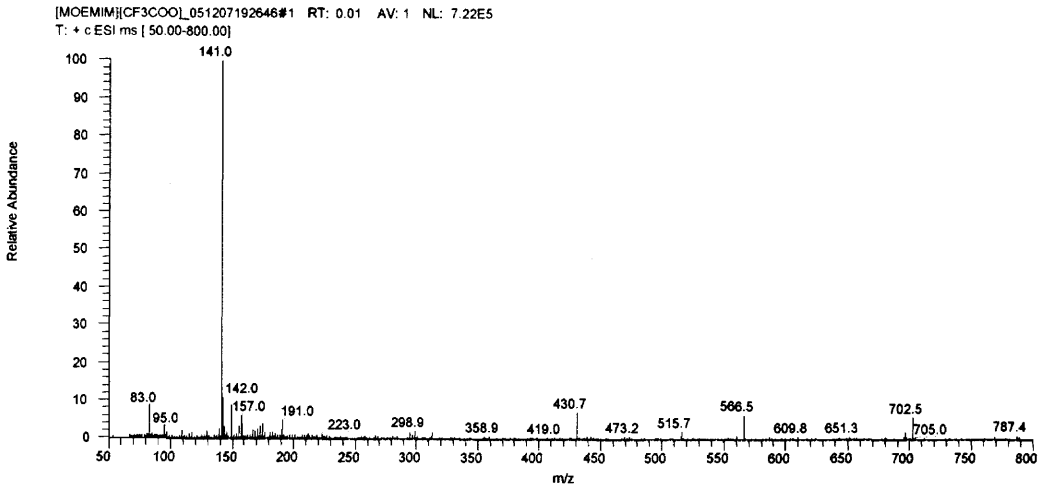

(a)

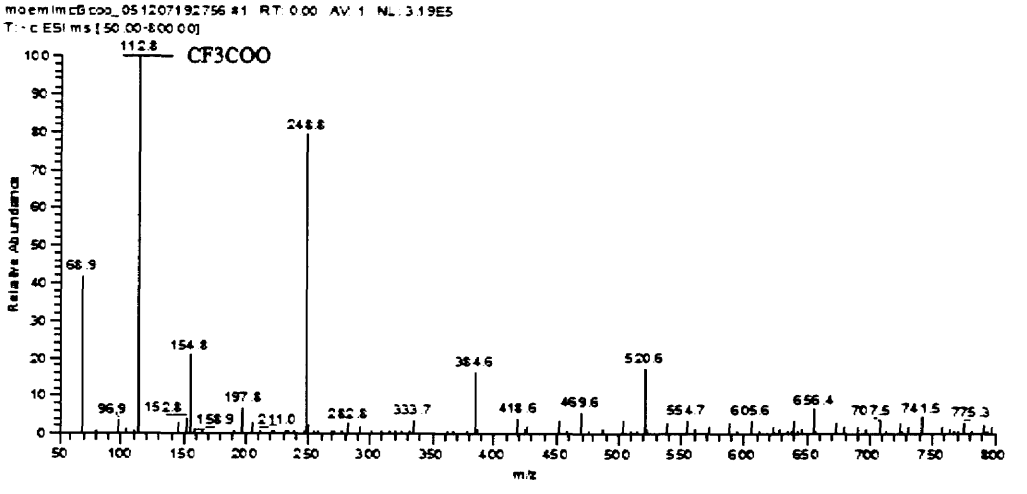

(b)

Figure 2.12 Mass spectra of [MOEMIM][CF_3COO]: (a) positive mode; (b) negative mode.

2.2.4 1-methoxyethyl-3-methyl imidazolium bis-trifluoromethane sulfonamide ([MOEMIM][Tf_2N])

2.2.4.1 Synthesis. [MOEMIM][Cl] (10.4g, 0.059 mol) was dissolved in water (50 mL) in a conical flask and added to $LiTf_2N$ (20.29g, 0.077 mol). The reaction mixture was stirred

at room temperature for 6 hours to give the product as a viscous layer at the bottom. The water was decanted off and the product was dissolved in CH_2Cl_2 and further washed three times with water, dried over $NaSO_4$, concentrated on rotavapor and finally dried in a vacuum oven to give the desired product (22.04 g, 88.9% yield).

2.2.4.2 Identification and Characterization.

UV-Vis UV spectrum was shown in Figure 2.13. It is the same as those of all other [MOEMIM] based ILs.

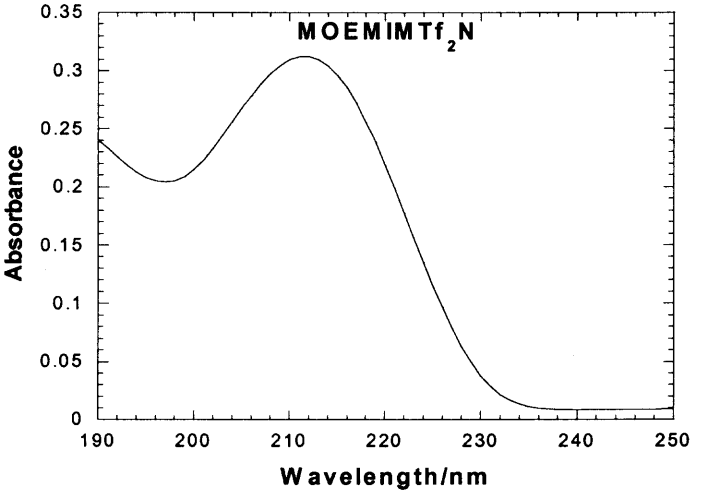

Figure 2.13 UV-vis spectrum of [MOEMIM][Tf_2N].

FTIR IR (film, neat): 3160, 3124, 2940, 2904, 2841, 1575, 1568, 1454, 1352, 1199, 1138, 1058, 740, 654, 617 cm^{-1}.

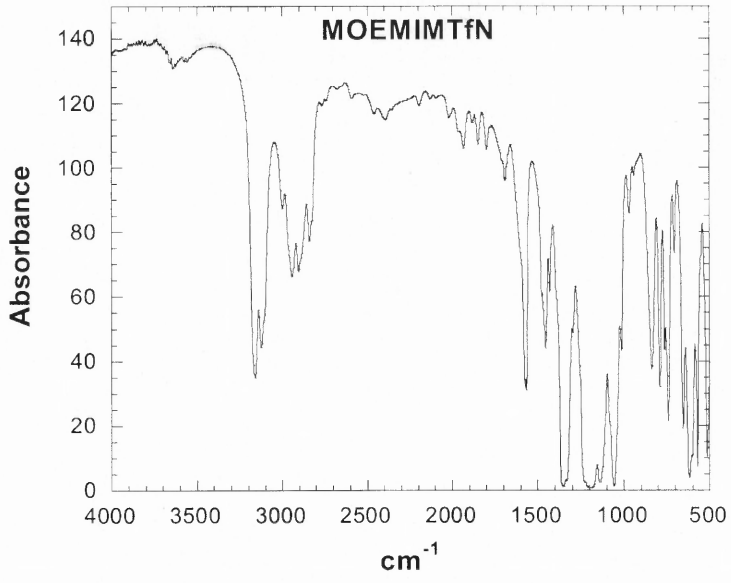

Figure 2.14 FTIR spectrum of [MOEMIM][Tf_2N].

MS Mass spectrum is shown in Figure 2.15.

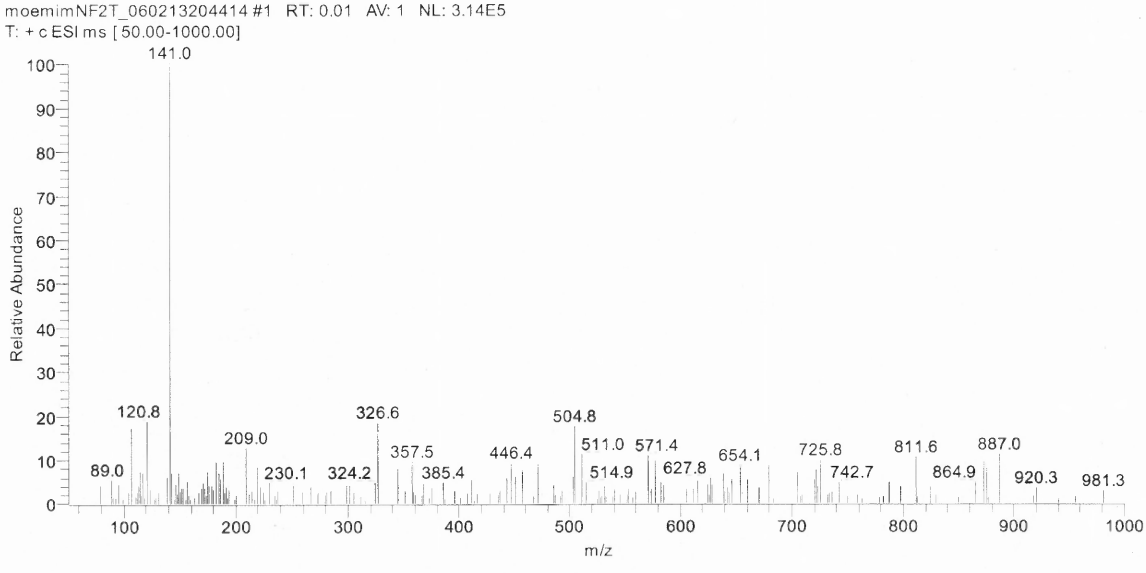

(a)

Figure 2.15 Mass spectra of [MOEMIM][Tf_2N]: (a) positive mode.

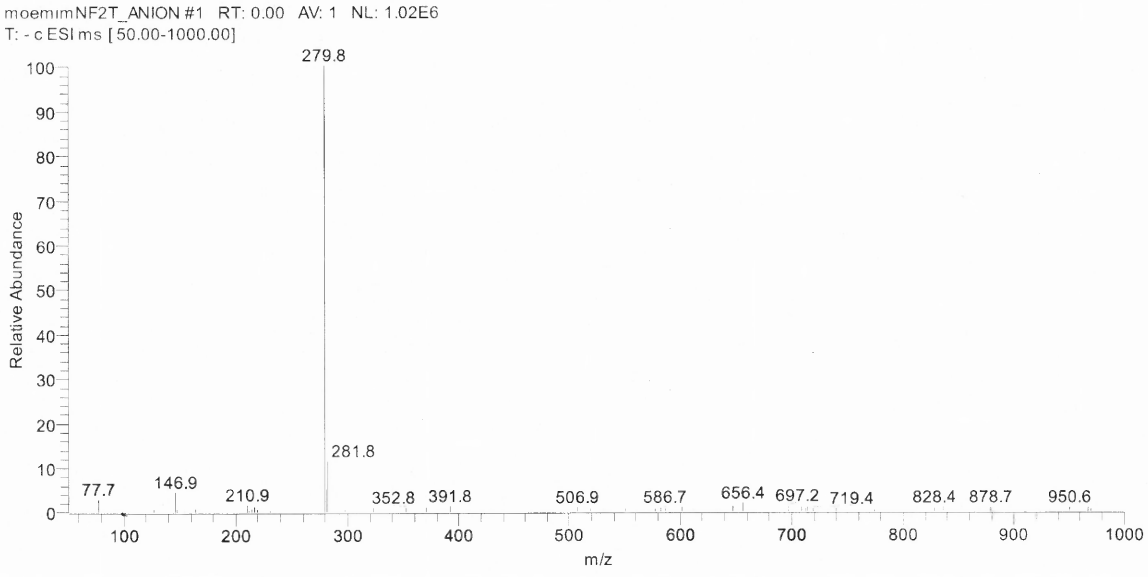

(b)

Figure 2.15 Mass spectra of [MOEMIM][Tf_2N]: (b) negative mode (Continuted).

NMR ^{1}H NMR (300 MHz, Acetone-d_6): δ3.35 (3H, s, OCH_3), 3.79 (2H, t, J = 4.8Hz, C-2'Hs), 4.04 (3H, s, N^3-CH_3), 4.49 (2H, t, J = 4.9Hz, C-1'Hs), 7.63 (1H, t, J = 1.8Hz, C-4H), 7.67 (1H, t, J = 1.8Hz, C-5H), 8.90 (1H, s, C-2H).

^{13}C NMR (75.5 MHz, Acetone-d_6): δ36.63 (OCH_3), 50.40 (C-2'), 58.86 (N^3-CH_3), 70.71 (C-1'), 120.92 (q, J = 321.24Hz, 2 x CF_3SO_3) 123.89 (C-4), 124.43 (C-5), 138.67 (C-2).

2.2.5 1-methoxyethyl-3-methyl imidazolium mthane sulfonate ([MOEMIM][OMS])

2.2.5.1 Synthesis. [MOEMIM][Cl] was taken in acetone in a conical flask and added to NaOMS. The reaction mixture was stirred at room temperature for 48 hours and then the NaCl precipitate was filtered through celite and the filtrate was concentrated on rotavapor

under vacuum. The product obtained was diluted with CH_2Cl_2 and passed through a silica gel column. The filtrate was concentrated, dried in a vacuum oven to give the product.

2.2.5.2 Characterization.

UV-Vis UV spectrum was given in Figure2.16. It is the same as UV spectra of other ILs.

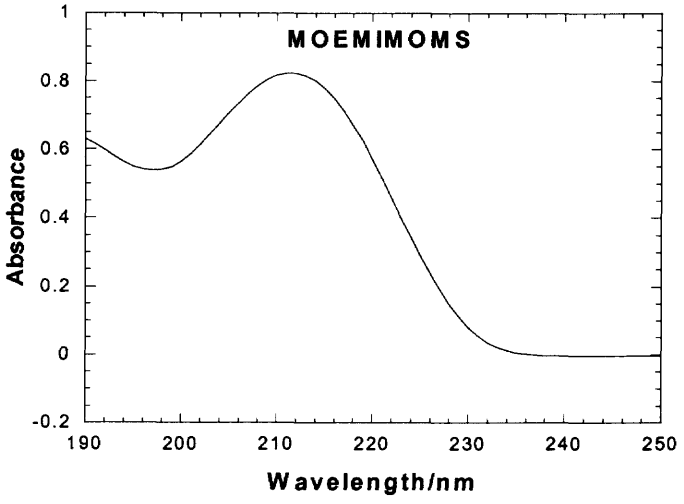

Figure 2.16 UV-vis spectrum of [MOEMIM][OMS].

FTIR Figure2.17 displays the FTIR of [MOEMIM][OMS].

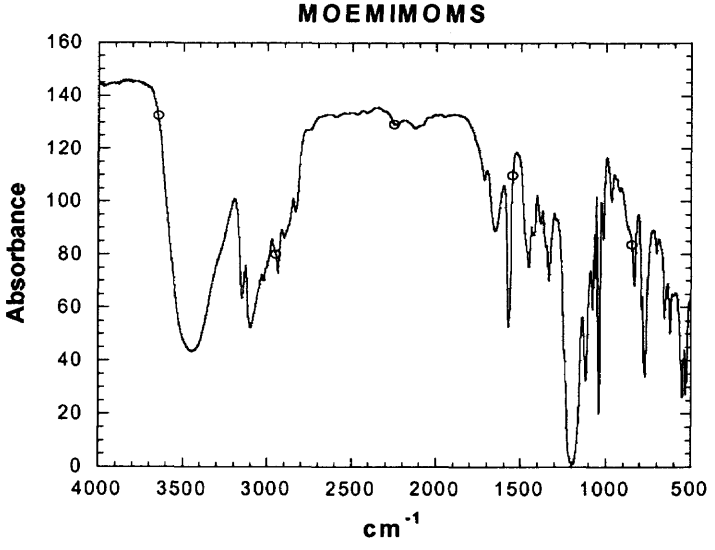

Figure 2.17 FTIR of [MOEMIM][OMS].

MS Mass spectra [MOEMIM][OMS] is shown in Figure 2.18. The 141 (m/e) represents MOEMIM cation in positive mode, and 95(m/e) corresponds to OMS anion in negative mode, proving this IL is [MOEMIM][OMS].

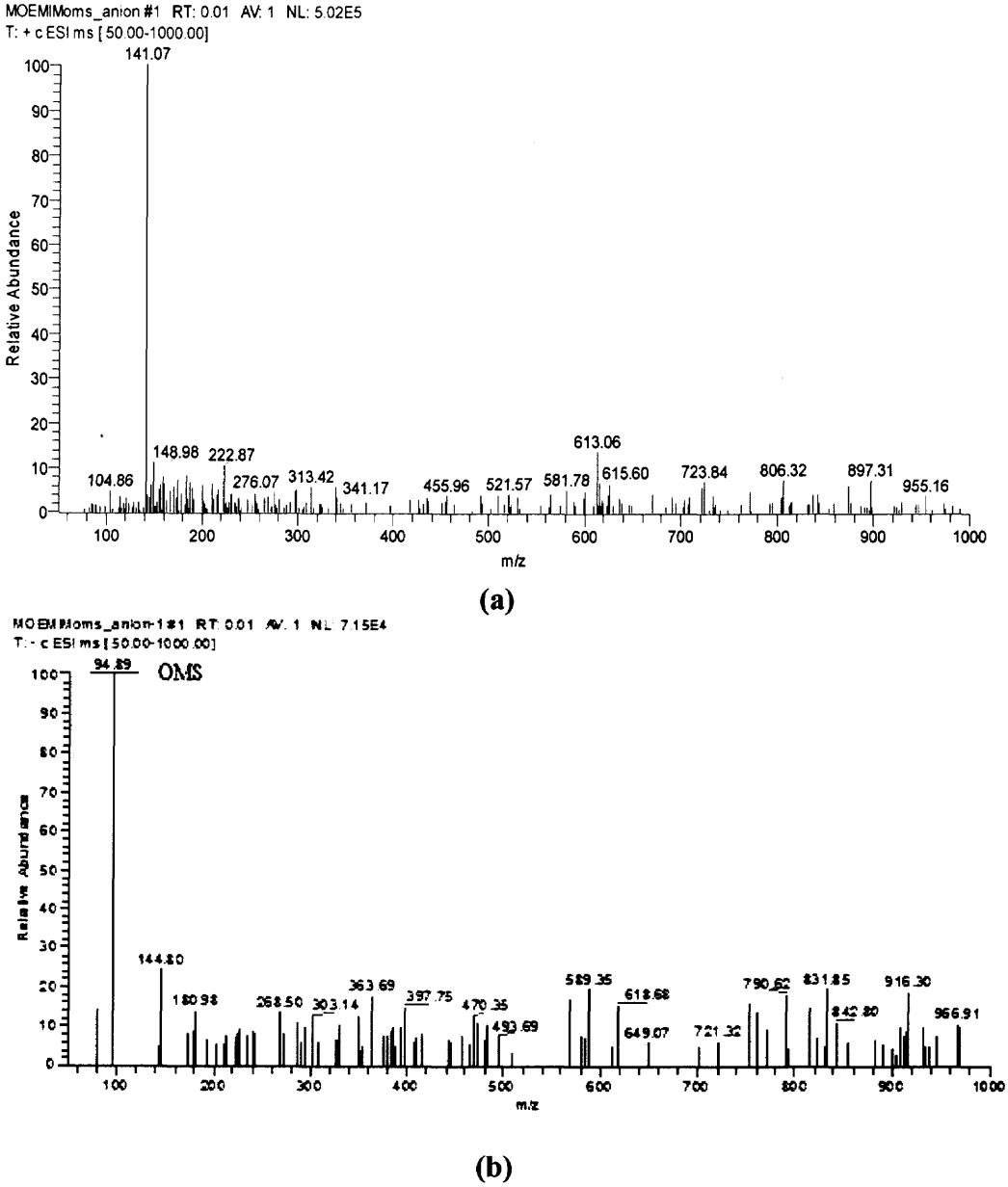

Figure 2.18 Mass spectra of [MOEMIM][OMS]: (a) positive mode; (b) negative mode.

2.2.6 3-methyl-1-(ethoxycarbonylmethyl) imidazolium acetate-[MECOOMIM][AC]

2.2.6.1 Synthesis.

Step1. Synthesis of [MECOOMIM][Br] To a stirred solution of 1-methylimidazole (4.1g, 40ml, 50mmol) in THF (50ml) at room temperature was added dropwise ethyl bromoacetate (10g, 6.7ml, 60mmol). The reaction mixture was stirred vigorously for 4 hours. The THF top phase was decanted and the IL washed with diethyl ether (3x10ml). Then residual solvent removed in vacuum. The product was dried at 60°C at 0.01mmHg for 72 hours to give a little bit yellow viscous hydroscopic oil.

Step 2. Exchange of Anion Add 1.745g [MECOOMIM][Br] and 0.516g CH_3COONa to an elementary flask containing 30ml acetonitril. Stir vigorously for 3 days. Then decant the solid, and remove the acetonitril by vacuum rotation. The residue was dissolved in 200 ml of Dichloromethane and eluted through silica gel column. The column was eluted 4-5 times. The eluent was collected and the dichloromethane was removed by vacuum rotator to get the desired IL.

2.2.6.2 Characterization.

UV-Vis [MECOOMIM][CH_3COO] shows a very different UV spectrum from [MOEMIM] based ILs. It has absorbance before 240nm, but there is no characteristic absorbance at 211nm as shown in [MOEMIM] based ILs.

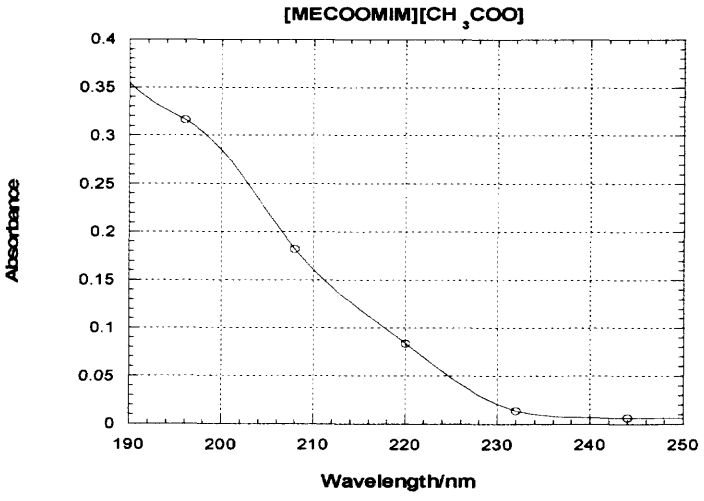

Figure 2.19 UV-vis spectrum of [MECOOMIM][CH_3COO].

MS 169(m/e) in positive mode represents $[MECOOMIM]^+$, while 62(m/e) in negative mode refers to $[CH_3COO]^-$, confirming this IL is [MECOOMIM][CH_3COO].

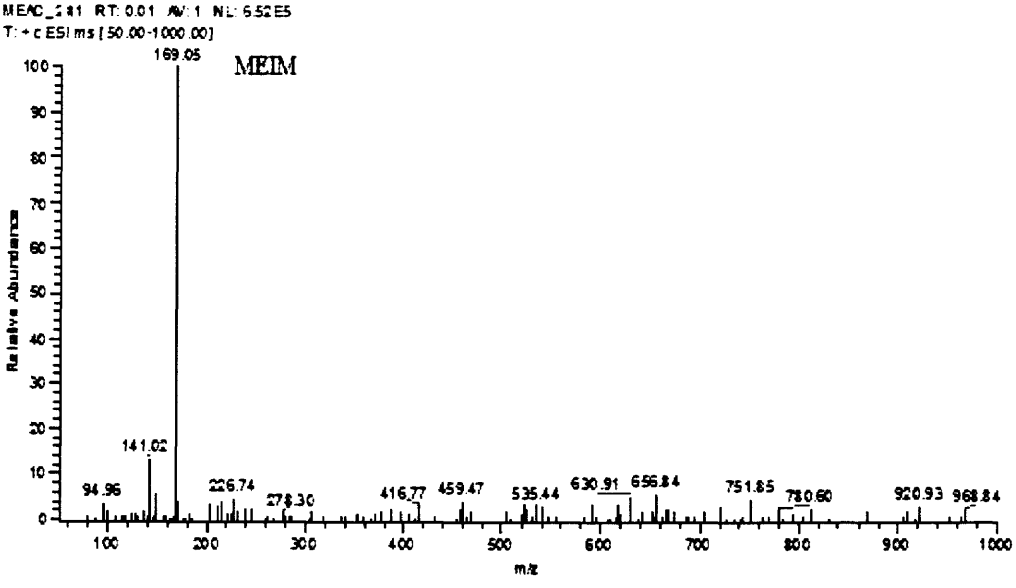

(a)

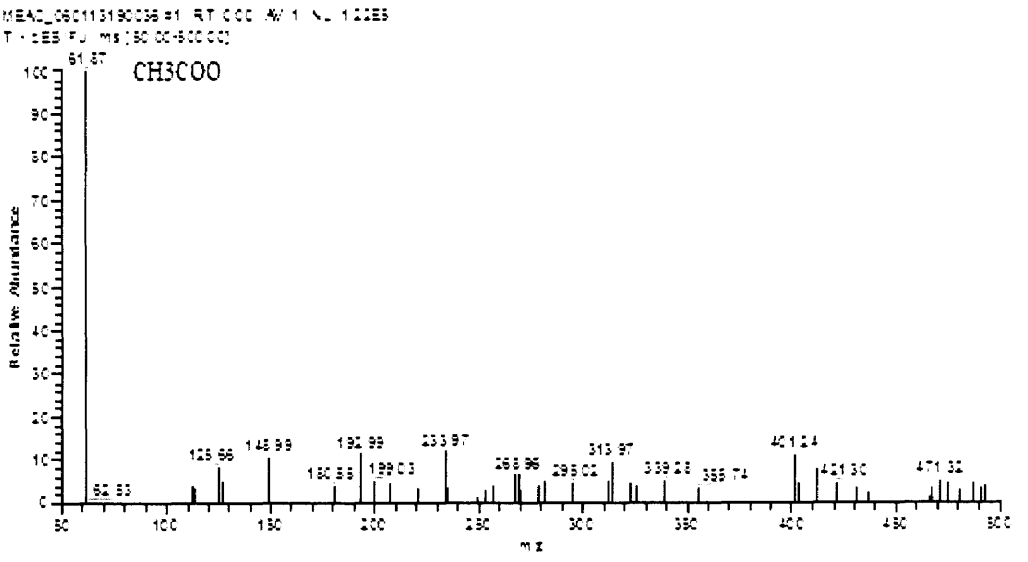

(b)

Figure 2.20 Mass spectra of [MECOOMIM][CH_3COO]: (a) positive mode; (b) negative mode.

2.3 Properties of Ionic Liquids

2.3.1 Status at Room Temperature

All ILs studied here are liquid at room temperature.

2.3.2 Density

All these ILs are yellow oily liquids and have a greater density than water.

Table 2.1 Density of ILs (g/ml)

	MOEMIM BF_4	MOEMIM PF_6	MOEMIM CF_3COO	MOEMIM OMS	MOEMIM Tf_2N	MECOO MIMAC
Density (g/ml)	1.267	1.404	1.302	1.216	1.476	1.229

2.3.3 Miscibility

[MOEMIM][PF_6] and [MOEMIM][Tf_2N] are hydrophobic, while all others are hydrophilic.

CHAPTER 3

CHARACTERIZATION OF URANIUM ASSOCIATED WITH IONIC LIQUIDS

3.1 Introduction

Actinides and lanthanides partitioning is achieved through solvent extraction from aqueous solutions. A large quantity of volatile or semi-volatile organic solvents has been widely used in the liquid/liquid extraction process to recover the radionuclides from low-level radioactive waste in an aqueous phase. Extractant/solvent miscibility problems or third-phase formation often happen during the liquid-liquid extraction. There is a real need for the exploration of new solvents that can replace the organic solvents and also enhance the liquid-liquid extraction.

Room temperature ionic liquids (RTILs) seem very promising substitutes for the traditional organic solvents used in the PUREX process to recover low-level U and Pu from waste. Visser and Roger et al. (2001) reported that the addition of $[C_{4\sim8}mim][PF_6]$ to an extractant like CMPO (octylphenyl-N,N-di-isobutyl carbamoylphosphine oxide)/TBP(tri-n-butyl phosphate) can significantly enhance the partitioning of actinides in these ILs. Also, a patented process demonstrated the dissolution of nuclear fuel cladding with $[BMIM][NO_3]$ with additional PUREX (Plutonium and Uranium Recovery by Extraction) processing to recover U and Pu.

However, there is little understanding of the mechanics by which partitioning-ability of actinides and other metals enhances. Therefore, it is important to investigate the interaction between the actinides and ILs. Choppin et al. (2003) have explored the uranyl

coordination environment in hydrophobic ionic liquids, and observed different inner-sphere coordination environments for the uranyl nitrate complex formed in organic solvent and in ILs. Gaillard et al. (2005) from Germany also investigated the uranyl complexation in different types of fluorinated acids. They found $[BF_4]^-$ and $[PF_6]^-$ can form monodentate complex with U(VI), while $[Tf_2N]^-$ did not complex with U(VI). However, the limitation on this study is the complexation-ability of an anionic part cannot be considered the same as the ILs, since ILs may behave as ion pair in aqueous solution and may not completely dissociate. In order to understand the coordination of ILs with actinides, in this study, I investigated the coordination chemistry of U(VI) and [MOEMIM]-based ILs.

3.2 Materials and Methods

3.2.1 Preparation of Uranium-IL mixture

Ionic liquids used in this study were synthesized and purified according to the methods described in chapter 2. Uranium was introduced as uranyl nitrate, $UO_2(NO_3)_2 \cdot 6H_2O$. The final concentration of U(VI) in the mixture was 5mM. Uranium and IL mixture consisting of 1: 1 and 1:2 molar ratio were prepared and equilibrated for 24 hours. All solutions were prepared with ultra-pure de-ionized water (Milli-Q plus, Millipore).

3.2.2 Characterization of the Interaction of Ionic Liquids with Uranium

pH change pH change during equilibration provides information on protonation or deprotonation, which indicates the interaction between uranium and ILs. In this study,

the pH change was determined by measuring the pH at the beginning of mixing and after 24 hours using Mettler Toledo MP 220 pH meter.

Potentiometric titration Complex formation was determined by potentiometric titration. Difference between titration curves from uranium and U-ILs mixture indicates if there is complexation between them. In this study, before titration, 1ml aliquot of the mixture was added to 19ml of 0.1M KCI to adjust the ionic strength. In addition, the sample and 0.01N NaOH solution were purged with pure nitrogen gas to keep it free of CO_2. The final U concentration in the solution was 0.25mM, and the initial pH was between 4 and 6. The change in pH of the mixture during the addition of 0.01N NaOH was determined by Mettler Toledo DL57 titrator. The glass electrode was calibrated before titration with three standard buffer solutions in the order of pH 10, pH 7 and pH 4.

UV-vis spectrometric analysis Uranium has a characteristic UV-vis absorption between 300nm and 500nm. The UV-visible spectra of uranium and the U in the ILs mixture were determined by a Hewlett Packard 8453 diode array scanning UV-vis spectrophotometer. A 1cm square cuvette made of quartz was used here. The U(VI) concentration in the mixture was 5mM.

Mass spectrometric analysis Mass spectrometry has the ability to determine the ratio of mass over charge of a molecule, from which molecular mass can be obtained. MS was used here to detect the complex molecules. Samples were analyzed by LCQ Advantage EIS-MS using electrospray ionization mass spectrometry, (*Thermo-Finnigan Inc.*) under the following conditions: sheath gas, nitrogen; spray voltage, 4.5kV; capillary temperature, 325°C; capillary voltage 35V.

Speciation of U-ILs by X-ray absorption spectroscopy (XAS) Molecular speciation of uranium associated with ILs was determined using X-ray absorption near-edge spectroscopy analysis (XANES) and extended x-ray absorption fine structure (EXAFS) analyses. XANES determines the oxidation state of the central atom by measuring the shift in absorption edge compared to a known standard. EXAFS measures the X-ray absorption as a function of energy and determines the local arrangement of atoms around a given absorbing atom. Analysis of the EXAFS allows obtaining the type, number of neighboring atoms, and the distance from the scattering atom.

Equimolar (20mM) of U-ILs mixture was prepared and equilibrated overnight. An aliquot of the mixture was sealed in a 5×4cm plastic bag made of polyethylene. Uranium was analyzed on beam line X11A at the National Synchrotron Light Source (NSLS) in Brookhaven National Laboratory at the U-L_{III} absorbance edge (17.166kev) using fluorescence detection. Six scans were collected and averaged to minimize the signal-to-noise ratio. The XANES spectra were background-subtracted and normalized to the edge jump, and the oxidation state of uranium in the samples determined by comparing the energy position at the inflection point with that from tetravalent uranium dioxide and hexavalent uranyl nitrate. Fourier transformed EXAFS data, a pseudo-radial distribution function representing the radial coordination shells of the near-neighbor atoms surrounding the metal, were obtained using a multi-step data analysis procedure, which included background subtraction and normalization to the edge-jump's height followed by Fourier transformation of the k^3-weighted EXAFS spectra. The theoretical EXAFS modeling code FEFF6 was used to calculate the back-scattering phase and amplitude information for individual neighboring atoms.

3.3 Results and Discussion

3.3.1 [MOEMIM][BF_4] and Uranium

3.3.1.1 pH change. Change of pH is displayed in Table 3.1. It is noted that pH change in both U and [MOEMIM][BF_4] after 24 hours are negligible, but the decrease in both 1:1 and 2:1 mixture was significant, i.e., 0.89 and 0.99 respectively. This indicates proton release, which may result from the strong interaction between [MOEMIM][BF_4] and U. As is known, $[BF_4]^-$ can hydrolyze to give out $[BF_3(OH)]^-$ and HF, resulting in pH drop (Mousa et al.,1997). To avoid the effect of hydrolysis, before using, [MOEMIM][BF_4] solution was stored for a few days until the hydrolysis was completed. Therefore the pH drop in the U-[MOEMIM][BF_4] mixture was just due to the complexation.

Table 3.1 pH Changes of [MOEMIM][BF_4]:U Mixture

	[MOEMIM][BF_4]:U		U	[MOEMIM][BF_4]
	1:1	2:1		
0 hr	3.22	2.99	3.05	4.23
24hr	2.33	2.00	3.06	4.19
Difference	0.89	0.99	0.01	0.04

3.3.1.2 Titration. Figure 3.1 shows the titration curves of U solution and U-[MOEMIM][BF_4] mixtures. Titration curve of U exhibited one sharp inflection point at 3mM OH^-/mM U at around pH 7.5, which means one uranyl needs three OH^-, as indicated by the equation below.

$$[UO_2(NO_3)_3]^- + H_2O \rightarrow [UO_2(NO_3)_2(OH)]^- + [NO_3]^- + H^+ \quad (3.1)$$

$$[UO_2(NO_3)_2(OH)]^- + H_2O \rightarrow [UO_2(NO_3)(OH)_2]^- + [NO_3]^- + H^+ \quad (3.2)$$

$$[UO_2(NO_3)(OH)_2]^- + H_2O \rightarrow [UO_2(OH)_3]^- + [NO_3]^- + H^+ \quad (3.3)$$

$[UO_2(NO_3)_3]^-$ is the major speciation in the solution, which has been confirmed by mass spectrometry. During the addition of NaOH, $[OH]^-$ started to replace the $[NO_3]^-$ that was associated with uranyl. And finally 3 $[NO_3]^-$ can be substituted by 3 $[OH]^-$.

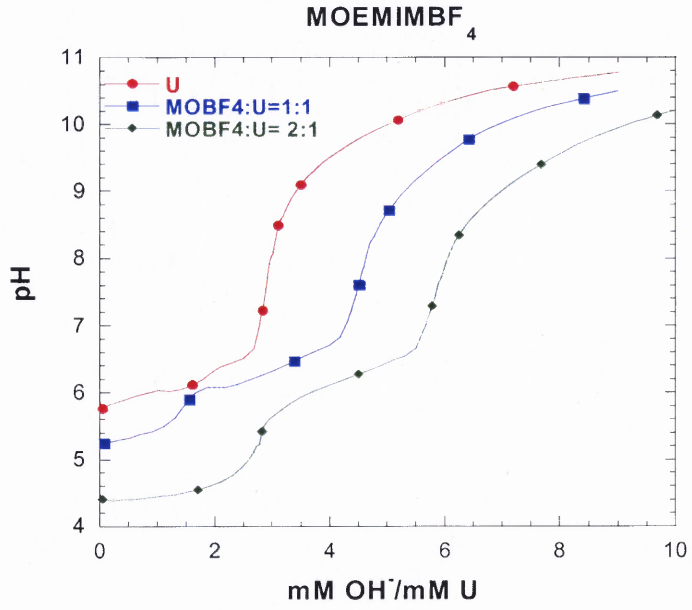

Figure 3.1 Potentiometric titration of U and U-[MOEMIM][BF_4] mixture.

Compared with the titration curve of uranyl nitrate, two inflection points were observed in both 1:1 and 2:1 mixtures. The first inflection point is considered as the result from the hydrolysis of BF_4^-, as described below, and the second is caused by the hydrolysis of uranyl, as described above.

Wamser (1948) carried out kinetic and equilibrium studies on the fluoroborate species in solution, and suggested the four ions BF_4^-, BF_3OH^-, $BF_2(OH)_2^-$ and $BF(OH)_3^-$ were formed by succession hydrolysis steps, as shown here:

$$BF_4^- + H_2O \rightleftharpoons BF_3OH^- + HF \quad (3.4)$$

$$BF_3OH^- + H_2O \rightleftharpoons BF_2(OH)_2^- + HF \quad (3.5)$$

$$BF_2(OH)_2^- + H_2O \rightleftharpoons BF(OH)_3^- + HF \quad (3.6)$$

The first hydrolysis step is slow while the subsequent steps are relatively fast. In 1:1 IL:U mixture, the first inflection was observed at 1.5mM OH-/mM U at pH 6, which was due to the hydrolysis of $BF4^-$, and the second one came up at around 4.5mM OH^-/ mM U at pH 7.6, which resulted from the hydrolysis of uranyl. The same thing happened to the 2:1 IL-U mixture, which displayed the first inflection point at 3mM OH-/ mM U at pH 5.5, and the second showed up at 6mM OH-/ mM U at pH 8. It is notable that, the first inflection point for 1:1 mixture was shown at 1.5 mM OH-/ mM U, while that for 2:1 mixture was displayed at 3 mM OH-/ mM U. This could be due to the addition of one more fold BF_4^-, which caused enhanced hydrolysis. That is, in 1:1 mixture, the hydrolysis is not accomplished through the 3 steps, but in 1:2 mixture the hydrolysis was completed. Anbar and Guttmann (1960) studied the effect of acidity on the hydrolysis of BF_4^-, disclosing that the increased acidity can enhance the hydrolysis of BF_4^-, due to the enhancement of the first hydrolysis step (1). In addition, from the first inflection point to the second, the both needed 3 more OH^-, indicating the complete hydrolysis of uranyl.

3.3.1.2 UV-vis. Figure 3.2 shows the UV-vis spectra of uranium and [MOEMIM][BF_4]-U mixtures. A characteristic absorbance of U (VI) is in the range between 350nm and 480nm.The absorption spectrum of U (VI) exhibits a maximum peak at 413nm, with two side shoulders at 403nm and 426nm, respectively. Another small peak is around 367nm. The spectra of both 1:1 and 2:1 [MOEMIM][BF_4]-U mixtures display the similar characteristic absorption, but the phase change is obvious. The maximum absorption peak shifted from 413nm to 418nm and the two shoulders also correspondingly shifted to

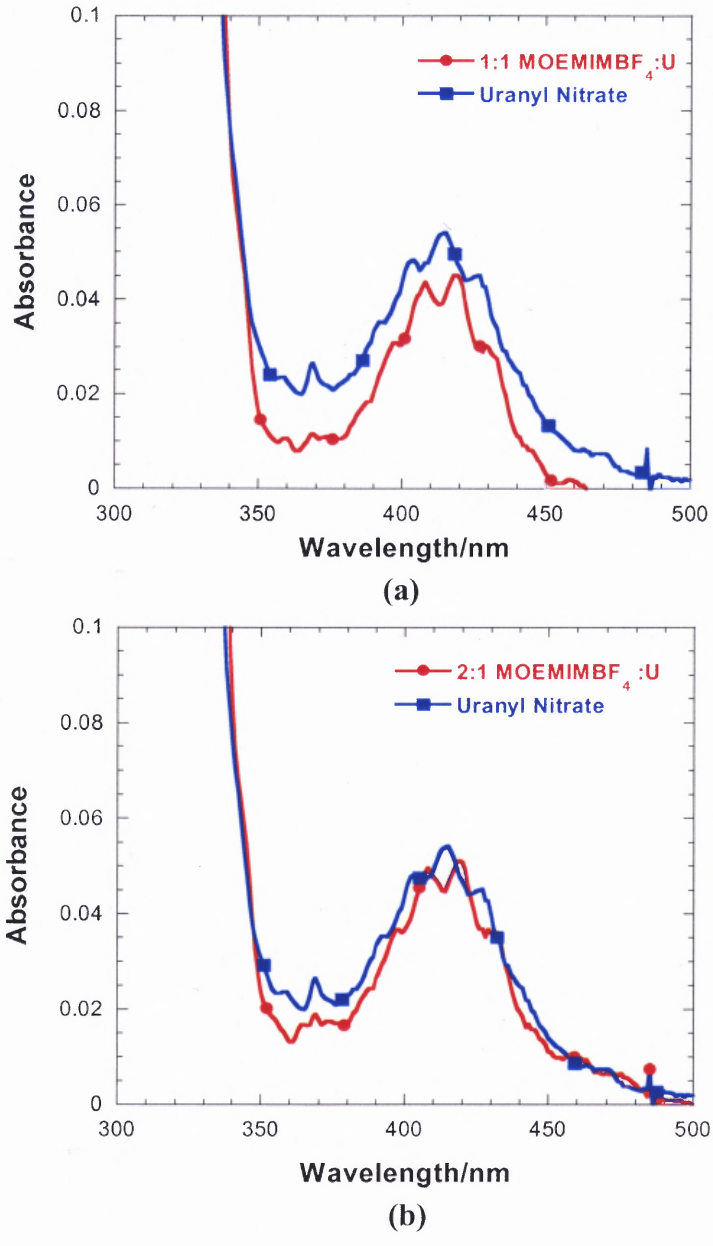

Figure 3.2 UV-vis spectra of 5mM U in: (a) 1:1 and (b)2:1 [MOEMIM][BF_4] -U mixture.

408nm and 429nm. In addition, the right shoulder that is originally at 426nm becomes unobvious. All the difference indicates the change of environment surrounding uranium atoms, indicating the formation of complex.

3.3.1.4 MS. ESI-MS was used to determine the molecular mass of the the complex molecule. Both positive and negative modes were monitored. Figure 3.3 shows the MS of uranyl nitrate solution at pH 3, and Figure 3.4 shows the MS of U-[MOEMIM][BF_4] mixture.

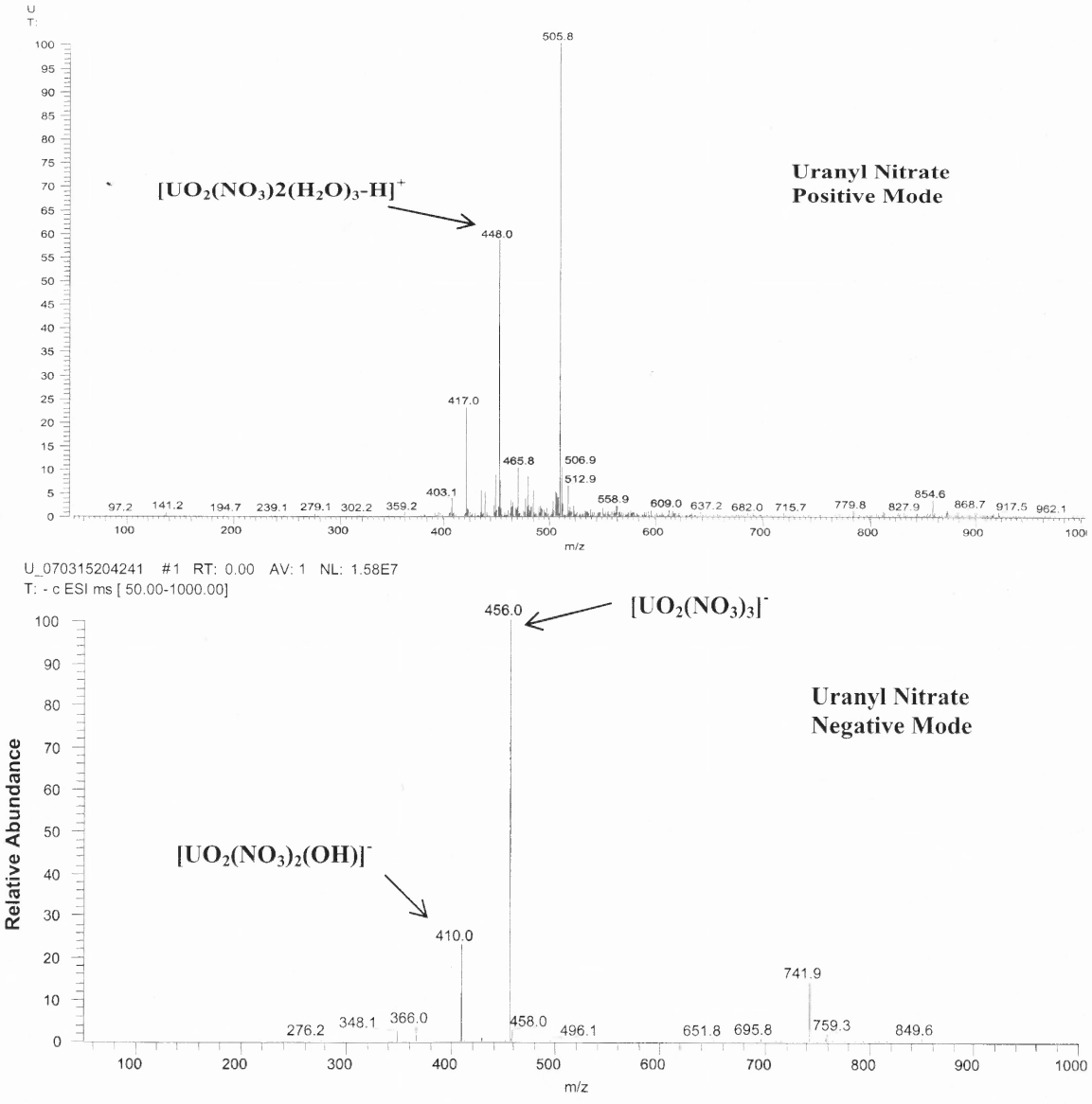

Figure 3.3 Mass spectra of uranyl nitrate solution at pH 3.

In positive mode, $[UO_2(NO_3)_2(H_2O)_3\text{-}H]^+$ at 448(m/e) is dominant. In negative mode, $[UO_2(NO_3)_3]^-$ at 456(m/e) is predominant, and $[UO_2(NO_3)_2(OH)]^-$ at 410(m/e) is another major speciation.

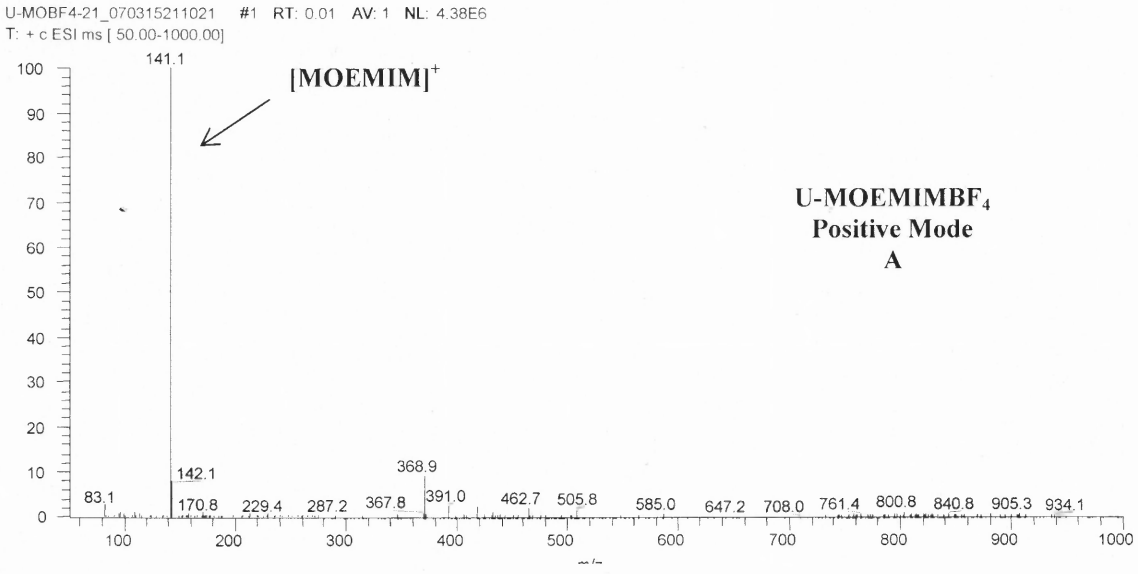

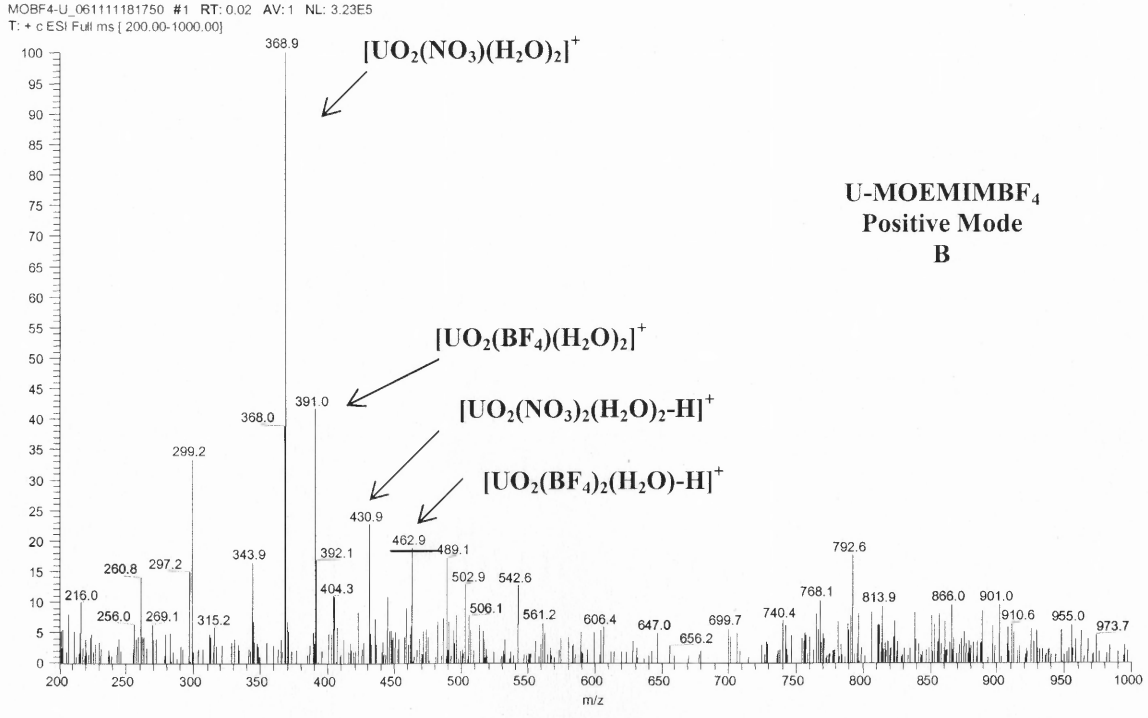

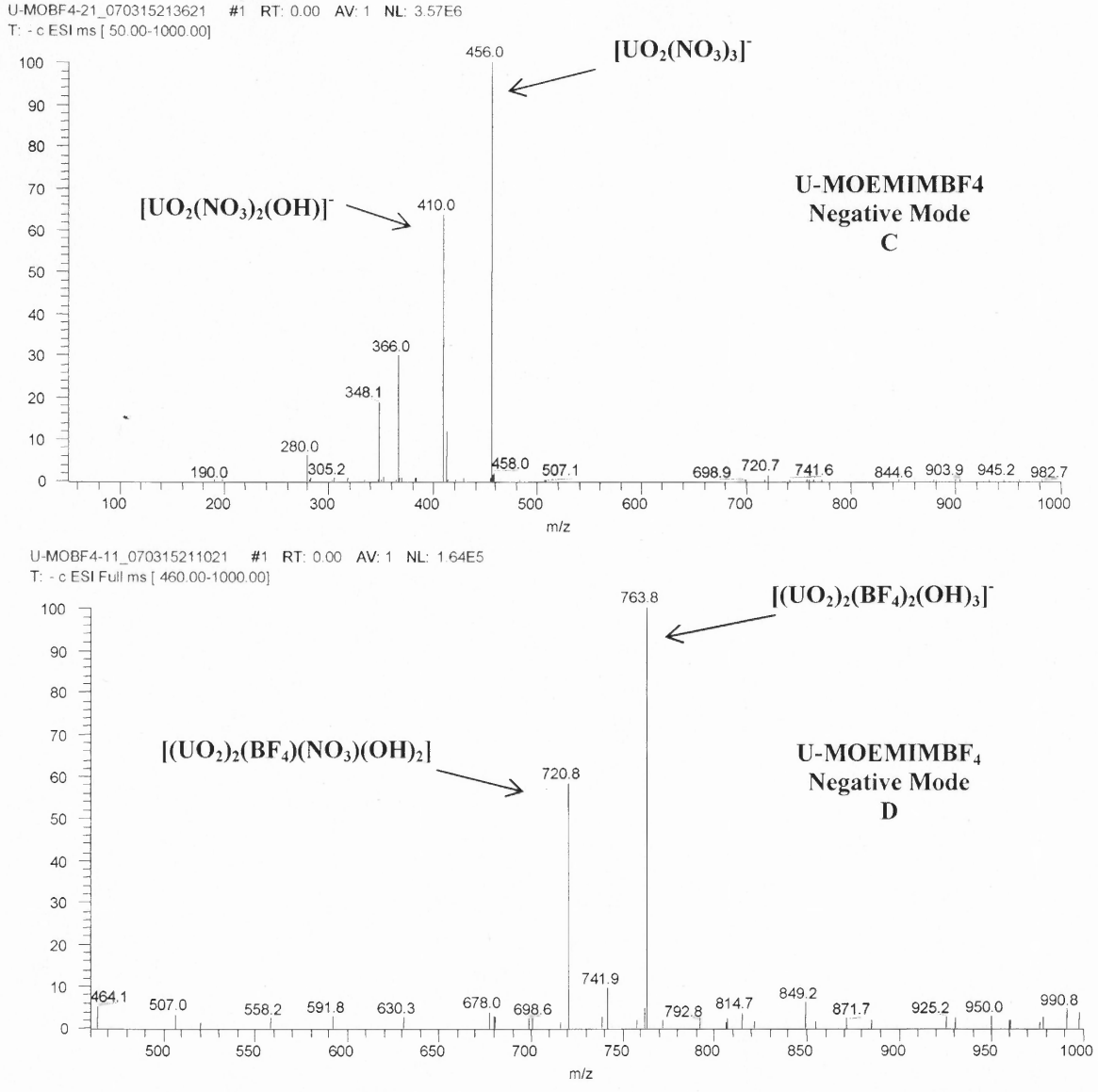

Figure 3.4 Mass Spectra of [MOEMIM][BF_4]-U at pH 2: (A) positive mode between 50-1000(m/z); (B) positive mode between 200-1000(m/z); (C) negative mode between 50-1000(m/z); (D) negative mode between 460-1000(m/z).

Positive mode A displays the MS between 50-1000(m/z), in which the 141(m/e) that represents the $[MOEMIM]^+$ cation is dominant since it doesn't complex with uranyl. Positive mode B shows MS between 200 and 1000(m/e), in which 368(m/e) is the majority that corresponds to $[UO_2(NO_3)(H_2O)_2]^+$. However, two complex molecules are

also found in B, one of which is shown at 391(m/z), representing $[UO_2(BF_4)(H2O)_2]^+$, and the other is shown at 463(m/e), corresponding to $[UO_2(BF_4)_2(H_2O)]^+$.

In negative mode C, MS is shown between 50-1000(m/e), uranyl nitrate ions are still predominant, and before 460(m/e) no complex is found. However, in negative mode D, MS is displayed between 460-1000(m/e), and two complex molecules are found in 764(m/e), which could be $[(UO_2)_2(BF_4)_2(OH)_3]^-$, and the other found in 721(m/e) a possible result from the $[(UO_2)_2(BF_4)(NO_3)(OH)_2]$.

As we can see, in the pH 3 solution, the complexes are not the predominant speciation in both positive and negative modes, but we do find some uranyl complex associated with $[BF_4]^-$, suggesting the formation of complex.

3.3.1.5 XANES. As discussed before, XANES can determine the oxidation state of the central atom by measuring the shift in the absorption edge compared to a known standard. Figure 3.5 revealed that the uranium in all the mixtures has the same absorption edge energy (17166ev) as does the uranyl nitrate standard, indicating the speciation of U in the mixture was present as U (VI) (Dodge et al. 1994).

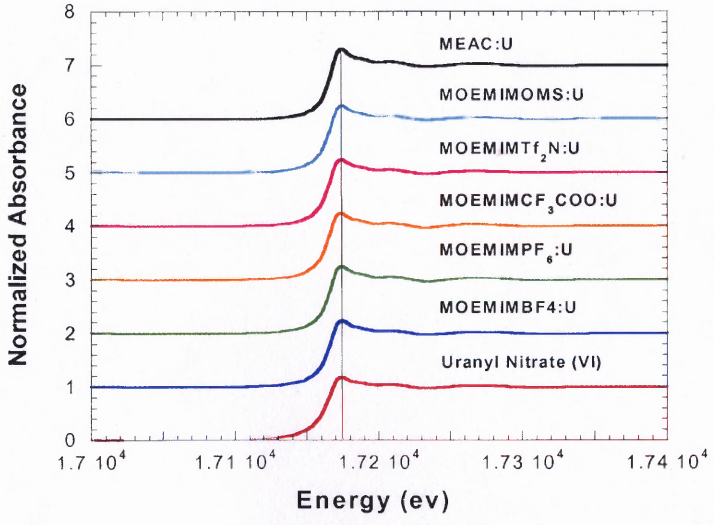

Figure 3.5 Normalized XANES spectra of various U-ILs mixtures.

3.3.1.6 EXAFS. The structure of $UO_2(NO_3)_2 \cdot 2H_2O$ is shown in Figure 3.6 (*www.3Dchem.com*).

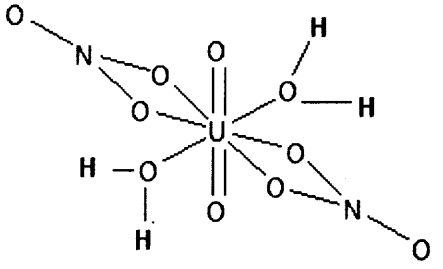

Figure 3.6 Molecular Structure of $UO_2(NO_3)_2 \cdot 2H_2O$.

The core uranium atom is surrounded by oxygen atoms. The first shell consists of two axial oxygen (O_{ax}) with a radius about 1.76Å. The second shell consists of 5 or 6 equatorial oxygen (O_{eq}), with the radius about 2.4 Å, provided by NO_3^- or H_2O (Kelly, et al., 2002; Antonio, et al, 2001). It has to be mentioned that the $NO3^-$ can form either a monodentate or bidentate with uranyl, and the number of water molecules can vary.

EXAFS is a useful method to measure the X-ray absorption as a function of energy. This helps to determine the local arrangement of atoms around a given absorbing atom, therefore, providing information about the type, number of neighboring atoms, and the distance from the scattering atom.

EXAFS spectra of uranyl nitrate at pH 3 and U-[MOEMIM][BF_4] at pH 2 were displayed in Figure 3.7 and 3.8, respectively. Figure 3.7(a) presents the raw k^3-weighted data over the range of 2.1 – 13.2 Å at the U-L_{III} edge for uranyl nitrate, and Figure 3.7(b) represents the Fourier transformed spectra of EXAFS. In Figure 3.7(b), the first peak corresponds to the axial shell at 1.76 Å, representing the scattering from the two collinear axial oxygen ligands. The second peak refers to the equatorial shell at about 2.41 Å, scattering from the equatorial oxygen atoms surrounding the uranium.

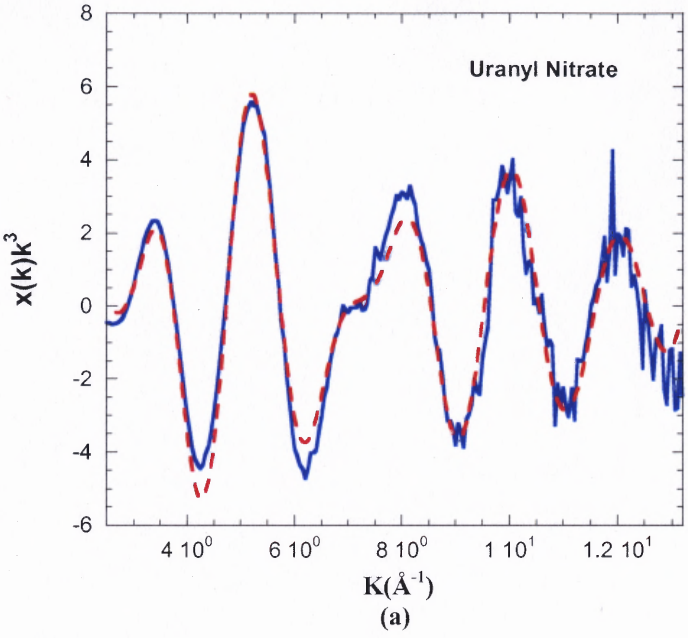

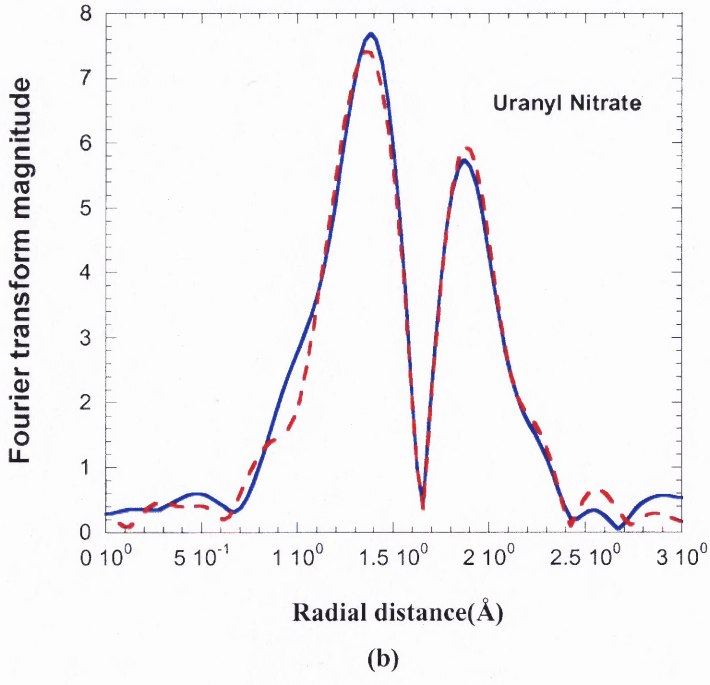

Figure 3.7 EXAFS spectra of uranyl nitrate at the U L_{III} edge: (a) k^3-weighted EXAFS spectra (2.5-13.2Å^{-1}); (b) Fourier transform of EXAFS. Experimental data (-); theoretical fit (--).

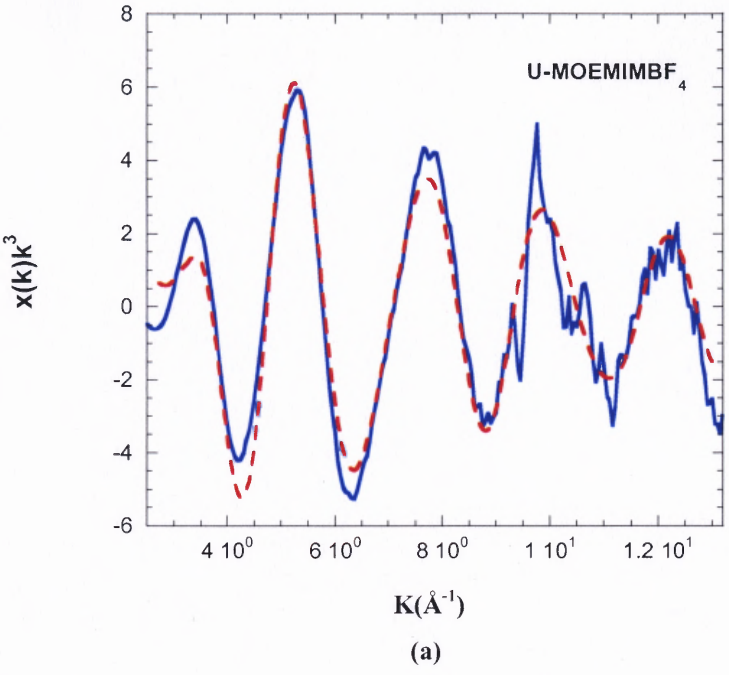

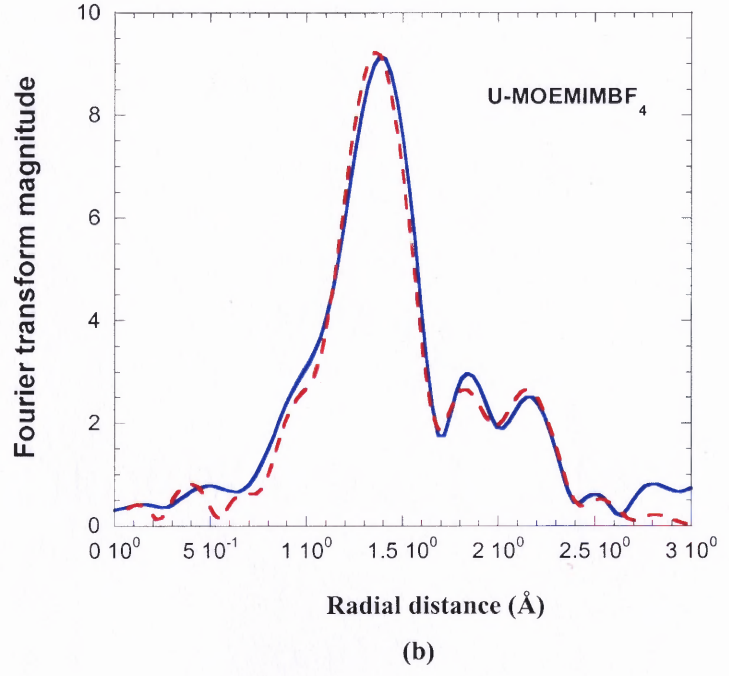

Figure 3.8 EXAFS spectra of U-[MOEMIM][BF_4] at the U L_{III} edge: (a) k^3-weighted EXAFS spectra (2.5-13.2Å^{-1}); (b) Fourier transform of EXAFS. Experimental data (-); theoretical fit (--).

Comparision of Figure 3.7 and 3.8 shows that the first peak of U-[MOEMIM][BF_4] is the same as the first peak of uranyl nitrate, indicating that the axial

shell is not influenced. However, it is obvious that the second peak of U-[MOEMIM][BF_4] is split into two peaks instead of one peak as shown in uranyl nitrate. This gave a hint that there is another bond formed in the equatorial shell. The new bond formed will most likely be the U-BF_4 bond. A fitting model has been made using FEFF6, and the results are shown in Table 3.2.

Table 3.2. EXAFS Structure Parameters for U and U-[MOEMIM][BF_4] Mixtures

Sample	Shell	N	R (Å)	σ^2 (Å^2)	R factor
[2]Uranyl Nitrate	U-Oax*	2	1.76±0.005	0.002	0.010
	U-Oeq	5±0.1	2.42±0.014	0.009	
[1]UO_2^{2+}/HBF_4	U-Oax	2	1.77	0.0029	0.009
	U-F	1	2.24	0.0068	
	U-Oeq	4	2.44	0.0075	
[2]UO_2^{2+}/[MOEMIM][BF4]	U-Oax*	2	1.77±0.008	0.004	0.021
	U-F	1±0.23[a]	2.26±0.038	0.007	
	U-Oeq	4	2.49±0.033	0.011	

(N) coordination number, (R) interatomic distance, (σ^2) disorder parameter, (R factor) reliability factor.
* Axial oxygen fixed at 2.
[a] n(U-F) = 5 – n(U-O)
1 - data from Gaillard et al. (2005)
2 - data from this study

The fitting model for uranyl nitrate shows the presence of 2 axial oxygen (O_{ax}) at 1.76Å, and 5 equatorial oxygen (O_{eq}) at 2.42Å, that result from hydration and the nitrate anion. These data are consistent with those in literature (Allen et al., 1997; Gaillard et al., 2005), in which 2 O_{ax} was found at 1.76Å and about 5 O_{eq} at 2.41 Å.

In the modeling of U-[MOEMIM][BF_4], a U-F path was included. Since the number of F was unknown, it was assumed the total equatorial number ($N_F + N_O$) is equal to 5. The best fitting model consists of 2 O_{ax} at 1.77Å, 1 F at 2.26Å, and 4 O_{eq} at 2.49Å.

The bond distance of U-O_{ax} is pretty close to that of uranyl nitrate and in agreement with the data in literature. The bond distance of U-F, on the other hand, is a little longer than the 2.24Å that is commonly found in uranyl fluoride solid compounds

(Mak, T. et al., 1985). As we know, the distance of one molecule to uranyl depends strongly on the number and the nature of the other molecules in this sphere. Fluoride can interact strongly with uranyl due to its strong electro-negativity. Compared with F^-, BF_4^- is much less electro-negative because the charge is much more diffuse. As a result, the attraction between uranyl and BF_4^- is reduced, leading to the increase of bond distance.

Furthermore, 2.49Å was found for the $U\text{-}O_{eq}$ bond distance in U-[MOEMIM][BF_4], which is 0.07Å longer than that in uranyl nitrate. It is hypothesized that the $[BF_4]^-$ associated with UO_2^{2+} can form a hydrogen bond with the H_2O that is also associated with the UO_2^{2+} nearby thus forming a six-membered ring with uranyl, and resulting in the longer $U\text{-}O_{eq}$ bond distance. This has been proposed by Gaillard et al. (2005) when investigating the uranyl complexation in fluorinated acids, including HF, HBF_4, HPF_6 and HTf_2N, by Time-resolved emission spectroscopy (TRES) and EXAFS. Their data is also shown in Table 3.2, and the structure is displayed in Figure 3.9.

It has to be mentioned that, in Gaillard's study HBF_4 acid was used to examine the coordination environment of uranyl, while in my study a [MOEMIM][BF_4] ionic liquid solution was used. Since the cation and anion are not associated to each other in solution and only an anion can form complex with uranyl, the cation seems unlikely to influence the complexation.

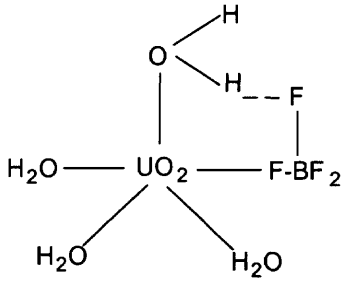

Figure 3.9 Proposed complex structure of U-[MOEMIM][BF_4].

3.3.2 [MOEMIM][CF_3COO] and Uranium

3.3.2.1 pH change. As is shown in Table 3.3, pH change is negligible in both 1:1 and 2:1 mixtures.

Tabel 3.3 pH Change in [MOEMIM][CF_3COO]:U Mixture

	[MOEMIM][CF_3COO]: U		U	[MOEMIM] [CF_3COO]
	1:1	2:1		
0 hr	3.17	3.23	3.05	6.09
24hr	3.09	3.16	3.06	6.02
Difference	0.08	0.07	0.01	0.07

3.3.2.2 Titration. Titration curves of both 1:1 and 2:1 mixtures are similar to that of U, showing only one inflection point around 3mM OH-/ mM U where the hydrolysis of uranyl took place. There is no complex found from titration.

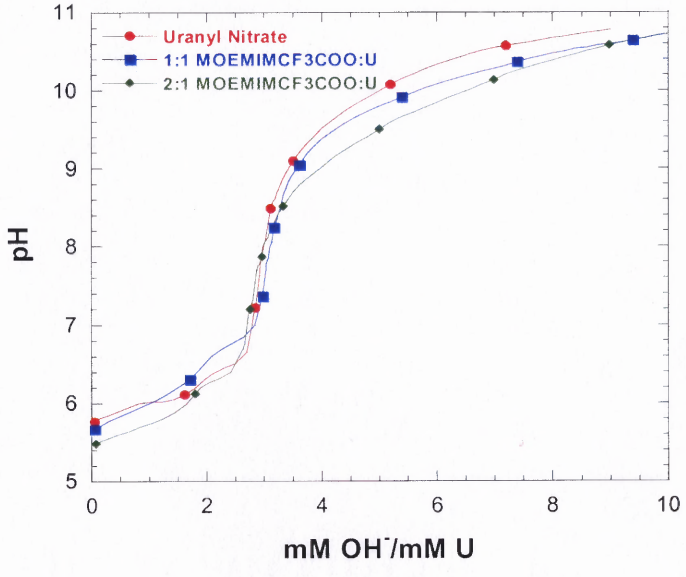

Figure 3.10 Potentiometric titration of [MOEMIM][CF_3COO]:U mixture.

3.3.2.3 UV-vis spectrum.

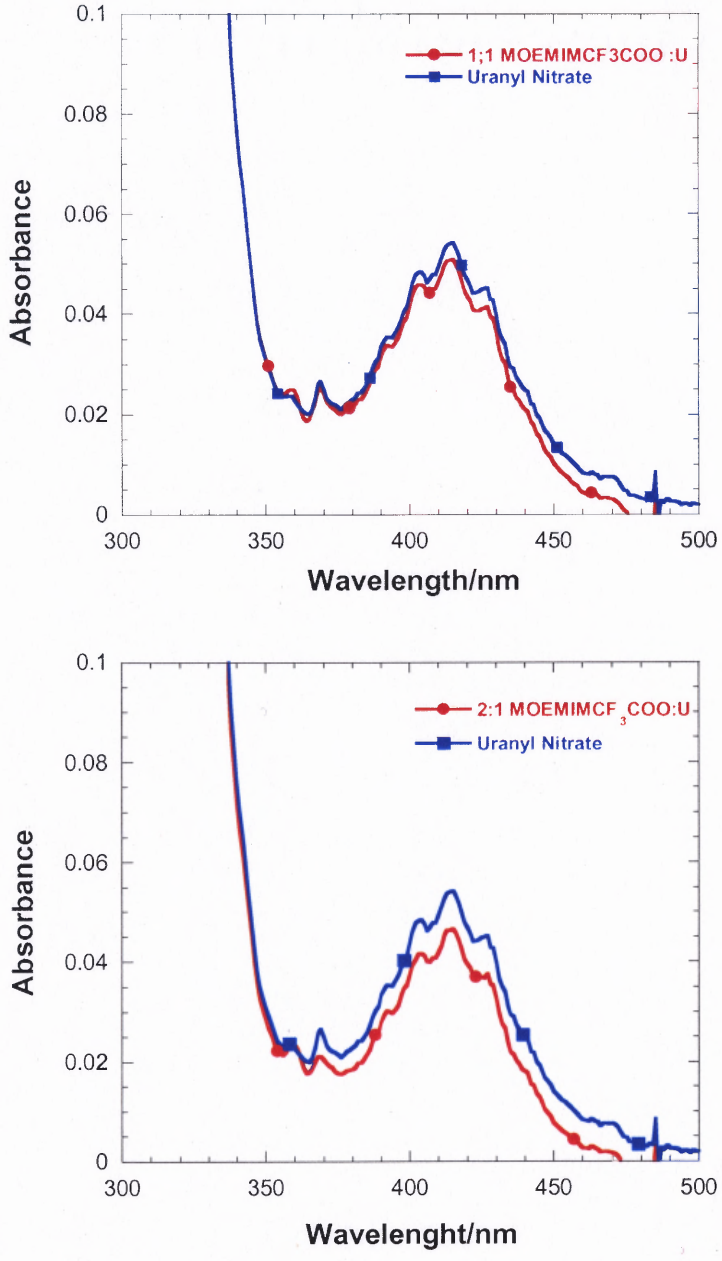

Figure 3.11 UV-vis spectra of [MOEMIM][CF_3COO]:U mixture.

Compared with the spectrum of uranyl nitrate, the absorbance intensity reduces a little bit in both 1:1 and 1:2 mixtures, but the phase and shape are almost the same, indicating the weak interaction between them.

3.3.2.4 MS. Mass spectrum of [MOEMIM][CF_3COO]:U is shown in Figure 3.12. In positive mode, only the cation, $[MOEMIM]^+$ was observed, and no complex was found. However, in negative mode, possible complex molecules were observed at 507(m/e) and 558(m/e), representing $[UO_2(NO_3)_2(CF_3COO)]^-$ and $[UO_2(NO_3)(CF_3COO)_2]^-$, respectively.

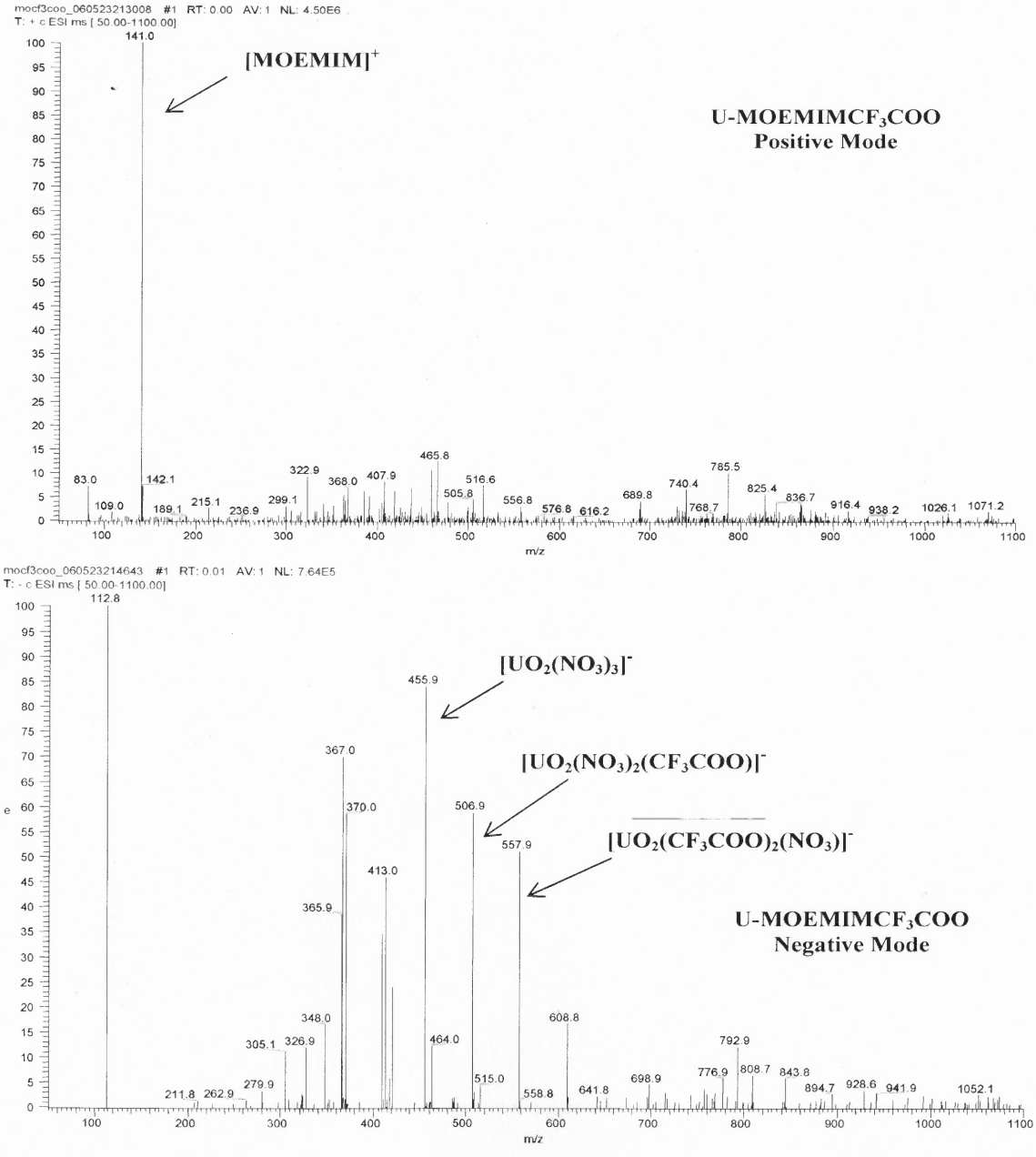

Figure 3.12 Mass Spectra of [MOEMIM][CF_3COO]:U mixture at pH 3.

3.3.2.5 EXAFS . Fourier transform of EXAFS is given in Figure 3.13.

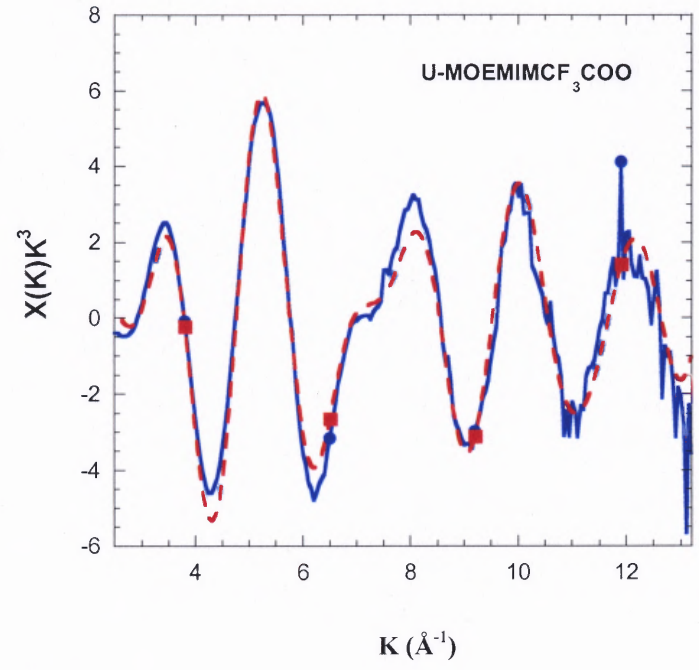

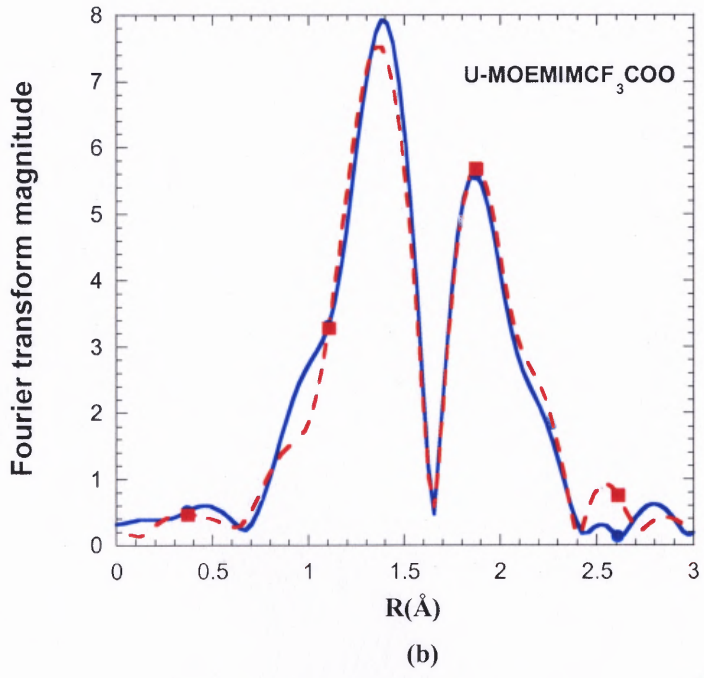

Figure 3.13 EXAFS spectra of U-[MOEMIM][CF3COO] at the U L_{III} edge: (a) k^3-weighted EXAFS spectra (2.5-13.2Å^{-1}); (b) Fourier transform of EXAFS. Experimental data (-); theoretical fit (--).

Comparison of the U and U-IL spectra shows no change, indicating they have similar near-range structures and the interaction between them was weak. The structure data of fitting model was given in Table 3.4.

Table 3.4 EXAFS Structure Parameters for U and [MOEMIM][CF_3COO]:U Mixture.

Sample	Atom type	N	R(Å)	σ^2	R factor
U+[MOEMIM][CH_3COO]	U-Oax*	2	1.76±0.006	0.002	0.015
	U-Oeq	5	2.42±0.0	0.008	

* Axial oxygen fixed at 2.

Two O_{ax} atoms were found at 1.76Å, and 5 O_{eq} at 2.41Å, which is almost the same as uranyl nitrate. No complexation information was provided by EXAFS.

3.3.3 [MOEMIM][PF_6] and Uranium

3.3.3.1 pH change. pH changes are shown in Table 3.5. From this table we can see the pH change in both mixtures is negligible, indicating little to no interaction between them.

Table 3.5 pH Change of [MOEMIM][PF_6]:U Mixture

	[MOEMIM][PF_6] : U		[MOEMIM][PF_6]	U
	1:1	2:1		
0 hr	3.36	3.48	5.79	3.05
24hr	3.33	3.49	5.74	3.06
Difference	0.03	-0.01	0.05	0.01

3.3.3.2 Titration. The titration curves of the three were very similar and their inflection points overlapped. No complexation information could be obtained from the titration.

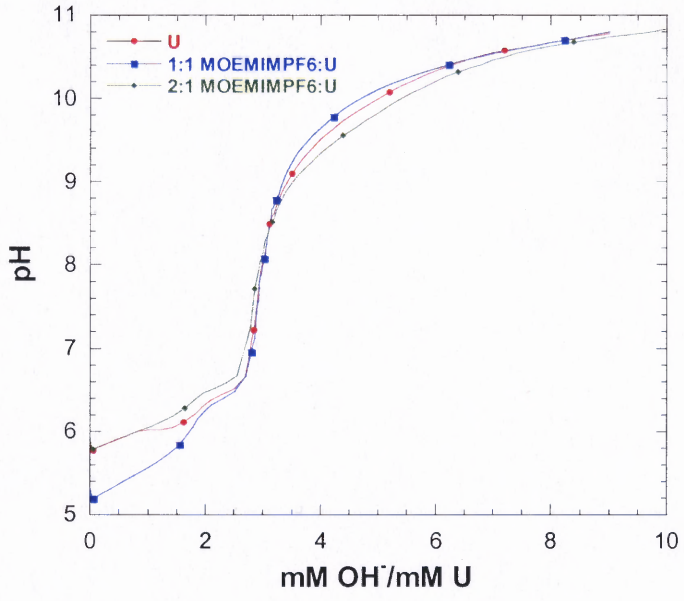

Figure 3.14 Potentiometric titration curve of [MOEMIM][PF_6]:U mixture.

3.3.3.3 UV-vis Spectrometry. The UV-vis spectrum of 1:1 mixture overlapped with the spectrum of uranyl nitrate. Moreover, the spectrum of 2:1 mixture was similar (except for the slightest decrease of intensity). No complexation evidence was found.

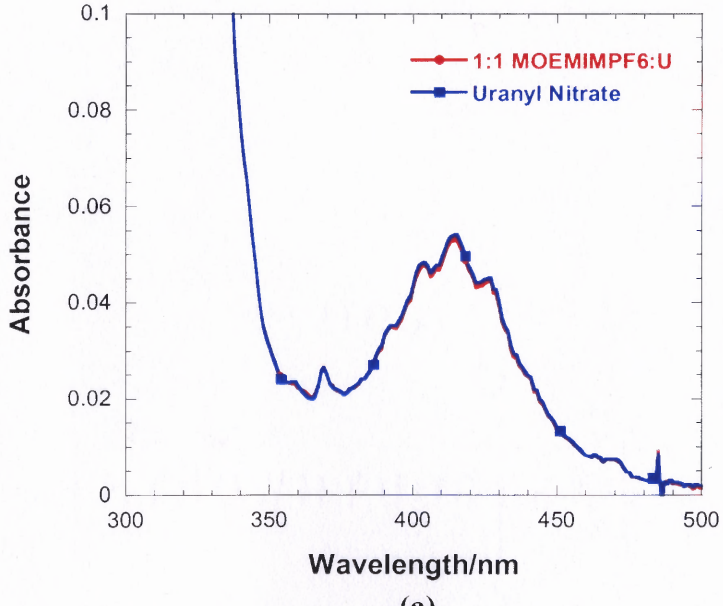

(a)

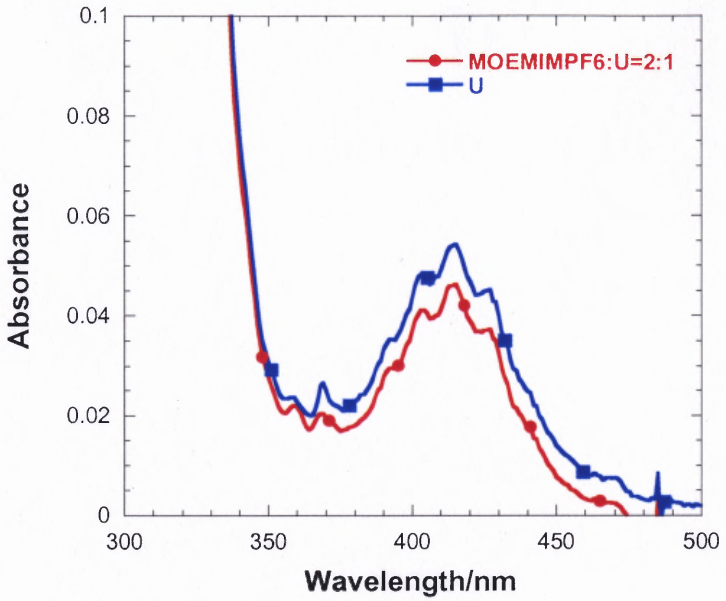

(b)

Figure 3.15 UV-vis spectra of [MOEMIM][PF_6]:U mixture.

3.3.3.4 Mass Spectroscopy. MS was displayed in Figure 3.16. In positive mode, 141(m/e) ([MOEMIM]$^+$) was the base peak. In negative mode, 145(m/e)([PF_6]$^-$) was dominant and another major peaks resulted from the uranyl ions. No uranyl complex associated with PF_6^- was found in either mode.

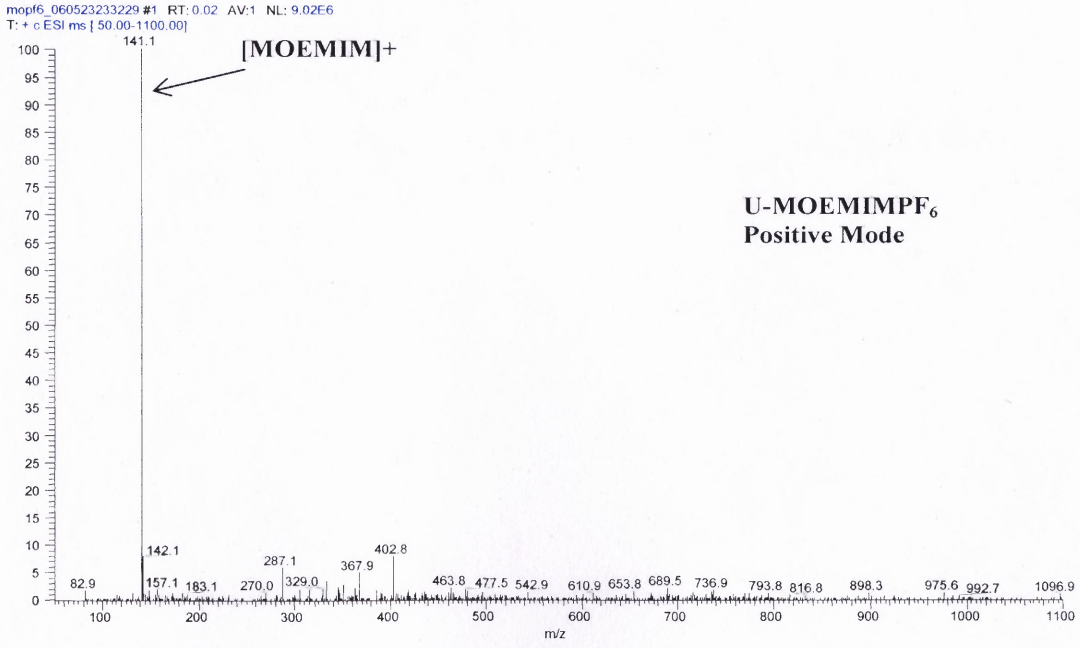

(a)

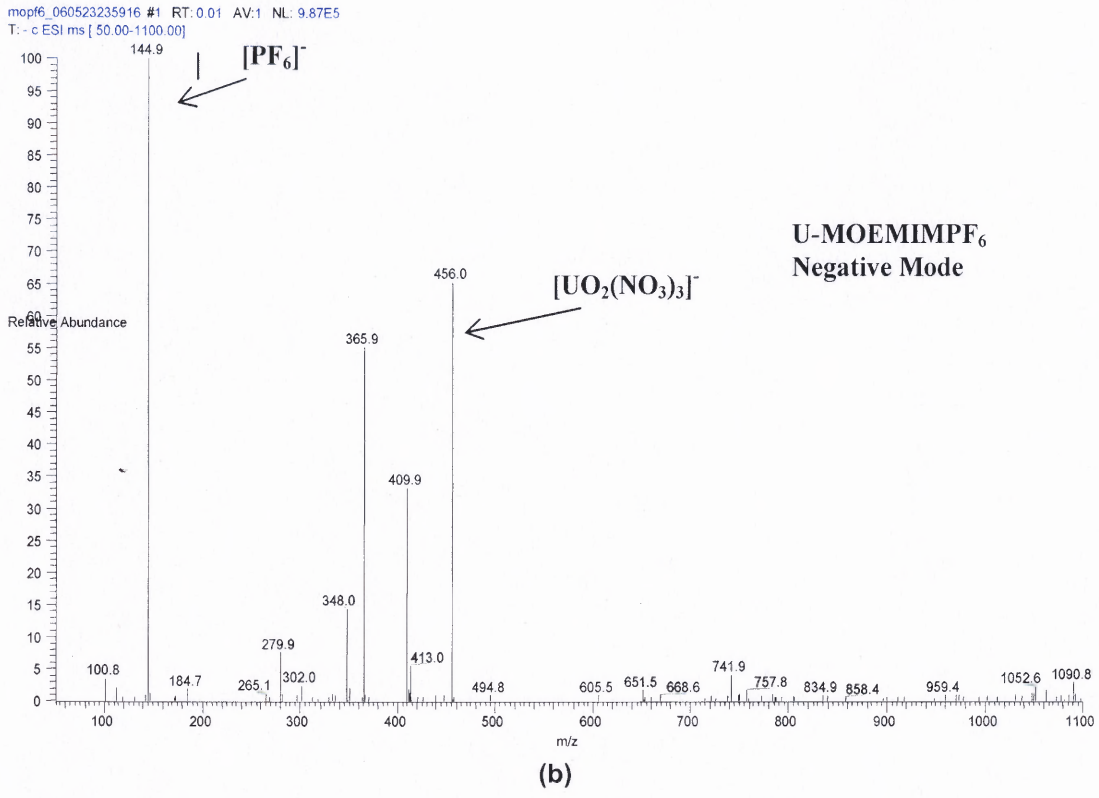

Figure 3.16 Mass spectra of [MOEMIM][PF_6]:U mixture at pH 3.5: (a) positive mode; (b) negative mode.

3.3.3.5 EXAFS.

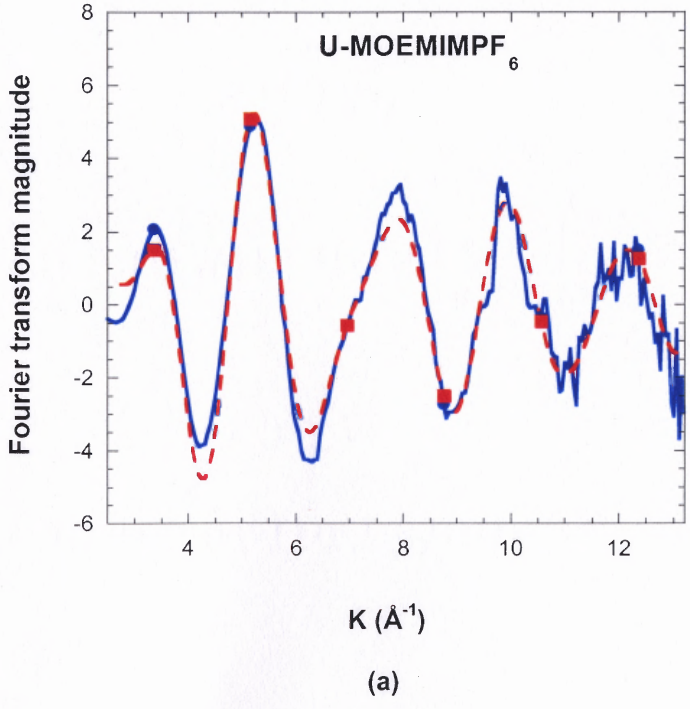

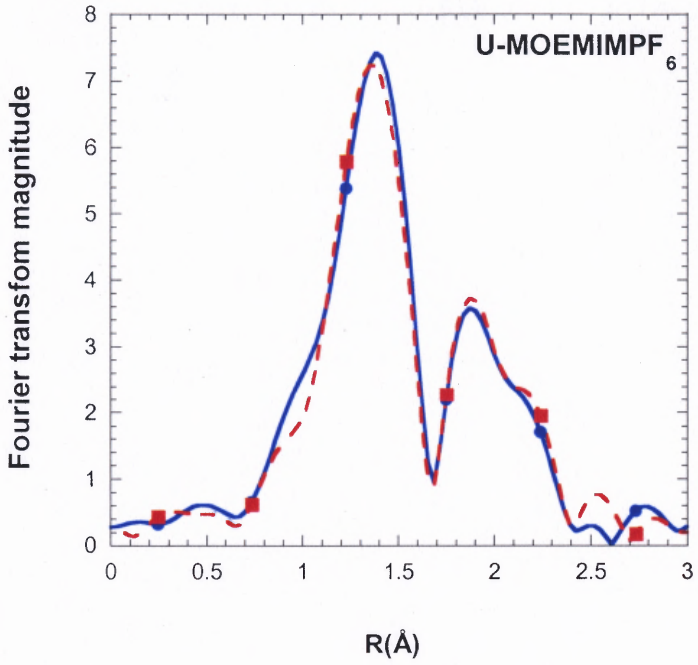

(b)

Figure 3.17 EXAFS spectra of U-[MOEMIM][PF_6] at the U L_{III} edge: (a) k^3-weighted EXAFS spectra (2.5-13.2Å^{-1}); (b) Fourier transform of EXAFS. Experimental data (-); theoretical fit (--).

The EXAFS spectra were displayed in Figure 3.17, and the best fitting model was given in Table 3.6.

Table 3.6 EXAFS Structure Parameters for U and U-[MOEMIM][PF6] Mixture

Sample	Atom type	N	R(Å)	σ2	R factor
U+[MOEMIM][PF6]	U-Oax	2	1.77±0.007	0.003	0.015
	U-Oeq	4	2.45±0.02	0.012	

Attempts to use a fit model with two equatorial shells (U-O and U-F) for this sample did not lead to a coherent fit. Therefore only one equatorial shell (U-O) was used in a fit model. Two axial oxygen atoms were found at 1.77Å, similar to those in U solution. 3 equatorial oxygen atoms were observed at the second shell, with a bond length of 2.45Å. Gaillarde et al.(2005) reported [PF_6]$^-$ interacts with uranyl quite similarly in

strength to water molecules, that is, there is competition of complexing with uranyl. The formation of a complex $UO_2PF_6^+$ was evidenced by TRES but could not be observed by the EXAFS technique, which requires higher uranium and [PF6]⁻concentnrations. In our study, we didn't find the complexation information from the EXAFS data either.

3.3.4 [MOEMIM][OMS] and Uranium

3.3.4.1 pH change. No significant pH change was found in 1:1 mixture after 24 hours, as shown in Table 3.7.

Table 3.7 pH Change of [MOEMIM][OMS]:U Mixture

	[MOEMIM][OMS]-U		[MOEMIM][OMS]	U
	1:1	2:1		
0 hr	3.33	3.52	4.28	3.05
24hr	3.35	3.50	4.34	3.06
Difference	-0.02	0.02	-0.06	0.01

3.3.4.2 Titration. The titration curve was exhibited in Figure 3.18. The three titration curves are very similar. They all have only one inflection point at 3mM OH^-/mM U and no complexation information was found here.

3.3.4.3 UV-vis. UV-vis spectra of both uranyl nitrate and [MOEMIM][OMS]:U were shown in Figure 3.19. Obviously, in both 1:1 and 2:1 mixtures, they all look very similar. No complexation information was found here.

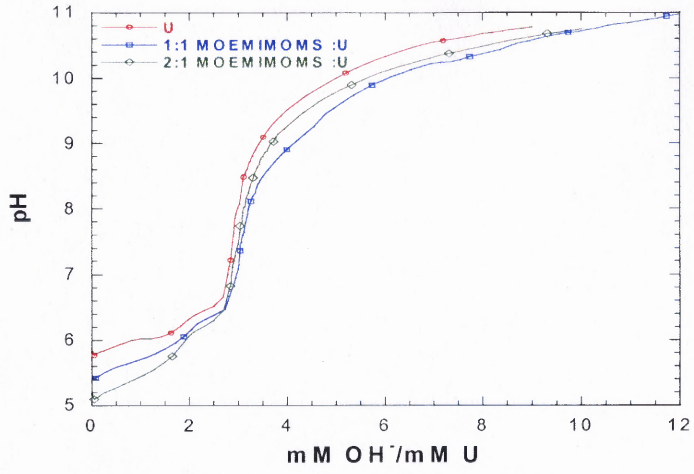

Figure 3.18 Potentiometric titration curve of [MOEMIM][OMS]-U mixture.

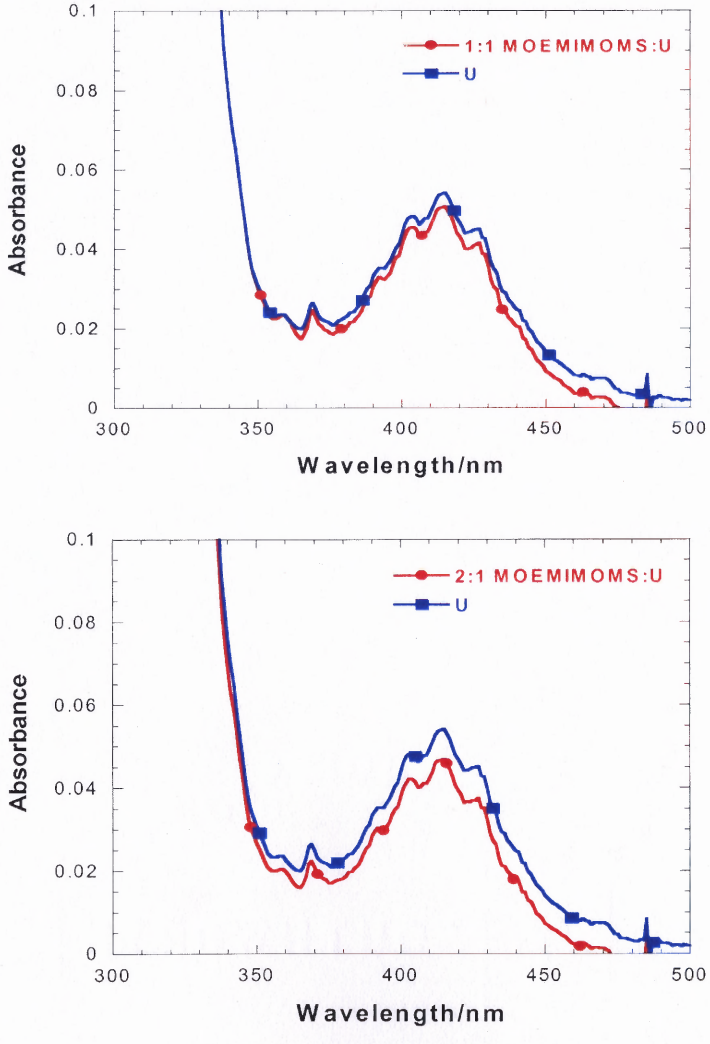

Figure 3.19 UV-vis spectra of [MOEMIM][OMS]-U mixture.

3.3.4.4 Mass Spectroscopy.

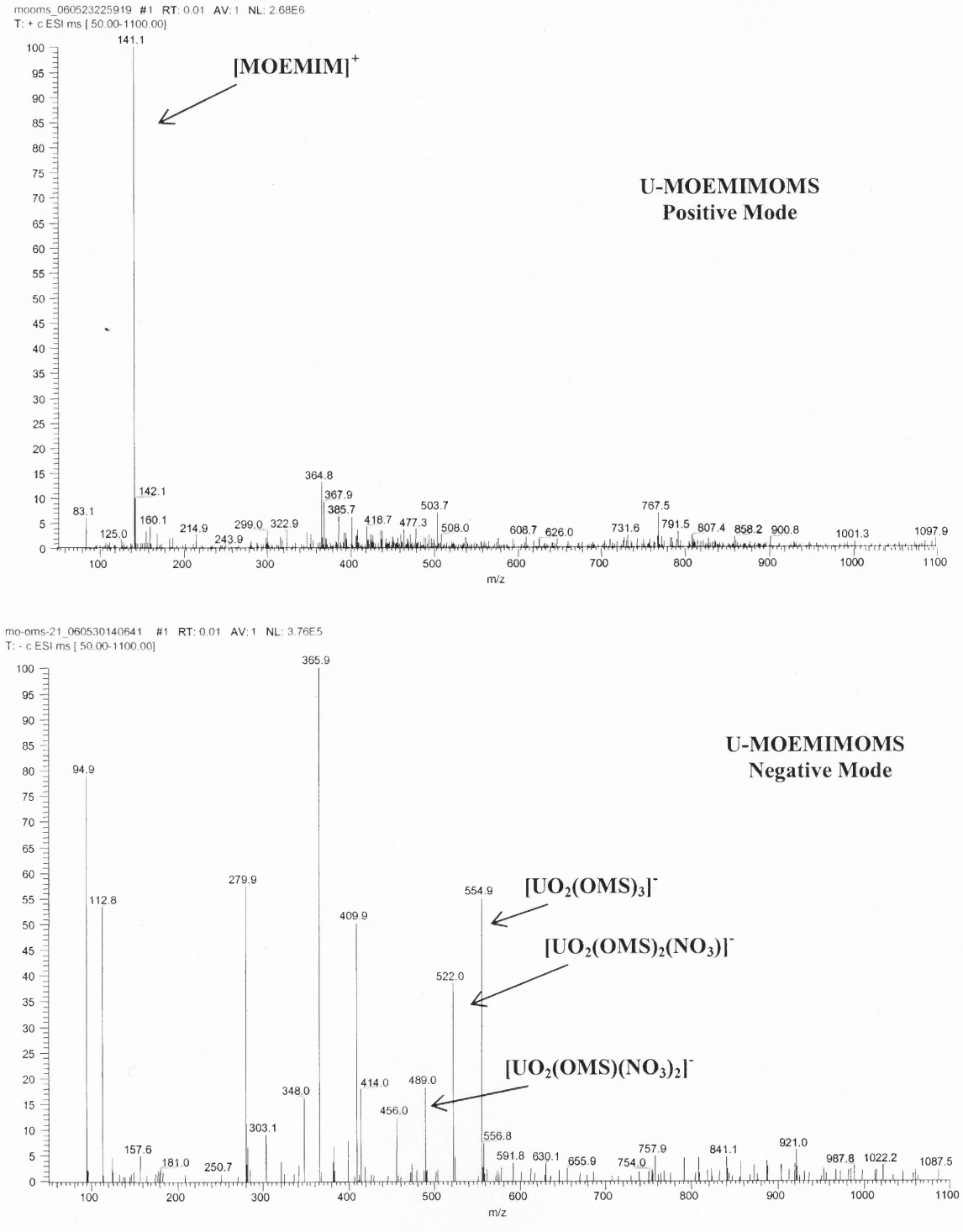

Figure 3.20 Mass spectra of [MOEMIM][OMS]:U mixture at pH 3.5.

No complex was found in positive mode. However, in negative mode, three complex molecules at 555(m/e), 522(m/e) and 489(m/e) were found, corresponding to $[UO_2(OMS)_3]^-$, $[UO_2(OMS)_2(NO_3)]^-$ and $[UO_2(OMS)(NO_3)_2]^-$, respectively.

3.3.4.5 EXAFS EXAFS spectra were shown in Figure 3.21, and the structure parameters of a fitting model are given in Table 3.8.

Table 3.8 EXAFS Structure Parameters for [MOEMIM][OMS]:U Mixture

Sample	Atom type	N	R(Å)	σ2	R factor
U+[MOEMIM][OMS]	U-Oax	2	1.76±0.005	0.003	0.007
	U-Oeq	4	2.42±0.011	0.006	

The Fitting model discloses that two O_{ax} atoms were found at 1.76Å, and 4 Oeq at 2.42Å. These structure data are similar to those of uranyl nitrate, except that there are only about 4 O_{eq} in the second shell.

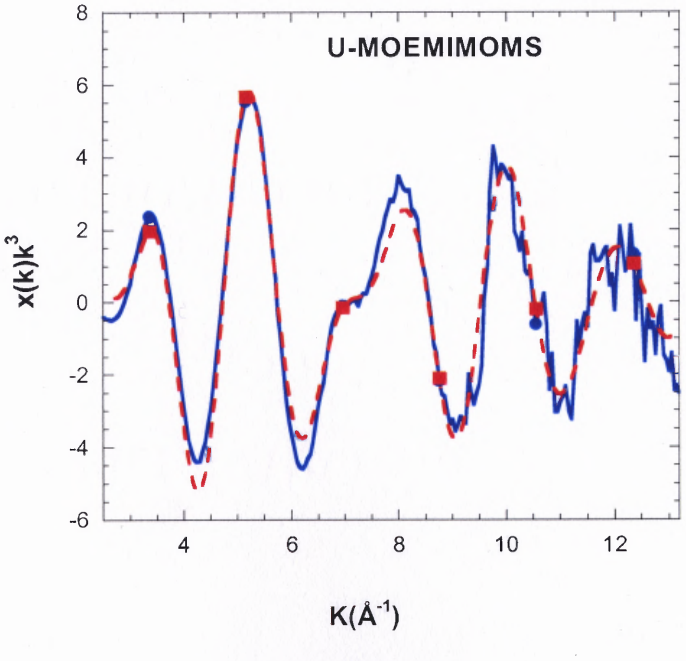

(a)

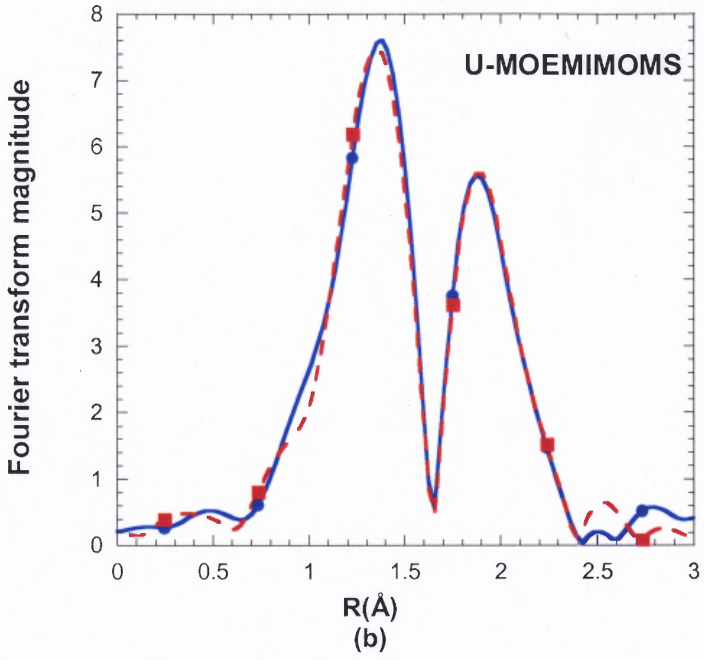

Figure 3.21 EXAFS spectra of U-[MOEMIM][OMS] at the U L_{III} edge: (a) k^3-weighted EXAFS spectra (2.5-13.2Å^{-1}); (b) Fourier transform of EXAFS. Experimental data (-); theoretical fit (--).

3.3.5 [MOEMIM][Tf_2N] and Uranium

3.3.5.1 pH Change. pH changes in both 1:1 and 2:1 mixtures are negligible.

Table 3.9 pH Change of [MOEMIM][Tf_2N]:U Mixture

	[MOEMIM][Tf_2N]-U		U	MOEMIMTf_2N
	1:1	2:1		
0 hr	3.41	3.46	3.05	5.89
24hr	3.32	3.32	3.06	5.72
Difference	0.09	0.14	0.01	0.17

3.3.5.2 Titration.

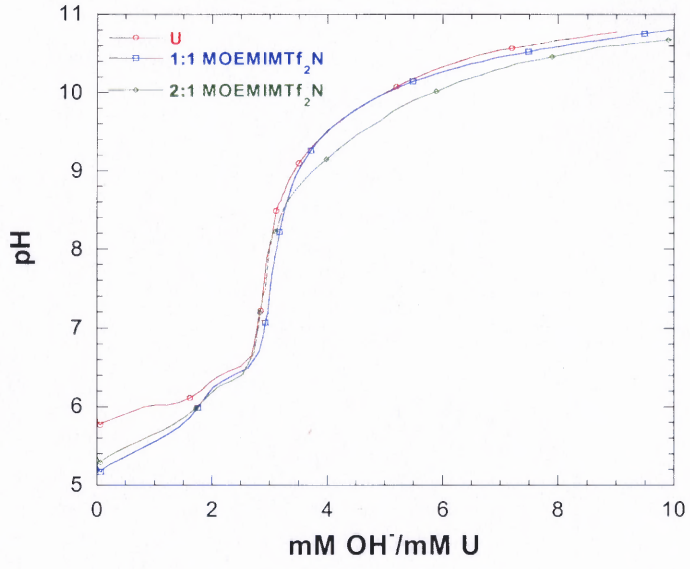

Figure 3.22 Potentiometric titration of [MOEMIM][Tf_2N]:U mixture.

Titration curves of the three are almost the same and all of them have the same inflection point at 3mM OH^-/mM U. No complex information was found here.

3.3.5.3 UV-vis. Similarity of UV-vis spectra indicates no interaction or weak interaction happens between them.

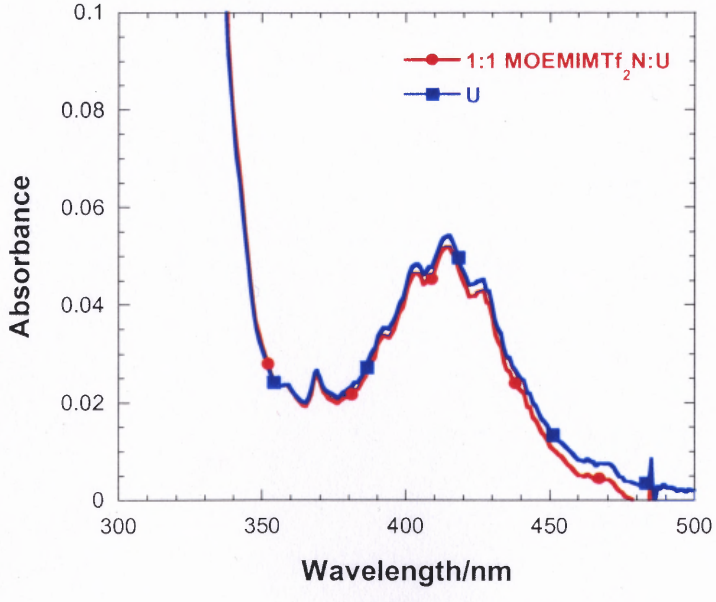

(a)

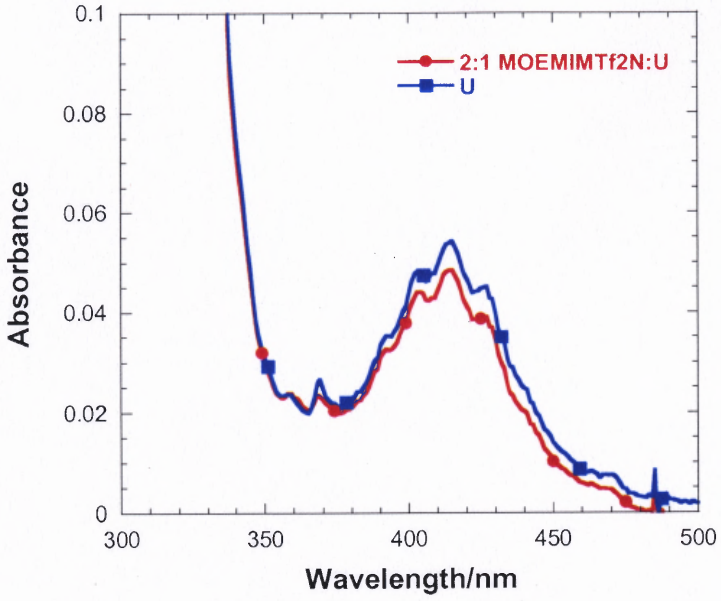

(b)

Figure 3.23 UV-vis spectra of [MOEMIM][Tf_2N]:U mixture: (a) 1:1; (b) 2:1.

3.3.5.4 Mass Spectroscopy.

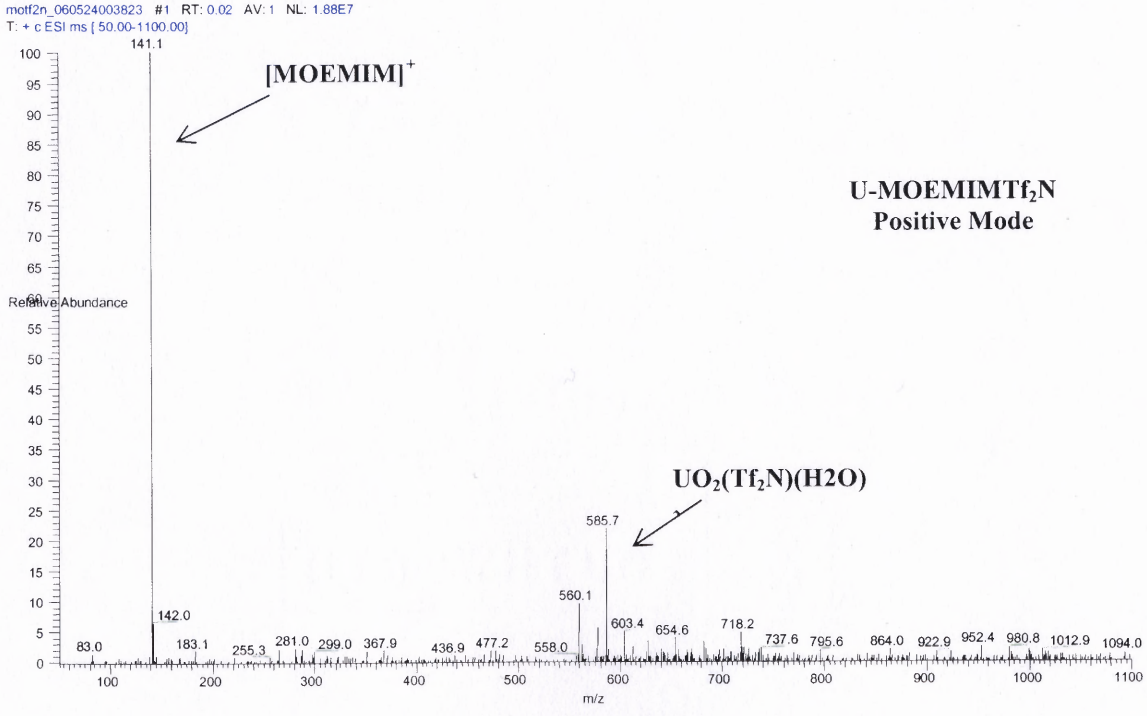

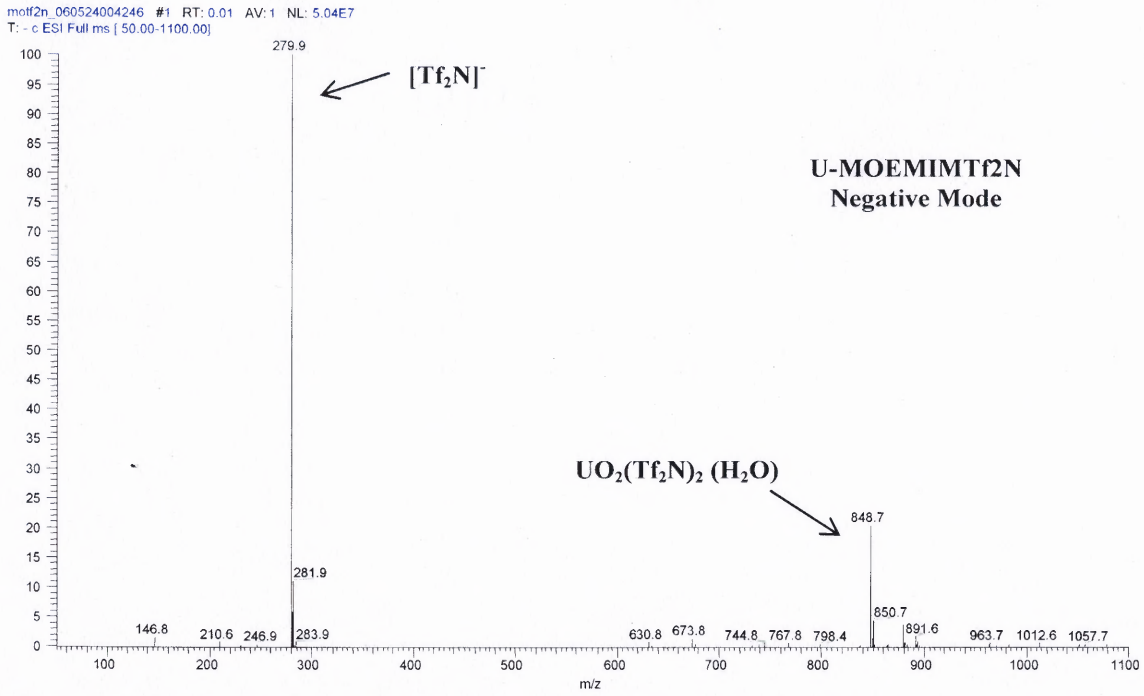

Figure 3.24 Mass spectra of [MOEMIM][Tf_2N]:U mixture at pH 3.

In positive mode, 141 represents the $[MOEMIM]^+$, and 585 could be $[UO_2(Tf_2N)(H_2O)_2]^+$. In negative mode, 280 represents the $[Tf_2N]^-$, and 848 could result from $UO_2(Tf_2N)_2(H_2O)$.

3.3.5.5 EXAFS.

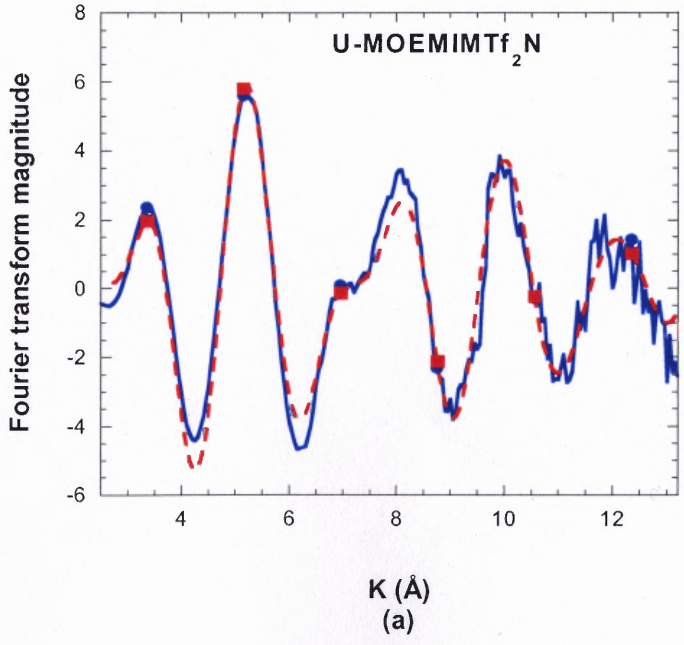

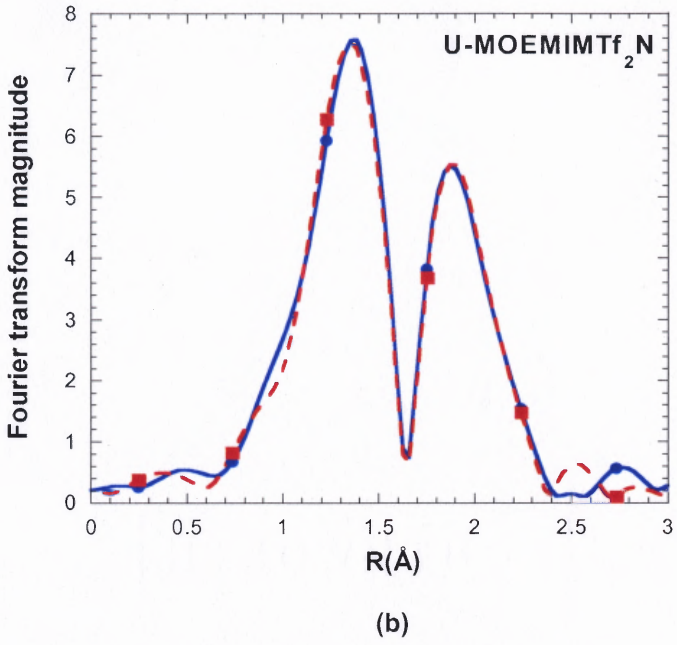

(b)

Figure 3.25 EXAFS spectra of U-[MOEMIM][Tf_2N] at the U L_{III} edge: (a) k^3-weighted EXAFS spectra (2.5-13.2$Å^{-1}$); (b) Fourier transform of EXAFS. Experimental data (-); theoretical fit (--).

Figure 3.25 displays the EXAFS spectra of U-[MOEMIM][Tf_2N]. The structure data of the best fitting model was given in Table 3.10.

Tabel 3.10 EXAFS Structure Parameters of U and U: [MOEMIM][Tf_2N]

Sample	Atom type	N	R(Å)	σ^2	R factor
U+[MOEMIM][Tf_2N]	U-O_{ax}	2	1.76±0.006	0.003	0.008
	U-O_{eq}	4	2.42±0.013	0.006	

U and [MOEMIM][Tf_2N]:U have very similar structure data, except that the former has 5 O_{eq} while the latter contains 4 O_{eq}. In Gaillard's study, they found that Tf_2N^- can not complex with uranyl.

3.3.6 [MECOOMIM][CH_3COO] and Uranium

3.3.6.1 pH Change. A significant pH change was found in both the 1:1 and 2:1 mixtures, indicating a proton released during the interaction between them.

Table 3.11 pH Change of [MECOOMIM][CH_3COO]:U Mixture

	[MECOOMIM][AC] and U		U	[MECOOMIM][AC]
	1:1	2:1		
0 hr	3.06	3.03	3.05	4.78
24hr	2.38	2.19	3.06	4.77
Difference	0.68	0.86	0.01	0.01

3.3.6.2 Titration. The inflection point of U, the 1:1mixture and 1:2 mixtures are 3mM OH-/ mM U, 3.28mM OH-/ mM U and 3.56mM OH-/ mM U, respectively. The shift of inflection points to the right indicates the proton was released in the mixtures, as a result of the interaction of [MECOOMIM][CH_3COO]:U.

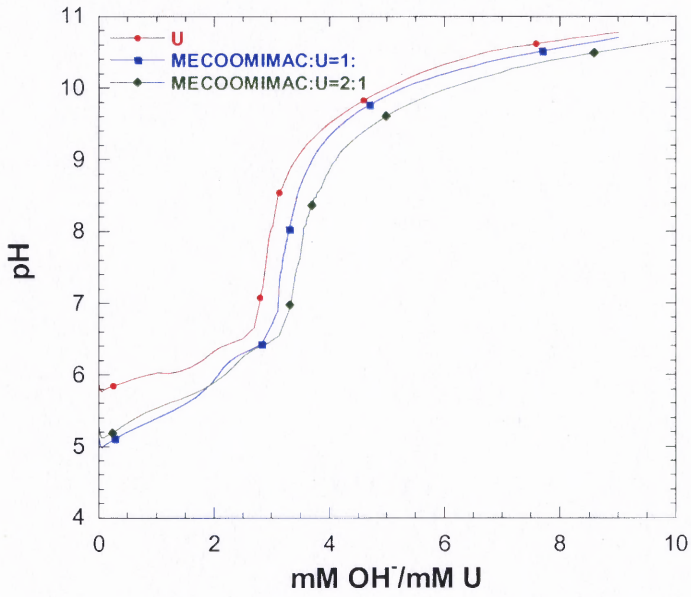

Figure 3.26 Potentiometric titration of [MECOOMIM][CH_3COO]:U mixture.

3.3.6.3 UV-vis. UV-vis spectra are given in Figure 3.27. Compared with the U standard, the absorption intensity decreased a little bit in both 1:1 and 2:1 mixture, but no phase shift was observed. No conclusive complex information can be obtained here.

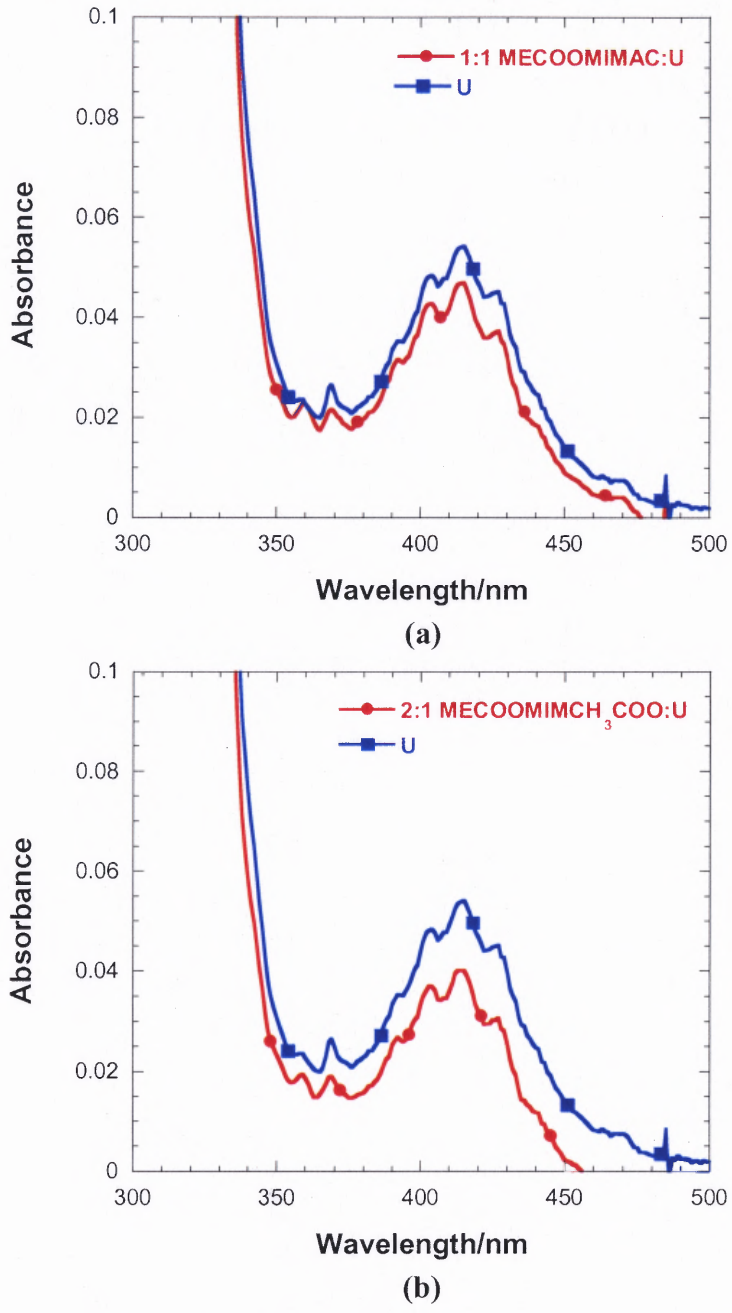

Figure 3.27 UV-vis spectroscopy of [MECOOMIM][CH_3COO]:U mixture.

3.3.6.4 Mass Spectroscopy. Peak 169 in positive mode represents the $[MECOOMIM]^+$. Another peak 490 corresponded to $[(UO_2)(MECOOMIM)(OH)_2(H_2O)]^-$. It is noteworthy that, there is an ester group in the cation side chain, and that the oxygen in carbonyl

contains lonely pair electrons; furthermore, this has the affinity to uranyl and capability to form the complex.

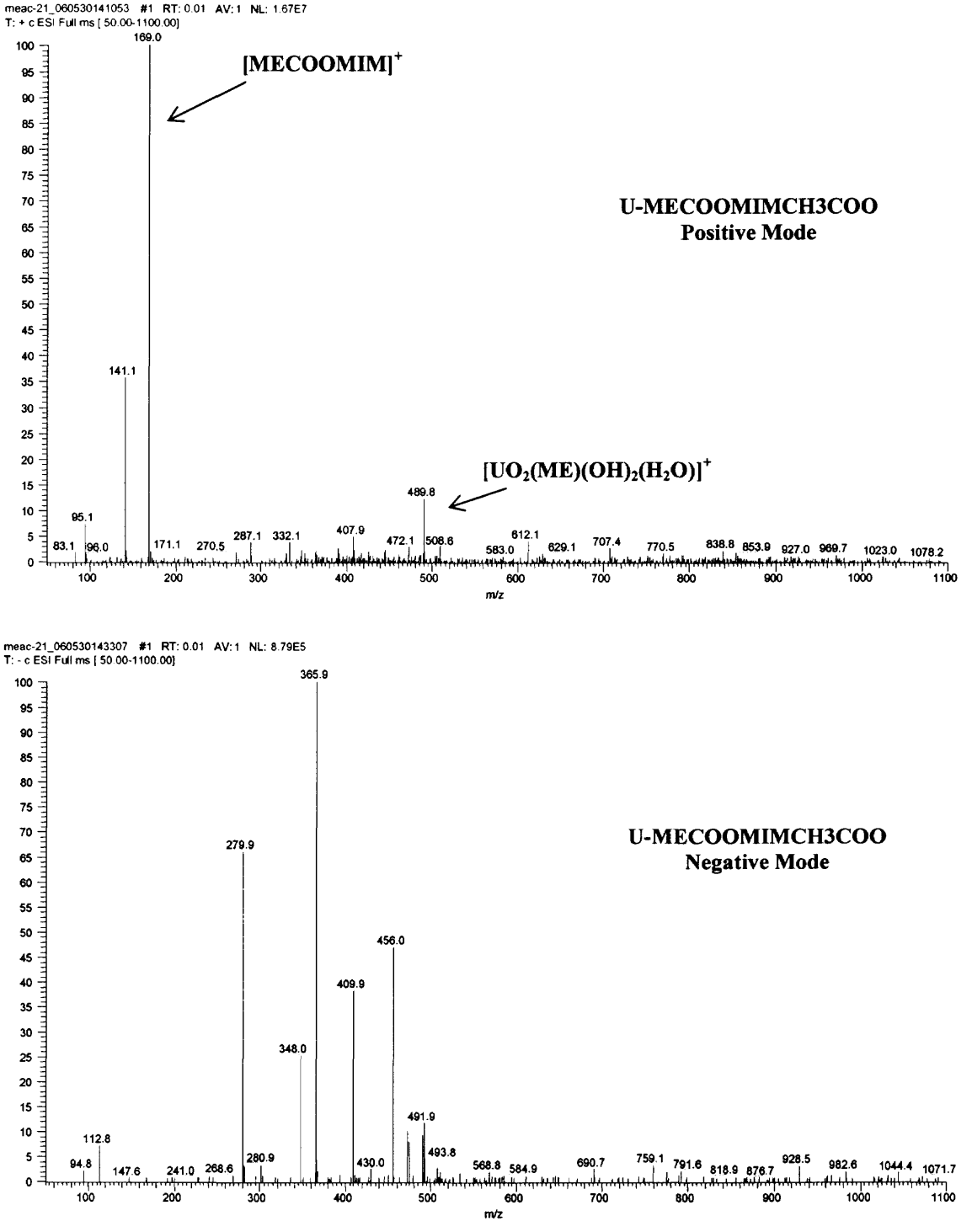

Figure 3.28 Mass spectra of [MECOOMIM][CH_3COO]:U mixture at pH 2.3.

3.3.6.5 EXAFS. EXAFS spectra are exhibited in Figure 3.34, and the structure data of the fitting model is given in Table 3.14.

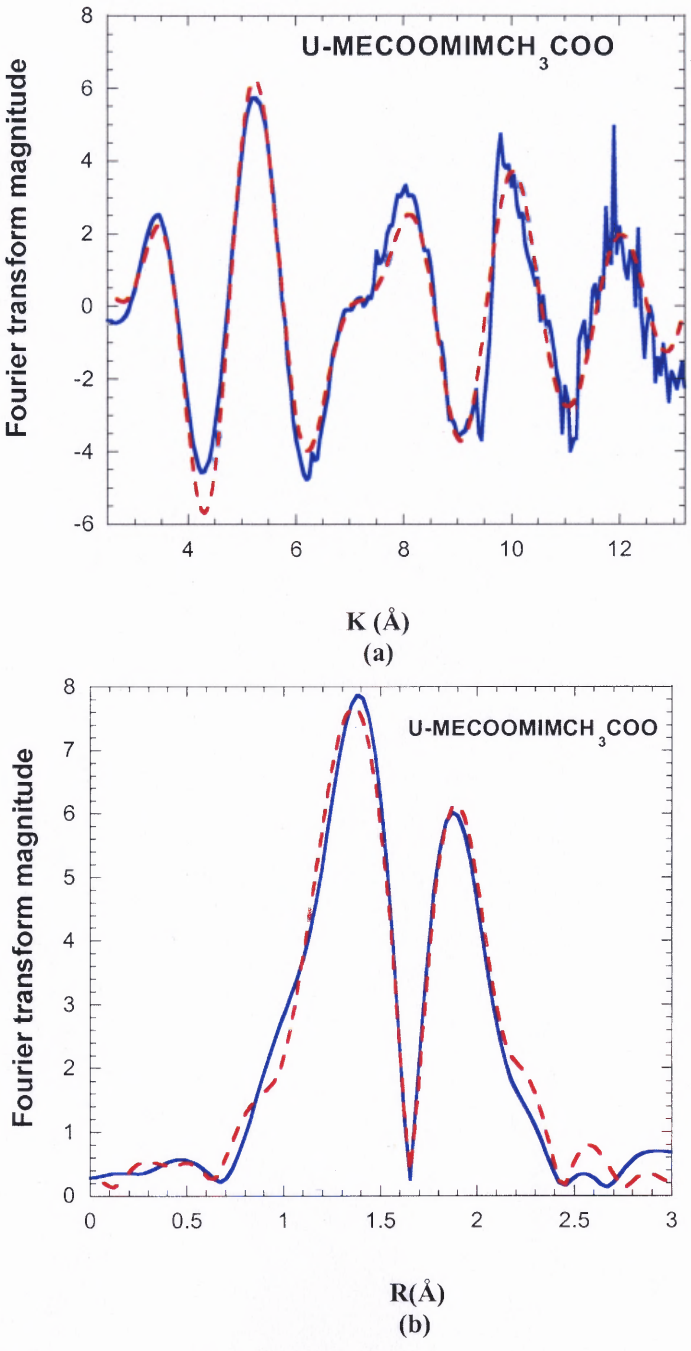

Figure 3.29 EXAFS spectra of U-[MOEMIM][CH3COO] at the U L_{III} edge: (a) k^3-weighted EXAFS spectra (2.5-13.2Å^{-1}); (b) Fourier transform of EXAFS. Experimental data (-); theoretical fit (--).

Table 3.12 EXAFS Structure Parameters of U and U: [MOEMIM][CH_3COO]

Sample	Atom type	N	R(Å)	σ^2	R factor
U+[MOEMIM][CH3COO]	U-Oax	2	1.76±0.009	0.003	0.013
	U-Oeq	4	2.43±0.009	0.007	

The best fitting model has 2 axial oxygen atoms at 1.76Å, and 4 equatorial oxygen atoms at 2.43Å, similar to those of uranyl nitrate.

3.4 Summary

Experimental results are summarized in Table 3.13. Positive (+) means there is complexation between U and the ILs, and negative (-) represents no complexation found between them.

Table 3.13 Summary of Determination of Complexation by Different Methods

	pH					
	1:1	2:1	UV-vis	Titration	MS	EXAFS
[MOEMIM][CF3COO]	-	+	-	-	+	-
[MOEMIM][BF4]	**+**	**+**	**+**	**+**	**+**	**+**
[MOEMIM][PF6]	-	-	-	-	-	-
[MOEMIM][OMS]	-	+	-	-	+	-
[MOEMIM][Tf2N]	-	-	-	-	+	-
MECOOMIMAC	+	+	-	+	+	-

Among all of the ILs studied here, only [MOEMIM][BF_4] shows positive to all different analytical methods, indicating complexation associated with uranyl. Other ILs show positive to some methods, but negative to the rest, hence there is no conclusion that can be drawn. However, there is no one method that can single-handedly determine complexation evidence.

CHAPTER 4

EFFECTS OF IONIC LIQUIDS ON BIOREDUCTION OF U(VI) TO U(IV) BY *CLOSTRIDIUM* SP.

4.1 Introduction

U (VI) is highly soluble in water while U (IV) is insoluble in water. However, soluble U (VI) can be reduced by microorganism to U (IV) and can precipitate out of an aqueous phase. Several microorganisms have proven to be able to convert U (VI) to U (IV). These bacteria include the Fe (III)-reducing *Geobacter* sp. and *Shewanella* sp. (Lloyd, et al., 2002), the Fe (III)- and sulfate-reducing *Desulfotomaculum* sp. (Pietzsch, et al., 1999), the sulfate-reducing *Desulfovibrio* sp. (Yong, et al., 2002), and the fermentative anaerobic *Clostridium* sp (Francis, et al., 1994).

Both organic and inorganic ligands can form a complex with uranium, thus increasing their solubility and leaching capability. In addition, different ligands play an important role in the biotransformation of uranium. A study by Robinson et al. (1998) disclosed that, among the complexes of uranium with acetate, oxalate or citrate, the reduction rate of the acetate-complexed uranium was the fastest while the reduction rate of the citrate-complexed uranium was the slowest. Francis et al. (2000) also found that the bidentate complex of citric acid and uranium was much less bioreducible than monodentate complex. In addition, Tucker et al. (1998) demonstrated an elevated NO_3^- and/or SO_4^{2-} concentration can decrease the bioreduction of U (VI) by *Desulfovirio*. Markich et al. (2002) investigated the effect of uranium complex with various inorganic ligands and humic substances on the bioreduction of uranium. Reduced bioreduction was observed in this experiment.

After studying the physic-chemical interactions between uranium and ILs, we were curious about how bioreduction could be affected by the interaction of U-ILs. The results of our experiments are reported here.

4.2 Materials and Methods

4.2.1 Chemicals

Ionic liquids used in this study include [MOEMIM][BF_4], [MOEMIM][CF_3COO], [MOEMIM][OMS], [MOEMIM][PF_6] and [MOEMIM][CH_3COO]. The uranium used here is a uranyl nitrate solution.

4.2.2 Bacterium

Clostridium sp. is an anaerobic fermentative bacterium that is gram positive stained and rod-shaped. This bacterium is able to reduce Fe (III) to Fe(II), Mn(IV) to Mn(II), Tc(VII) to Tc(IV), and U(VI) to U(IV) (Francis, et al., 1994; 1998; 2002).

A mineral salts medium composed of glucose (5.0g), glycerol phosphate (0.3g), $MgSO_4.7H_2O$ (0.2g), $FeSO_4.7H_2O$ (2.8mg), $CaCl_2$ (0.5g), Peptone (0.1g), and yeast extract (0.1g) was used to culture *Clostridium* sp. All the ingredients were dissolved in 1000 ml of distilled water, and the pH was adjusted to 6.5. The medium was pre-reduced by the process of boiling and purging with N_2 gas for 15min to remove dissolved oxygen. During the purging process the mixture was allowed to cool down. Once complete, it was moved to a glove box to dispense. A 40ml medium was dispensed into a 60ml serum bottle. The bottle was then sealed by a butyl rubber stopper with an aluminum cap and autoclaved.

4.2.3 Analysis of U(VI) and U(IV)

Determination of U (IV) in solution U (IV) in solution is measured by the colorimetric method based on the reaction below.

$$U^{4+} + 2Fe^{3+} \rightleftharpoons U^{6+} + 2Fe^{2+}$$
$$Fe^{2+} + o-phenanthroline \rightarrow red\ color$$

The ferric ion can re-oxidize U(IV), reduced by *clostridium* sp., to U(VI), and produce a ferrous ion. A ferrous ion forms a complex with o-phenanthroline to give a red color solution. The concentration of ferrous complex was determined by UV spectrometer at 510 nm. A calibration curve can be obtained by ferrous standards with different concentrations. The uranium concentration was half of the concentration of ferrous complex.

Preparation of color development mixture 14ml of 1 mM $FeCl_3$ solution containing concentrated HCl (6.4 ml/liter mixture) was mixed with 3 ml of 10 mM o-phenanthroline and 3 ml of 1M acetate buffer (pH 5).

Sample measurement Sample preparation was carried out in a glove box. An aliquot of 0.25 ml filtered sample was added to the cell containing 0.25 ml of de-oxided, de-ionized water and 0.5ml of color development mixture. It was placed in a dark chamber for 2 hours for color development. Subsequently, the UV-vis absorbance was measured at 510nm. Standards containing 0.01, 0.025, 0.05 and 0.07 mM ferrous ion were used to prepare a calibration curve. The culture solution without uranium was utilized to eliminate any background ferrous ion in the medium and/or any ferrous ion released by the metabolism of bacteria.

4.2.4 Determination of Total U in solution

After U(IV) was determined, an aliquot of this sample was taken and diluted. The total U(VI) in solution (after the U(IV) was re-oxided to U(VI))was then measured by KPA (Kinetic Phosphorescence Analyzer). The difference between the total U (VI) determined by KPA, and the U (IV) measured by colorimetric method, yields the un-reduced U (VI).

4.2.5 Determination of U(IV) and Total U in precipitate

A 40 ml sample was centrifuged at 10,000 rpm for 20min and washed three times with 5 ml of pre-reduced 20mM KCl. 10 ml of 5mM citric acid was then added to extract both U (IV) and U(VI). The sample was kept in darkness to avoid the photo degradation of the citric acid. Both U (IV) and U(VI) were determined by the methods described above.

4.2.6 Experiment Methods

Effect of Different ILs on Bioreduction A certain amount of uranyl nitrate solution and ILs were added to a cell and diluted with pre-reduced DI water to 3ml. The mixture was kept overnight and allowed to reach equilibrium. It was then added to an 18-hour-old *Clostridium* sp. culture, giving a final concentration of 0.235mM for Uranium and 10mM for the ILs. Two sets for each IL were prepared: 1) for kinetic study and 2) for a study of the mass balance. For the kinetic study, an aliquot was withdrawn periodically for up to 42 hours. The sample was filtered with a 0.45μm membrane and the concentrations of U (IV) and U(VI) in solution were determined. For the mass balance study, however, the other set of sample was kept intact for 48 hours. An aliquot was then taken from the solution to determine the U(IV) and U(VI) concentrations. The remains

were centrifuged and washed three times with 20mM KCl. Citric acid was added to extract all the uranium in the precipitate in order to determine the concentrations of reduced U(IV) and unreduced U(VI) therein.

Effect of Different Concentration of [MOEMIM][BF4] on Bioreduction Five different concentrations of [MOEMIM][BF_4] (0mM, 1mM, 5mM, 10mM and 20mM) were tested to determine the best in bioreduction efficiency. Two sets were prepared: one for kinetic study and the other for a mass balance calculation. The concentrations of both U(IV) and U(VI) were measured by the method described above.

4.3 Results and Discussion

4.3.1 Effects of Various ILs on U Bioreduction

4.3.1.1 Kinetic Study. A Kinetic study conducted for 24 hours is shown in the Figure 1. The original U(VI) concentration was 0.235mM and ILs concentration was 10mM. In a BC1 medium containing only uranium nitrate and no bacteria, the uranium precipitated out of the solution quickly, due to the formation of uranium phosphate and a hydroxyl at pH of 6.5. As shown in Figure 4.1, in all cases except for [MOEMIM][BF_4], the U(VI) in solution decreased very quickly for the first 4 hours (from 0.235Mm to about 0.05mM), and then continued to drop down gradually to below 0.01mM. Comparatively, the concentration of U(IV) in solution increased rapidly for the first 6 hours (from 0 up to 0.05mM), and then decreased gradually. It is noteworthy that in the presence of [MOEMIM][BF_4], bioreduction showed distinctive differences from the samples: 1) the U(VI) in solution did not decrease as much compared with other ILs. After 42 hours, about 0.115mM U(VI) was still present in the solution; 2) there was a higher

concentration of U(IV) in the solution. After 42 hours, it reached about 0.7mM, which was 5 times more than that in other ILs. (Figure 1(b)).

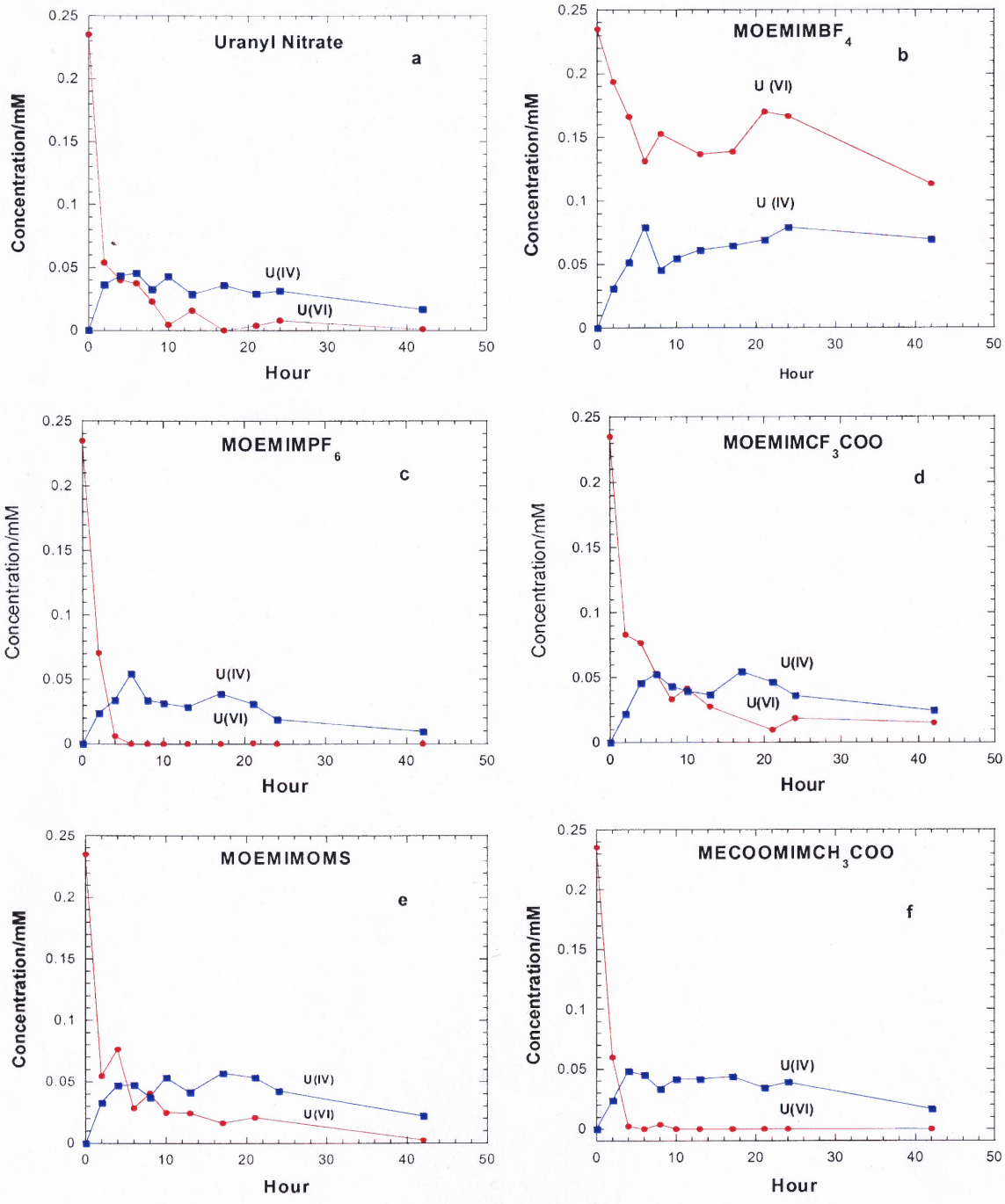

Figure 4.1. Concentrations of U(VI) and U(IV) in various ILs solutions: (a) Control, (b) [MOEMIM][BF_4], (c) [MOEMIM][PF_6], (d)[MOEMIM][CF_3COO], (e) [MOEMIM][OMS], (f) [MECOOMIM][CH_3COO].

In addition, we observed that, even after 72 hours, the solution with [MOEMIM][BF_4] was still cloudy, indicating most of the bacteria suspending in the solution, while the solutions with other ILs were clear and most of the bacteria precipitated out at the bottom.

As discussed in chapter 3, [MOEMIM][BF_4] can form a strong complex with uranium thus enhancing the solubility of both U(VI) and U(IV) in an aqueous phase. As a result, more uranium is present in the solution. However, other ILs can only form weak complexes with uranium and have no effect on its solubility.

4.3.1.2 Mass Balance of U Speciation in Presence of Various ILs.

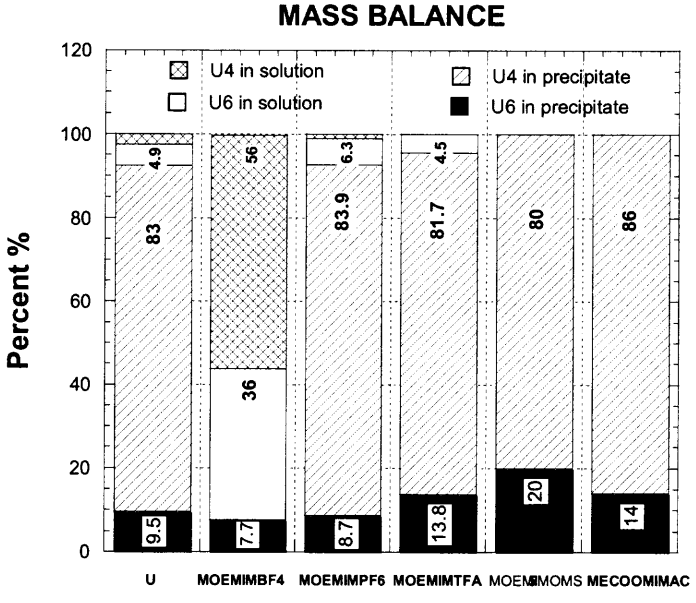

Figure 4.2 Mass Balance of U in different ILs after Reduction.

The U(IV) and U(VI) concentrations in both solution and precipitation were determined and the percentage for each was calculated. Figure 4.2 displays the distribution of uranium speciation in the presence of various ILs. Based on the data, we found that: 1) U(IV) in precipitate predominated, except in presence of the

[MOEMIM][BF_4], accounting for more than 80% of total U; 2) U(VI) made up the second major part of the precipitate (from 9% to 20%); (3) there was little of either U(VI) or U(IV) present in the solution except in the presence of [MOEMIM][BF_4]; 4) over 92% of the total U (36% from U(VI) and 56% from U(IV)) was in the aqueous phase in the presence of [MOEMIM][BF_4], and no U (IV) was observed in precipitate.

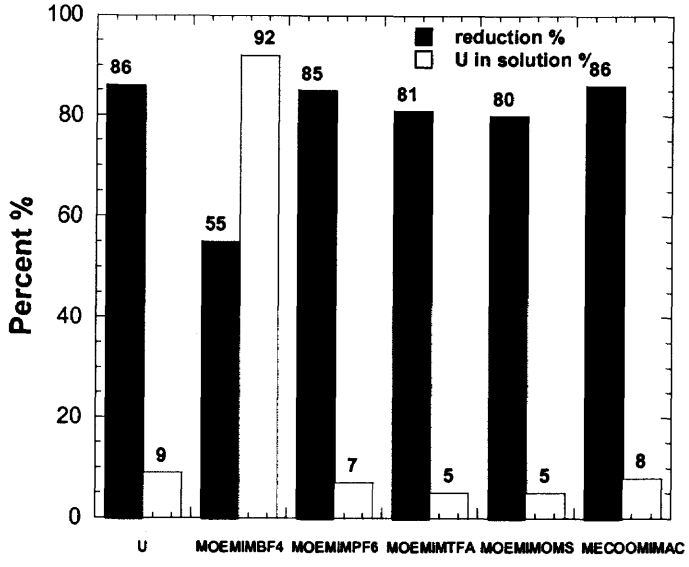

Figure 4.3 Percentage of U reduction and U in solution in presence of various ILs.

The percentage of bioreduction and total U in solution were calculated (Figure 4.3). As for bioreduction, the addition of 10mM of any ILs other than [MOEMIM][BF_4] bore no effect on bioreduction efficiency. For example, U was reduced 86% in the absence of any IL, while 85% with [MOEMIM][PF_6], 81% with [MOEMIM][CF_3COO], and 80% with [MOEMIM][OMS]. However, in the presence of 10mM [MOEMIM][BF_4], the bioreduction was inhibited and dropped to about 55%. This could result from the complexation of U and [MOEMIM][BF_4] as discussed before. After the

formation of a complex, it becomes difficult for bacteria to approach UO_2^+, and, therefore, the availability of UO_2^+ is reduced; thus leading to the overall decrease in U reduction.

Based on these results, it is obvious that [MOEMIM][BF_4] is able to keep more than 90% of its total U in the aqueous phase, whereas, other ILs can only maintain less than 10% of their total U in solution. As we discussed in 3.1.1, the increase in solubility of U is due to the formation of a complex in the solution.

4.3.1.3 UV-vis Spectrometry.

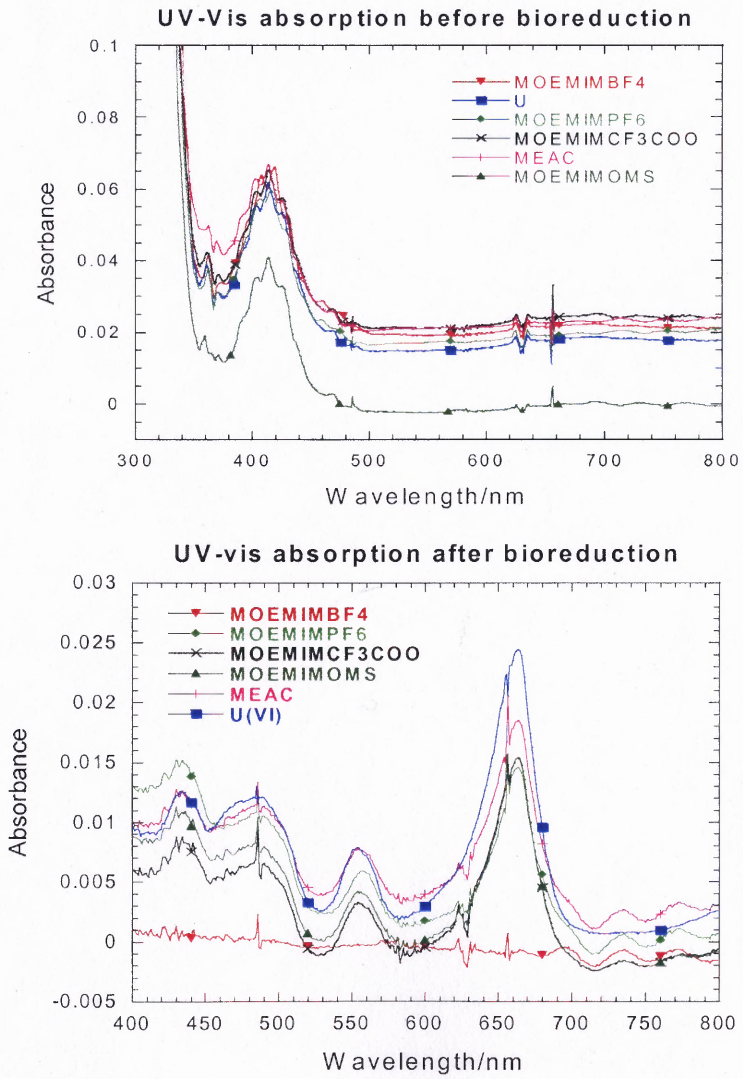

Figure 4.4 UV-Vis absorption of U in presence of various ILs.

UV-Vis spectra of U before and after bioreduction are given in Figure 4.4. Comparison of Figs. 4 (a) and (b) shows that the maximum absorbance of uranium has shifted from 413nm to 663nm, which is the characteristic absorbance for U (IV), thus proving that U(VI) has been reduced to U(IV). In addition, it should be noted that the absorbance for [MOEMIM][BF_4] after reduction was very weak. This is because most of U was maintained in the solution and not in the precipitate. Therefore, the U concentration in the citric acid used as the extractant for the U was very low.

4.3.2 Effects of Various Concentrations of [MOEMIM][BF_4] on Bioreduction

[MOEMIM][BF4] demonstrates a unique ability to increase the solubility of both U(IV) and U(VI) in solution. Further study was carried out to determine at what concentration [MOEMIM][BF_4] was optimized for both bioreduction efficiency and enhanced solubility.

4.3.2.1 Kinetic Study. The kinetic study results of five different concentrations of [MOEMIM][BF_4] are shown in Figure 4.5. As can be seen here, U(VI) concentration in solution decreased quickly, from 0.235mM to 0.02mM within 4 hours when no [MOEMIM][BF_4] was present, while the U(IV) concentration increased from 0 to 0.04mM. An addition of 1mM [MOEMIM][BF_4] slowed down the rate of the U(VI) decrease while increasing the U(IV) concentration a little, (from 0.02mM to 0.03mM). However, in the presence of 5mM [MOEMIM][BF_4], the U(VI) in solution was maintained as high as 0.12mM (10 times higher than the control) after 24 hours. At the same time, the U(IV) increased to 0.12mM, (6 times more than the control). In the

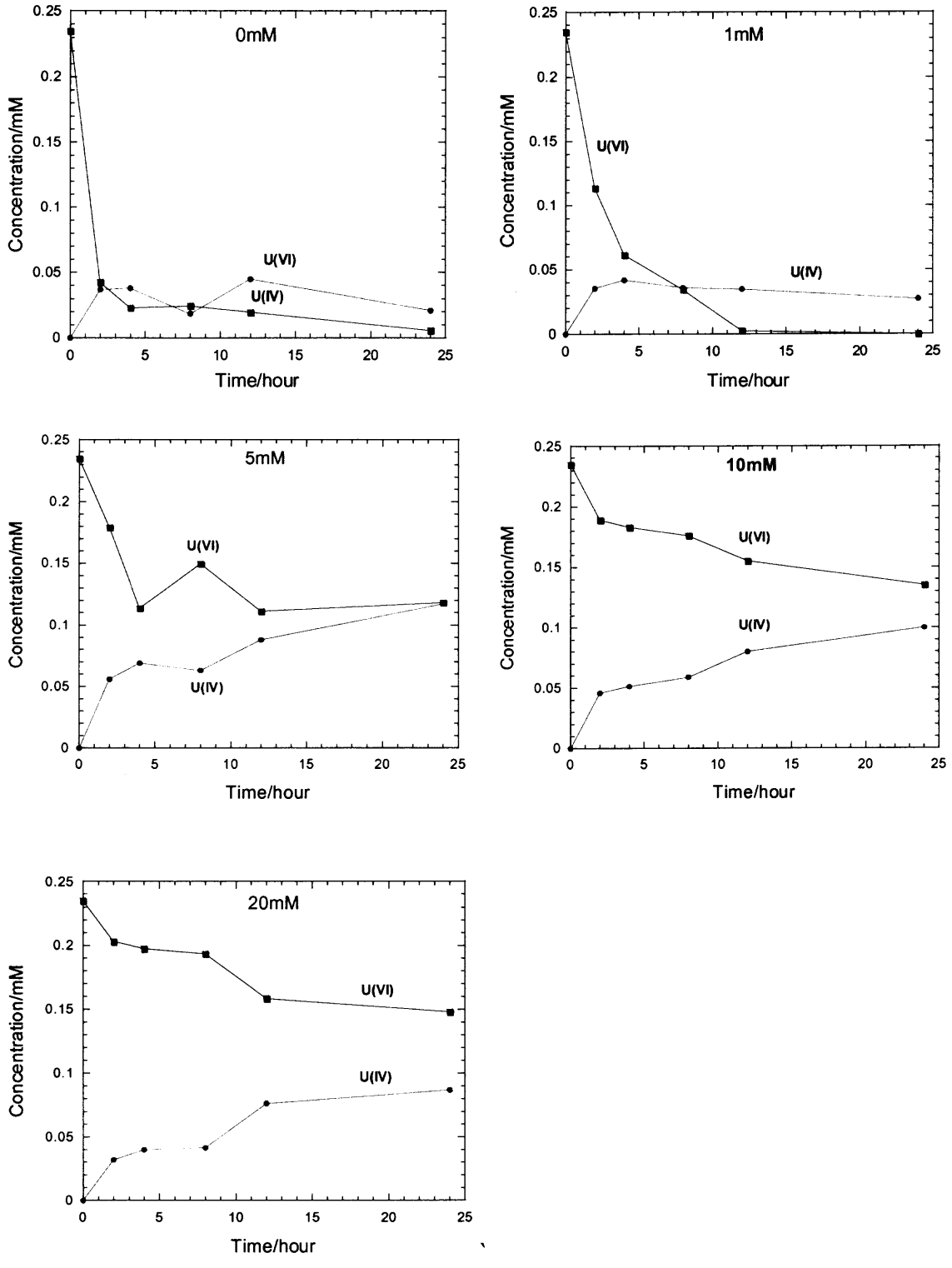

Figure 4.5 Concentrations of U(VI) and U(IV) in [MOEMIM][BF_4] with various concentrations.

presence of 10mM of [MOEMIM][BF_4], 0.135mM U(VI) stayed in solution while 0.1mM U(IV) maintained in solution. With the addition of 20Mm of [MOEMIM][BF_4], the concentration of U(VI) continued to increase to 0.15mM while the concentration of U(IV) dropped a little to 0.09mM.

Based on the data above, it can be concluded that: 1) an increase of [MOEMIM][BF_4] concentration can lead to the continuous increase of the U(VI) concentration in solution. This could be due to the formation of a complex as described before; 2) along with the rise of [MOEMIM][BF_4] concentration, U(IV) in solution increases first, and then decreases a little. It is hypothesized that, on the one hand, the elevated concentration of [MOEMIM][BF_4] improves complexation and leads to the increase of U(IV) in solution; while on the other hand, a raise in concentration enhances the toxicity of [MOEMIM][BF_4] to bacteria, resulting in less U(VI) converted to U(IV).

4.3.2.2 Mass balance of U after bioreduction in the presence of [MOEMIM][BF_4] with various concentrations.

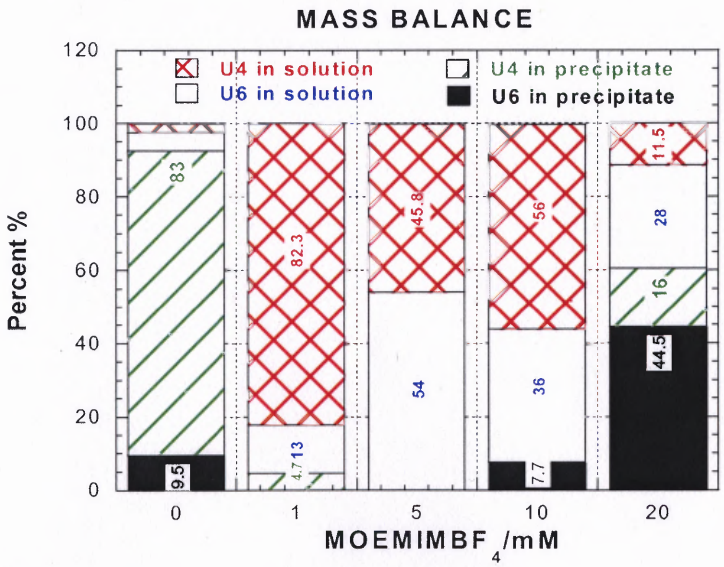

Figure 4.6 Mass Balance of U in different ILs after reduction.

Based on the data shown in Figure 4.6, we can say that: 1) in the absence of [MOEMIM][BF_4] solution, about 92.5% U precipitated out of solution, (83% U(IV) / 9.5% U(VI)). However, in the presence of [MOEMIM][BF_4], both U(IV) and U(VI) in solution increased. For instance, in a 1mM [MOEMIM][BF_4] solution, the U(IV) in solution reached 82.3% of the total U, (almost 31 times the U(IV) percentage in 0mM [MOEMIM][BF_4] solutions). Also, 13% U(VI) was present in solution, (about 3 times higher than the U(VI) percentage in the 0mM [MOEMIM][BF_4] solution); 2) the U(IV) in solution increased at the beginning, and then decreased when the [MOEMIM][BF_4] concentration increased. There was only 2.6% U(IV) in the 0mM [MOEMIM][BF_4] solution, but it increased to 82.3% in 1mM [MOEMIM][BF_4] solution, and then subsequently decreased to 56% in 10mM of [MOEMIM][BF_4] solution. When the concentration reached 20mM, only about 11.5% U (IV) was maintained in the solution; 3) as the [MOEMIM][BF_4] concentration increased, so did the unreduced total U(VI) in both solution and precipitate.

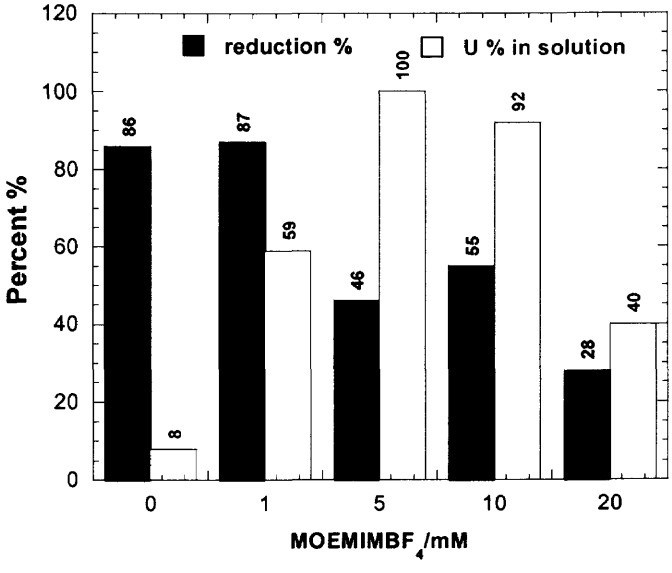

Figure 4.7 Percentage of U reduction and U in solution in various concentrations of [MOEMIM][BF_4] solution.

The total bioreduction percentage (for both in solution and precipitate) and total the uranium percentage in solution (for both U (VI) and U (IV)) were concluded as shown in Figure 4.7.

As for the reduction percentage, we found that the ability (or inability) of [MOEMIM][BF_4] to effect bioreduction efficiency depends on its concentration. In the control, 86% reduction was achieved. The addition of 1mM [MOEMIM][BF_4] could maintain the same reduction efficiency as 87%. However, the addition of 5mM and/or 10mM [MOEMIM][BF_4] inhibits bioreduction capability about 50%. Moreover, when the concentration reached 20mM, only about 28% reduction was obtained.

As to the U percentage in solution, there's no doubt that [MOEMIM][BF_4] could improve the solubility of total U in solution. Compared with 8% of the total U in 0mM solution, 59% of the total U was kept in a 1mM solution, while 100% and 92% of total U were maintained in 5mM and 10mM solutions respectively.

As described before, [MOEMIM][BF_4] is able to form a complex with uranium in solution, leading to the increase of uranium solubility in an aqueous phase. This explains why the addition of [MOEMIM][BF_4] caused more uranium to remain in solution. Both U(IV) and U(VI) were increased in the solution, indicating that [MOEMIM][BF_4] can form a complex with both of them. In addition, the elevated concentration inhibited the activity of bacteria due to the increased toxicity associated with the increased [MOEMIM][BF_4], thus leading to the decrease of bioreduction.

4.4 Summary

Different ILs have different effects on the bioreduction of U(VI).

- Except [MOEMIM][BF_4], other ILs form no or weak complexes with uranium, and produce little effect on overall bioreduction efficiency at low concentrations.

- [MOEMIM][BF4] can form a strong complex with uranium, leading to the significant increase of both U(VI) and U(IV) solubility.

- At the concentration of 1mM, [MOEMIM][BF_4] can maintain as much bioreduction efficiency as in the absence of [MOEMIM][BF_4], while also maintaining about 60% of the total U in solution. With the increase in [MOEMIM][BF_4] concentration, more U can be maintained in solution, but the toxicity also increases, inhibiting the activity of bacteria and thereby decreasing bioreduction efficiency.

CHAPTER 5

TOXICITY STUDY OF IONIC LIQUIDS ON *CLOSTRIDIUM* SP.

5.1 Intordution

Although Ionic Liquids have been extensively studied recently, information about the toxicity for most ILs remains scarce. In the existing science a few important discoveries should be highlighted. For example, it has been discovered that the structure of imidazolium ILs is similar to that of biologically active plant growth regulators (or cationic surfactants) which have known destructive impact on the Environment. Also, Docherty and co-workers (2005) have observed the antimicrobial properties of ILs. They examined the antimicrobial effects of 1000 ppm of butyl, hexyl and octyl imidazolium and pyridinium-based ionic liquids on the growth of a group of microorganisms. Generally speaking, hexyl and octyl imidazolium and pyridinium ILs exhibited higher inhibitive effects than those ILs containing a butyl chain. In addition, Pernak et al. (2004) also found that ILs exhibit antimicrobial activities, and that the alky chain length plays an important role in toxicity. The longer the alky chain, the more toxic the ionic liquid. Ranke et al. (2003) also studied the biological effects of imidazolium ILs with varying chain lengths in acute *vibrio fischeri* and WST-1 cell viability assays. The concentrations of ILs used in their study were generally of some orders of magnitude lower than the toxicity of conventional solvents like acetone, acetonitrile, and methanol. They also demonstrated the linear relationship between toxicity and alky chain length.

Building on these studies, we continued our research into ILs and toxicity. In our study, we used MOEMIM-based ILs with various anions to further examine the toxicity

to bacterium. In order to compare the toxicity with other ILs, BMIM-based ILs also were investigated here. Both the cation and anion effects on toxicity were examined.

5.2 Materials and Methods

5.2.1 Ionic Liquids

The Ionic liquids used for this study include [EtPy][CF_3COO], [BMIM][BF_4], [BMIM][CF_3COO], [MOEMIM][BF_4], [MOEMIM][PF_6], [MOEMIM][CF3COO], [MOEMIM][OMS], [MOEMIM][Tf_2N] and [MOEMIM][CH_3COO]. For each of the ILs, four concentrations were examined, including 0.10%, 25%, 0.5% and 1% (volume of IL/volume of water).

5.2.2 Bacterium

Clostridium sp. was studied for toxicity. A BC1 medium was used to culture *Clostridium* sp.,

5.2.3 Method

Ionic liquid was dispensed to the autoclaved BC1 in a glove box. For each concentration, two parallel samples were prepared; one was used for kinetic study, the other was kept intact for measurement of the gases produced by *Clostridium sp.*

Clostridium *sp.* was cultured in BC1 medium without any ILs for 18 hours to reach logarithm period of growth. 2ml of culture was then transferred to each bottle. Samples were withdrawn in intervals to determine the growth of *Clostridium sp.*

5.2.4 Indicators of Growth to be Measured

Optical density (OD) --- is proportional to the amount of cells, measured at 600nm by UV-Vis spectrometer.

pH pH change indicates the metabolism of bacteria. Here because *Clostridium* sp. consumes glucose, acid is released during growth. The lower pH, the greater bacteria growth.

Gases Produced by Bacteria Some gases, mainly carbon dioxide and hydrogen, will be generated during growth. The pressure was measured by gas gauge and the volume was calculated

Mass Spectroscopy After filtrated with 0.25um filter membrane, the sample was analyzed using LCQ Advantage ESI-MS to determine the production of metabolism.

5.3 Results and Discussion

5.3.1 Effects of [BMIM][BF_4]on *Clostridium* sp. growth

5.3.1.1 Optical Density (OD). The Kinetic study of OD values is shown in Figure 5.1. Obviously, addition of [BMIM][BF_4] inhibited the bacteria growth. The higher concentration led to lower growth. For example, in the control (without ILs), bacteria grew very well and OD reached to 0.73, while in the medium with 0.25% (v/v) [BMIM][BF_4], the OD dropped to 0.22. When the concentration increased to 0.5%, almost no cell growth occurred.

5.3.1.2 pH. pH change (along with the time duration) was displayed in Figure 5.2. During growth, *Clostridium* sp. consumed glucose and produced lots of acids by metabolism, which resulted in the significant pH decrease. Generally speaking, the more

[BMIM][BF_4] in the medium, the less the pH decrease (due to the [BMIM][BF_4]'s prohibition of cell metabolism).

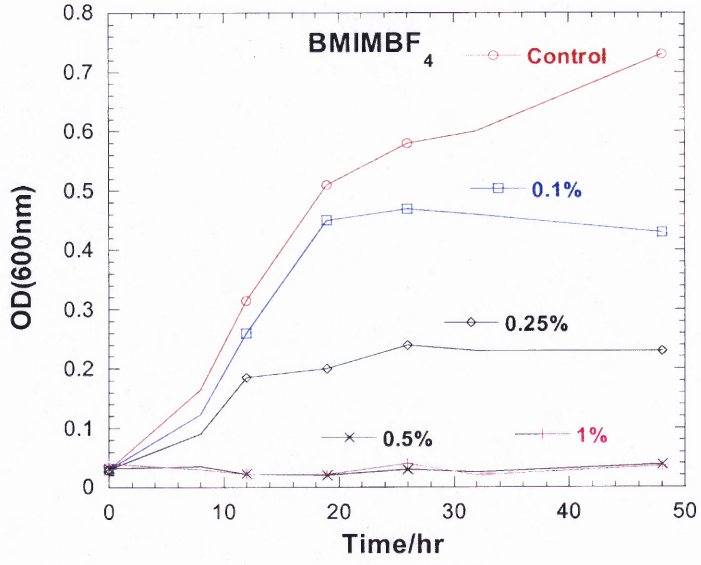

Figure 5.1 Bacteria growth in presence of [BMIM][BF_4].

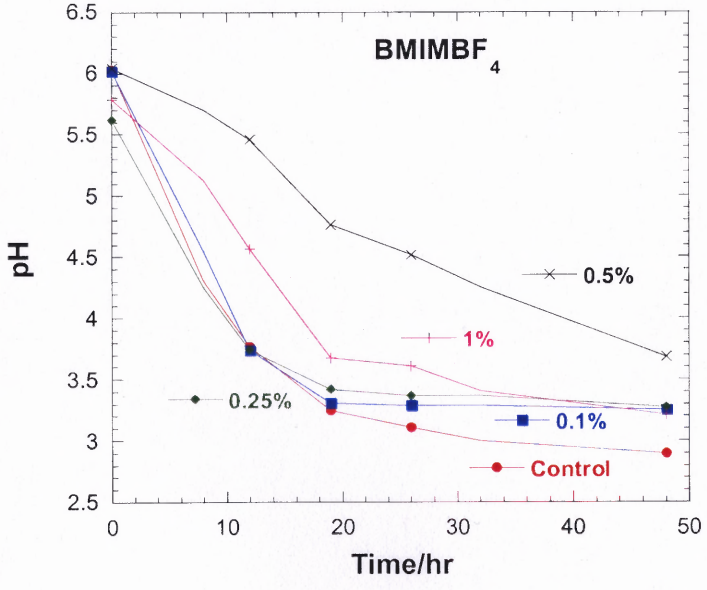

Figure5.2 Effects of [BMIM][BF_4] on pH change during incubation.

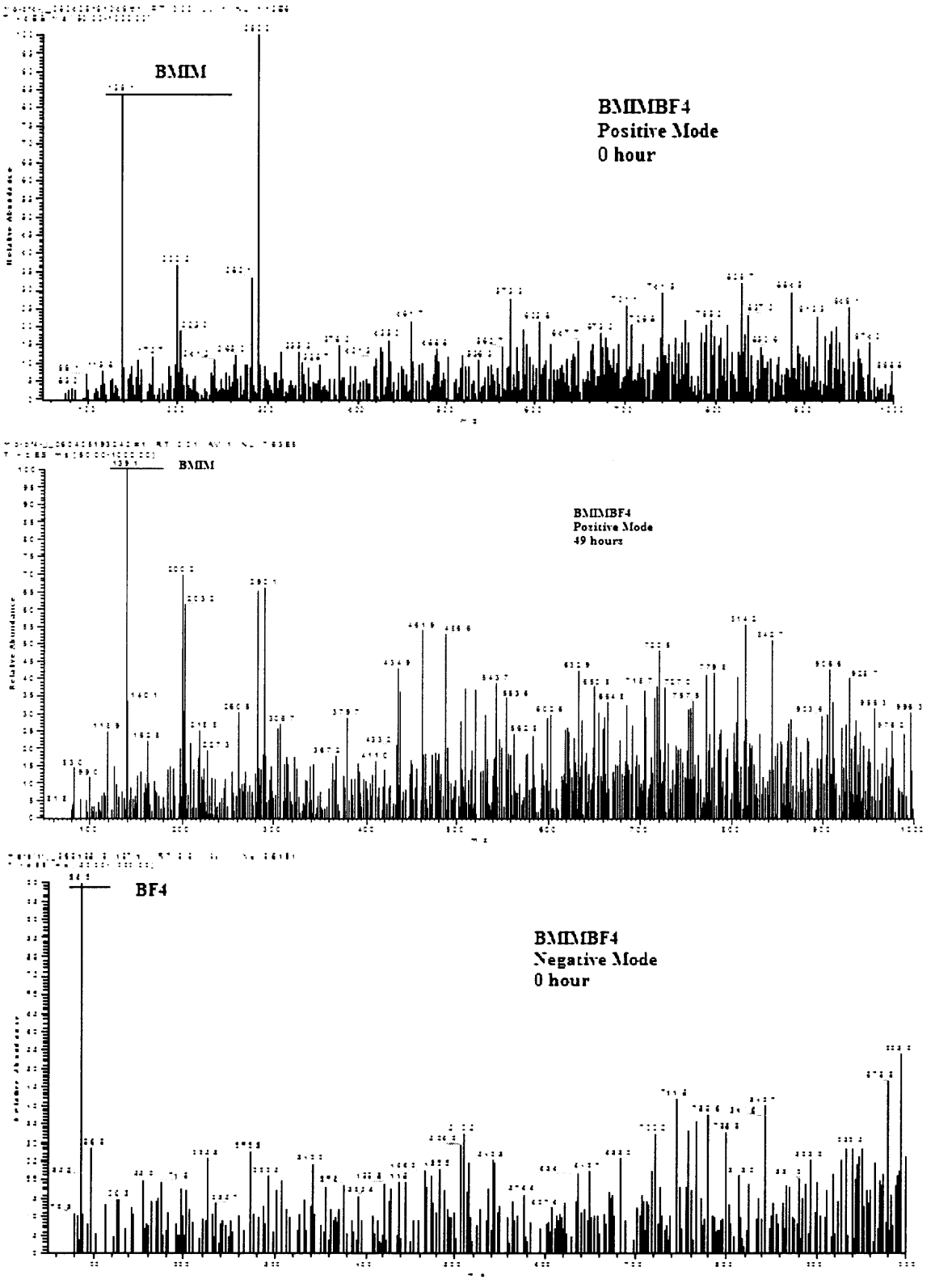

Figure 5.4. Mass spectra of medium containing [BMIM][BF_4] (0.1%).

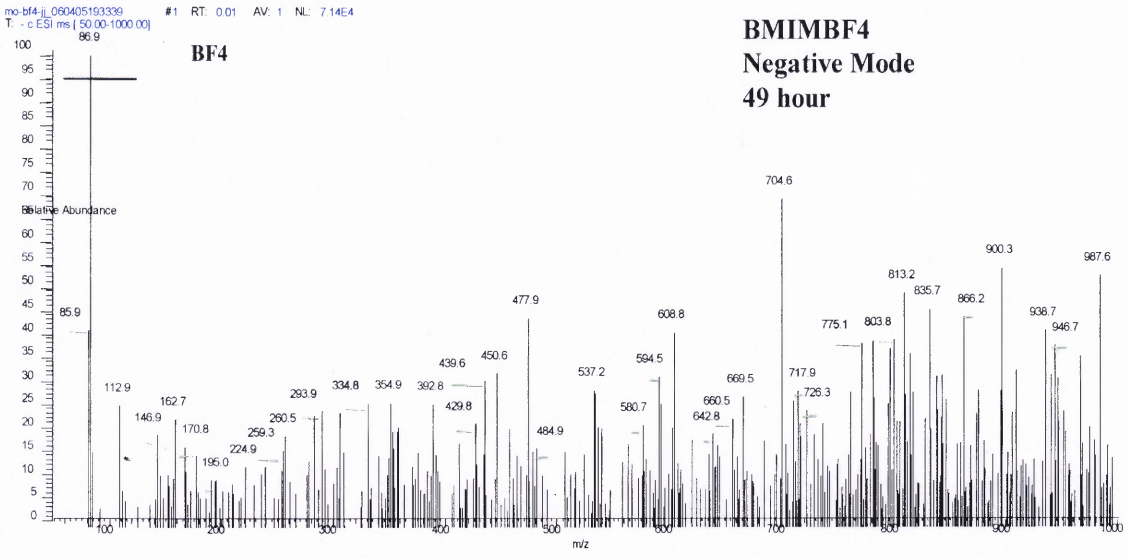

Figure 5.4. Mass spectra of medium containing [BMIM][BF_4] (0.1%)(Continued).

5.3.2 Effects of [MOEMIM][BF_4] on *Clostridium* sp. Growth

5.3.2.1 OD. OD was shown in Figure 5.5.

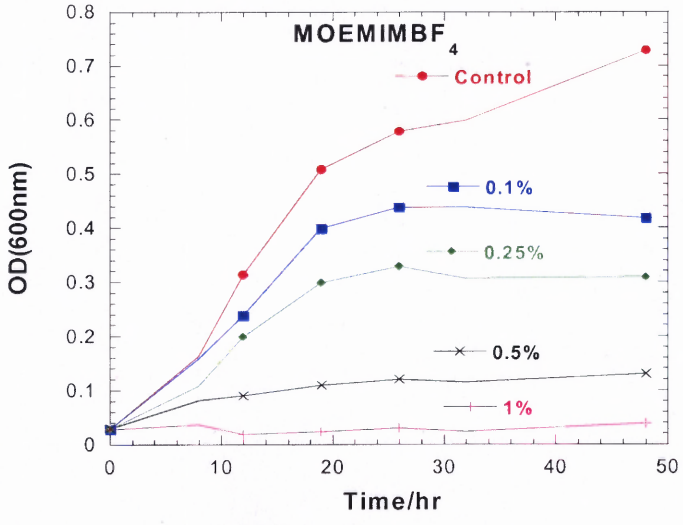

Figure 5.5 Bacteria growth in presence of [MOEMIM][BF_4].

OD decreased as the [MOEMIM][BF_4] concentration increased. The higher concentration led to the lower growth rate of bacteria. In 1% [MOEMIM][BF_4] medium, almost no bacteria grew.

5.3.2.2 pH. As it is shown in Figure5.6, the higher concentration of [MOEMIM][BF_4] resulted in less of a pH change, indicating the inhibiting factors of [MOEMIM][BF_4] on bacteria growth.

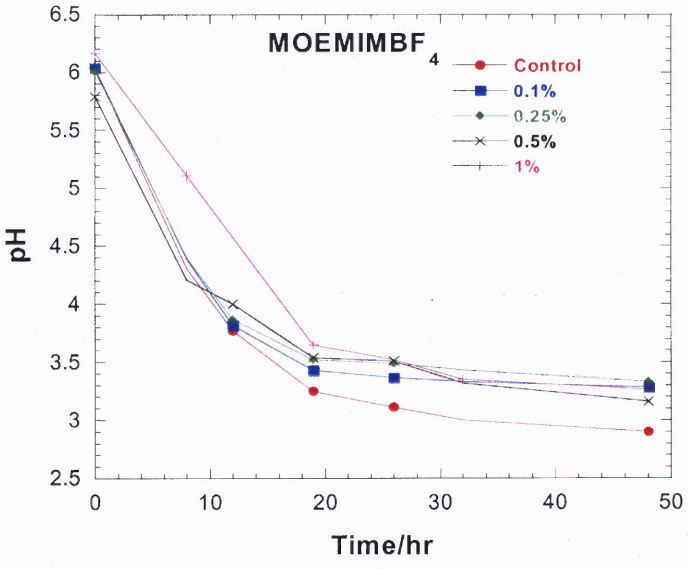

Figure 5.6 Effects of [MOEMIM][BF_4] on pH change during incubation.

5.3.2.3 Gas Production.

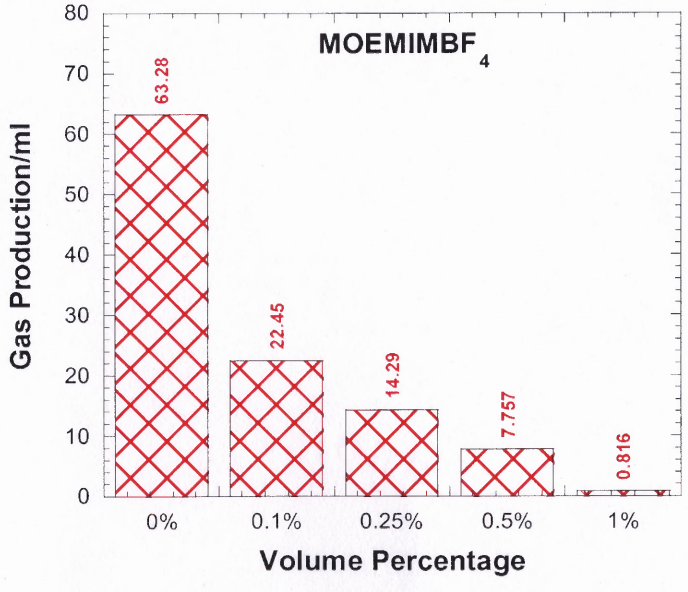

Figure 5.7 Effects of [MOEMIM][BF_4] on gas production during incubation.

It is obvious in Figure 5.7 that gas production decreased with the increase of [MOEMIM][BF_4].

5.3.2.4 Mass Spectroscopy. MS of 0.1% [MOEMIM][BF_4] was displayed in Figure 5.8. 141(m/e) in positive mode represents $[MOEMIM]^+$, while 86 in negative mode corresponds to $[BF_4]^-$. Based on MS data, [MOEMIM][BF_4] was not degraded by bacteria.

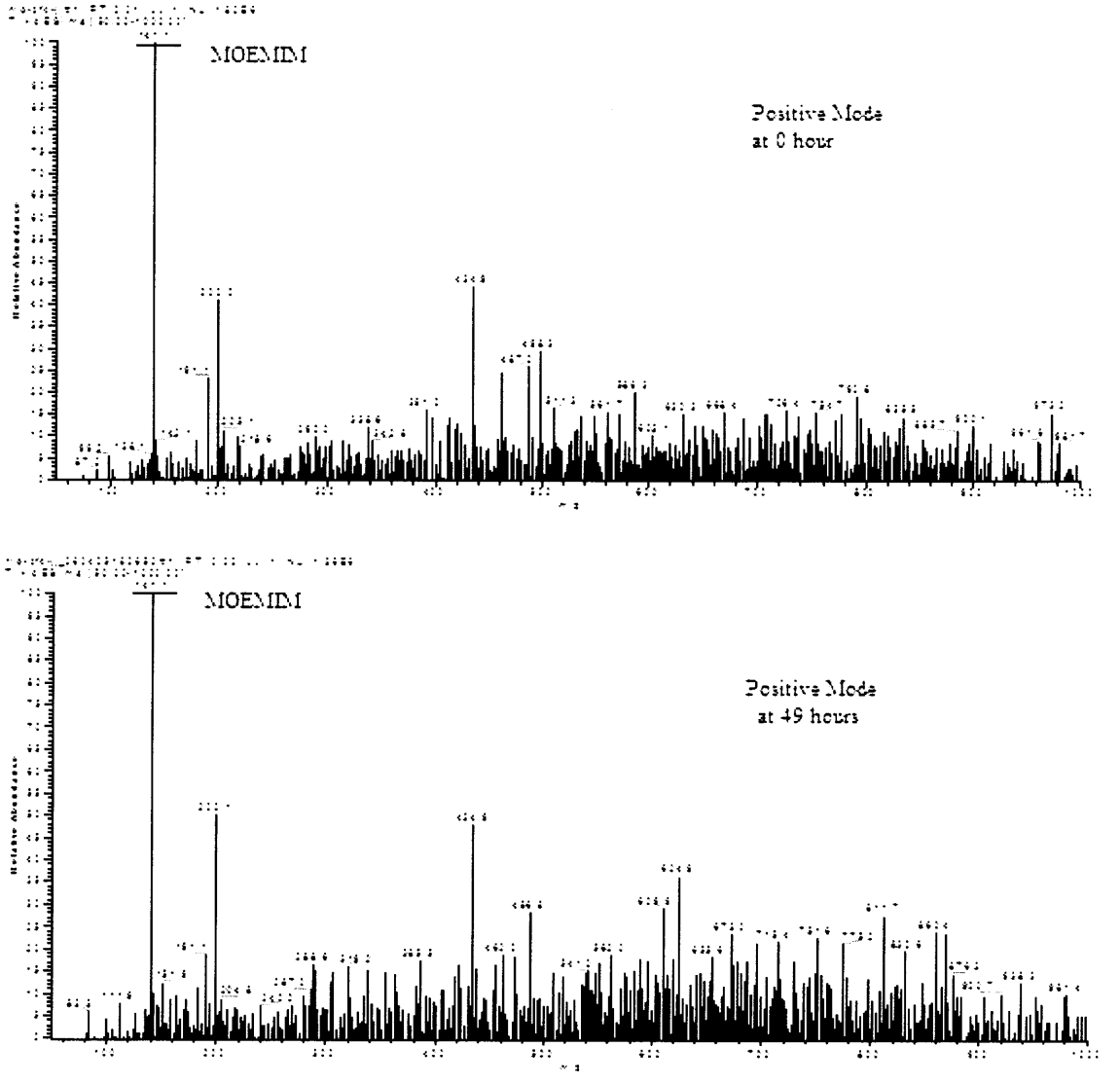

Figure 5.8 Mass spectroscopy of medium containing [MOEMIM][BF_4] (0.1%).

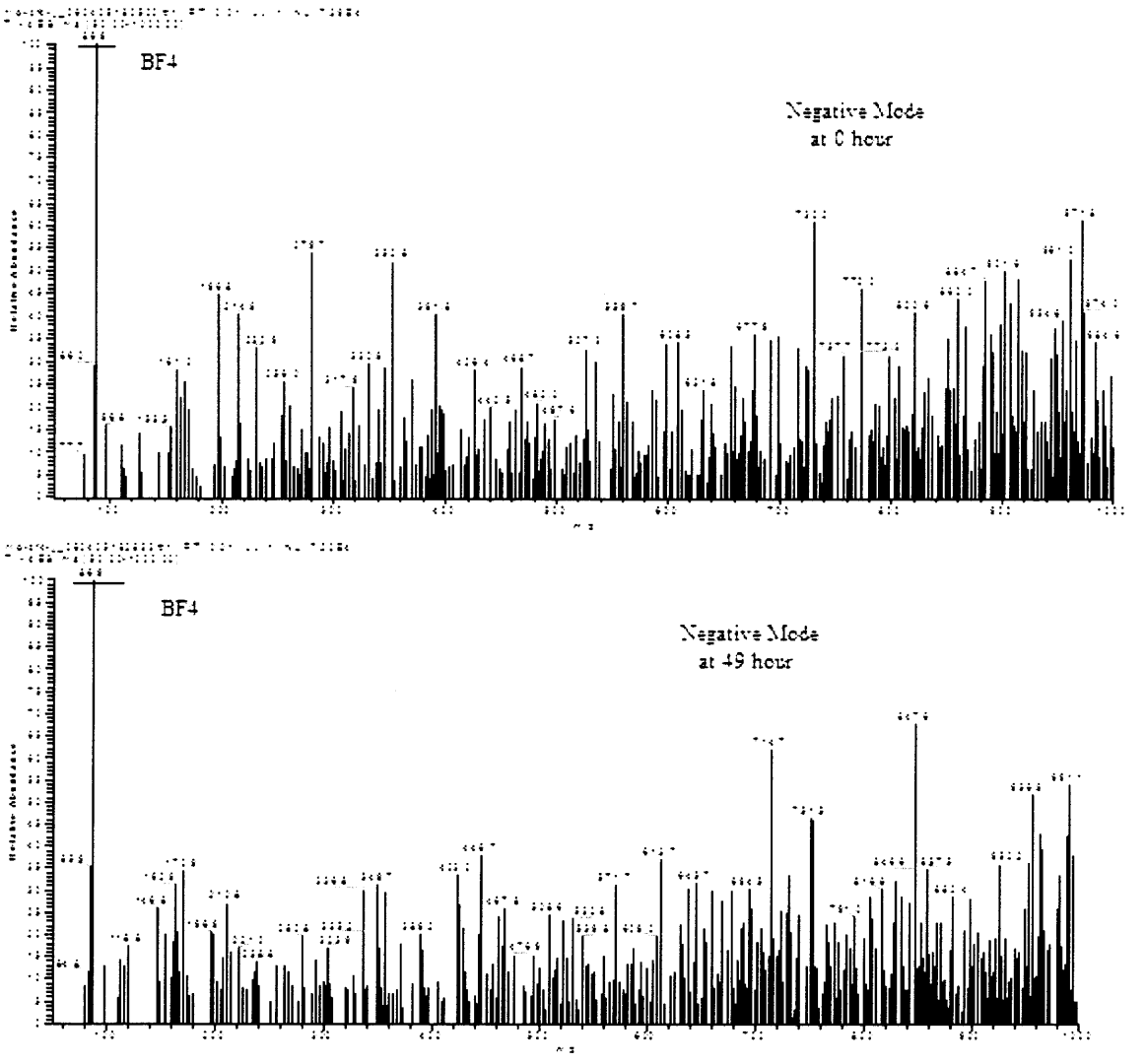

Figure 5.8 MS of medium containing [MOEMIM][BF_4] (0.1%)(Continued).

5.3.3 Effects of [MOEMIM][OMS] on *Clostridium* sp. Growth

5.3.3.1 OD. It is obvious in Figure 5.9 that, compared with other ILs, [MOEMIM][OMS] did not prove very toxic to bacteria. In the medium with 0.5% [MOEMIM][OMS], bacteria grew as well as bacteria in the control. Even in the 1% [MOEMIM][OMS] medium, OD can reach 0.48. Compared with other ILs, it is much less toxic.

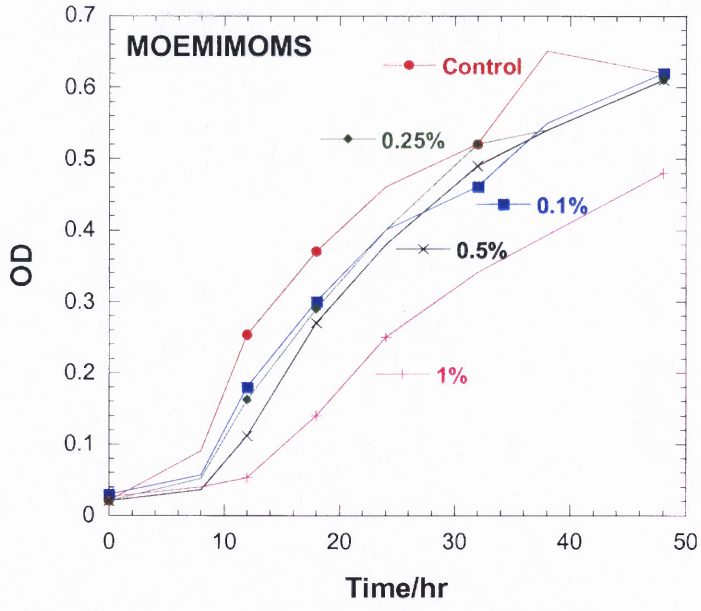

Figure 5.9 Bacteria growth in presence of [MOEMIM][OMS].

5.3.3.2 pH. pH change during inoculation was displayed in Figure 3.10. It proves that [MOEMIM][OMS] is much less toxic compared with other ILs. Except in the medium with 1% [MOEMIM][OMS], pH values remained very close to each other and the control. This indicates that the activity of bacteria was not much inhibited by its presence.

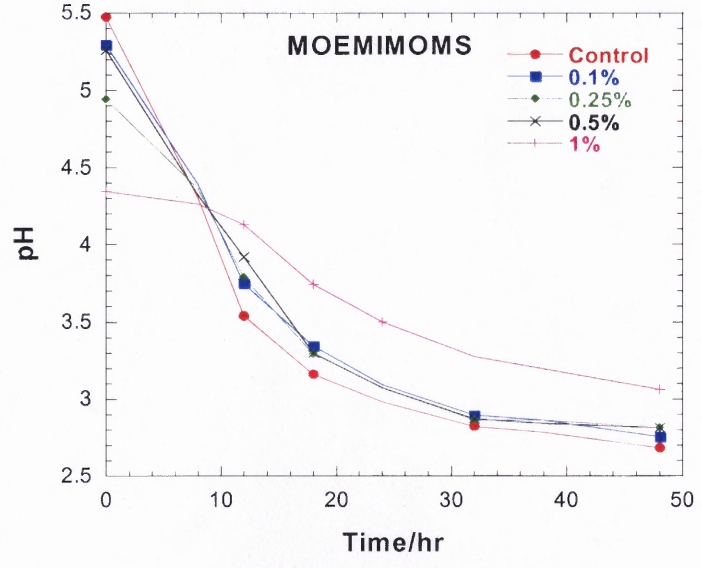

Figure 5.10 Effects of [MOEMIM][OMS] on pH change during incubation.

5.3.3.3 Gas Production. Figure 5.11 revealed that, up to 0.5% [MOEMIM][OMS], there is little difference in gas production as compared with the control, indicating much less inhibition on the *clostridium* s.p's activity. Even at 1%, bacteria can still grow well.

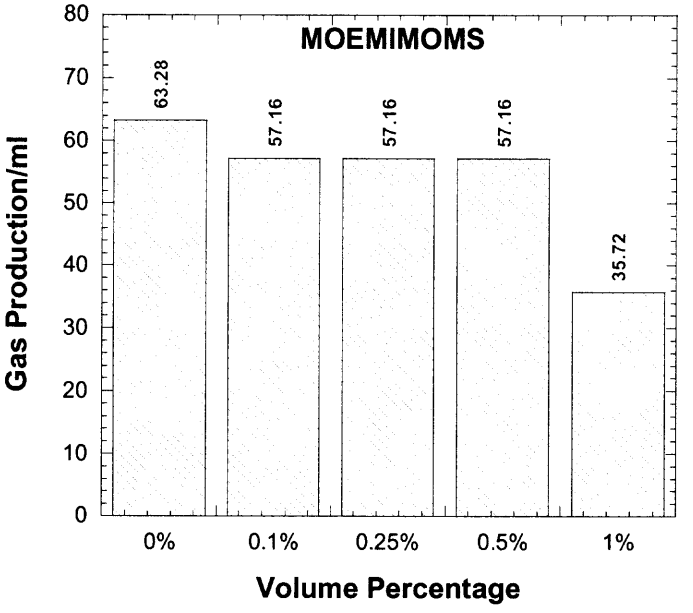

Figure 5.11 Effects of [MOEMIM][OMS] on gas production during incubation.

5.3.3.4 MS.

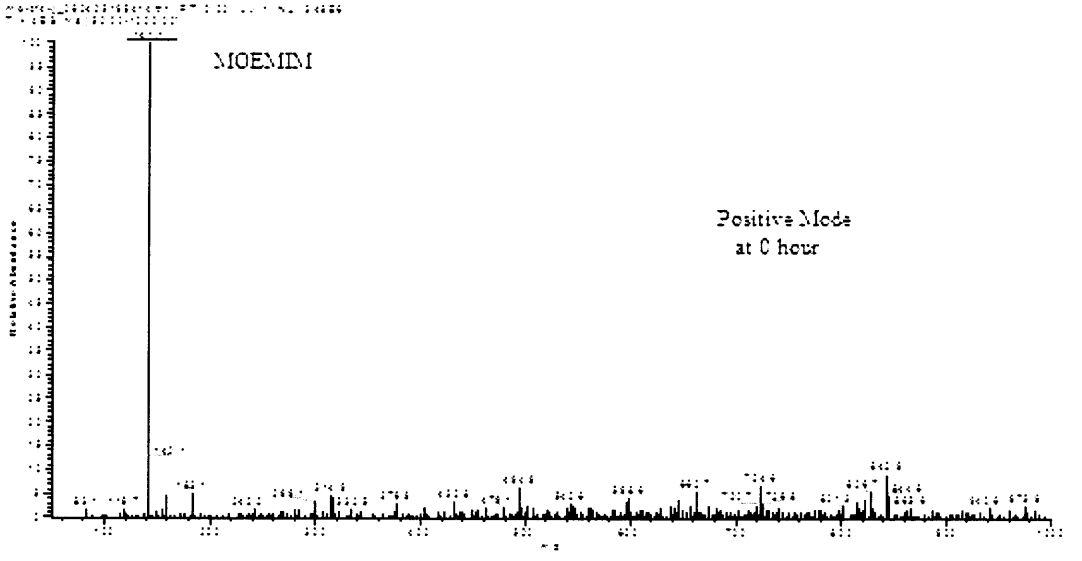

Figure 5.12 Mass spectra of medium containing [MOEMIM][OMS] (0.1%).

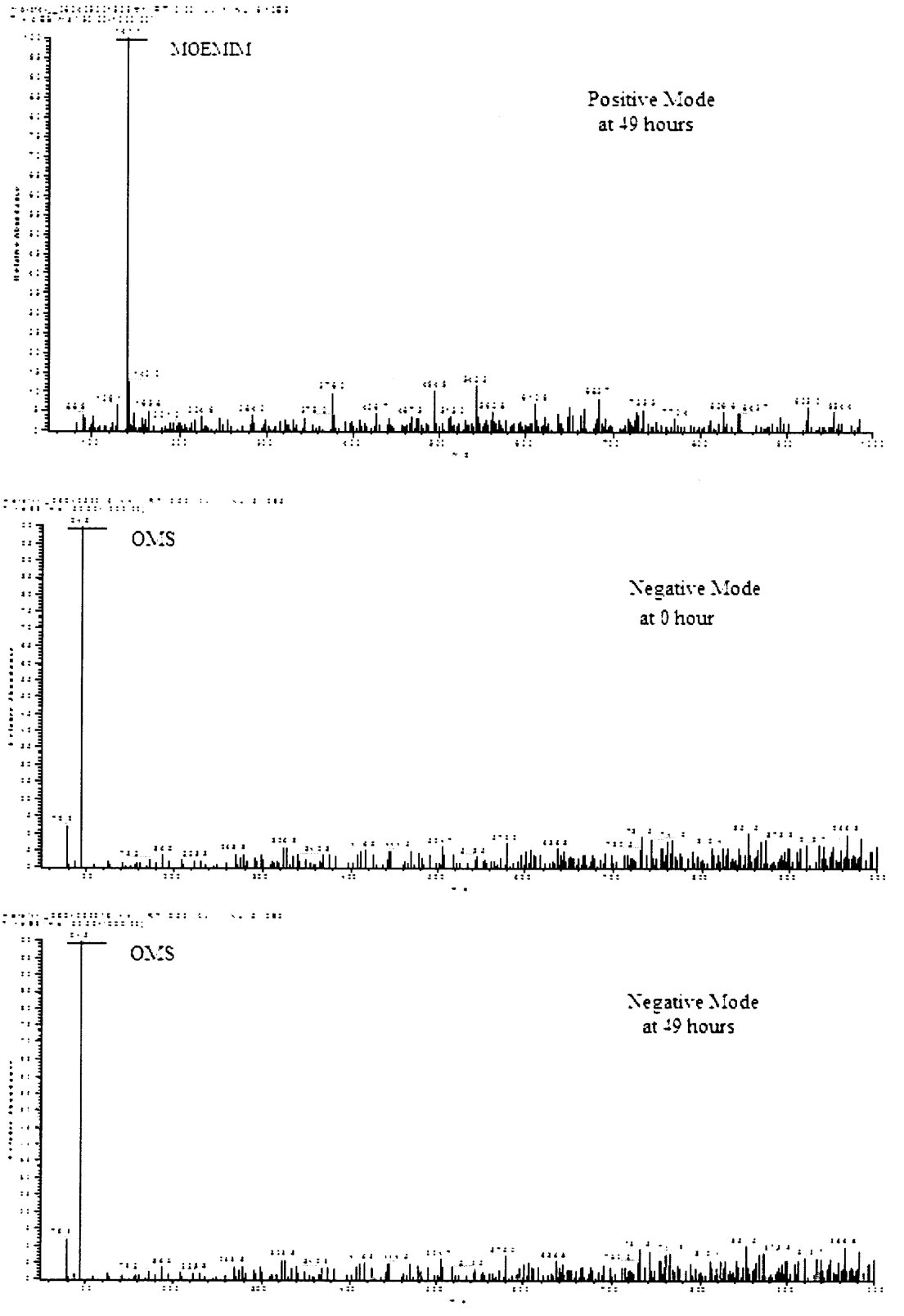

Figure 5.12 Mass spectra of medium containing [MOEMIM][OMS] (0.1%)(Continued).

141(m/e) represents [MOEMIM] cation in positive mode, and 95 reprsents [OMS] cation in negative mode. MS revealed that [MOEMIM][OMS] was not degraded by bacteria.

5.3.4 Effect of [MOEMIM][CF_3COO] on *Clostridium* sp.

5.3.4.1 OD. [MOEMIM][CF_3COO] did inhibit the growth of *Clostridium* sp. In the presence of 0.1% [MOEMIM][CF_3COO], the OD value after 48 hours was just 0.28, while that of the OD control was 0.65. At 1% concentration, 0.12 was observed for OD.

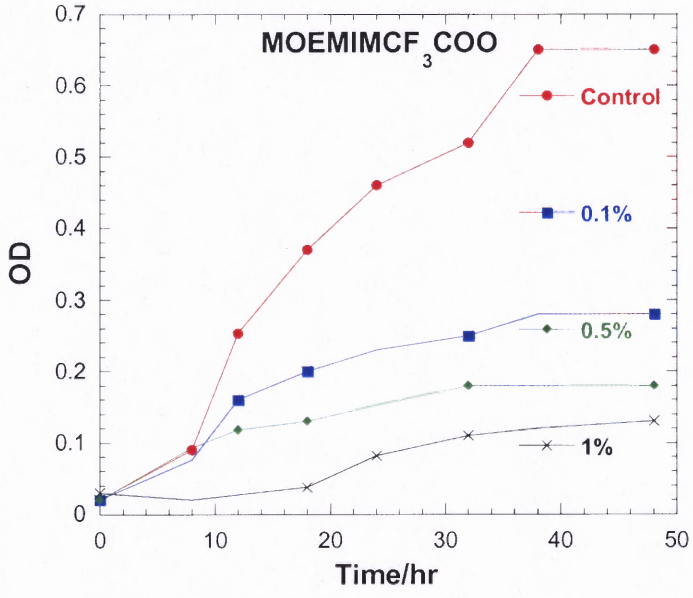

Figure 5.13 Bacteria growth in presence of [MOEMIM][CF_3COO].

5.3.4.2 pH. After 48 hours, the pH in the control dropped from 5.5 to 2.6, while the pHs in the 0.1%, 0.5% and 1% media are 3.3, 3.5 and 3.8 respectively, indicating this ionic liquid's influence on metabolism.

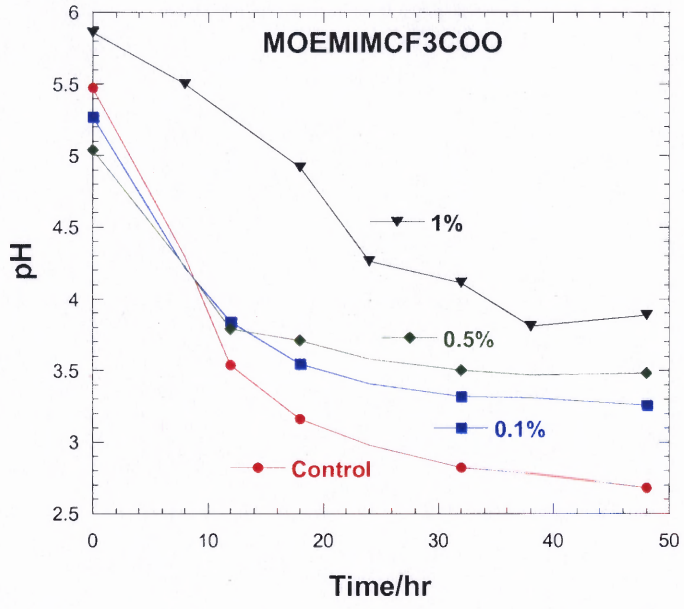

Figure 5.14 Effects of [MOEMIM][CF_3COO] on pH change during incubation.

5.3.4.3 Gas Production.

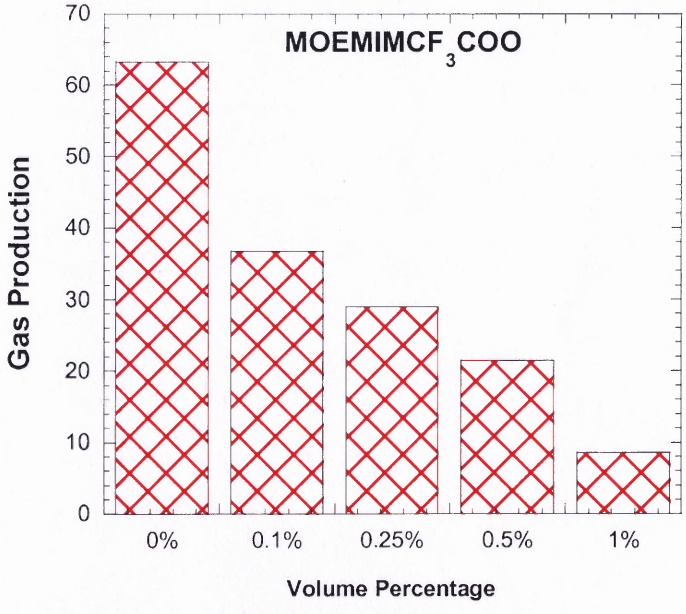

Figure 5.15 Effects of [MOEMIM][CF_3COO] on gas production during incubation.

5.3.4.4 MS. MS is shown in Fig 5.16. 113 (m/e) corresponds to [CF_3COO] anion. There is no degradation of this IL found in MS.

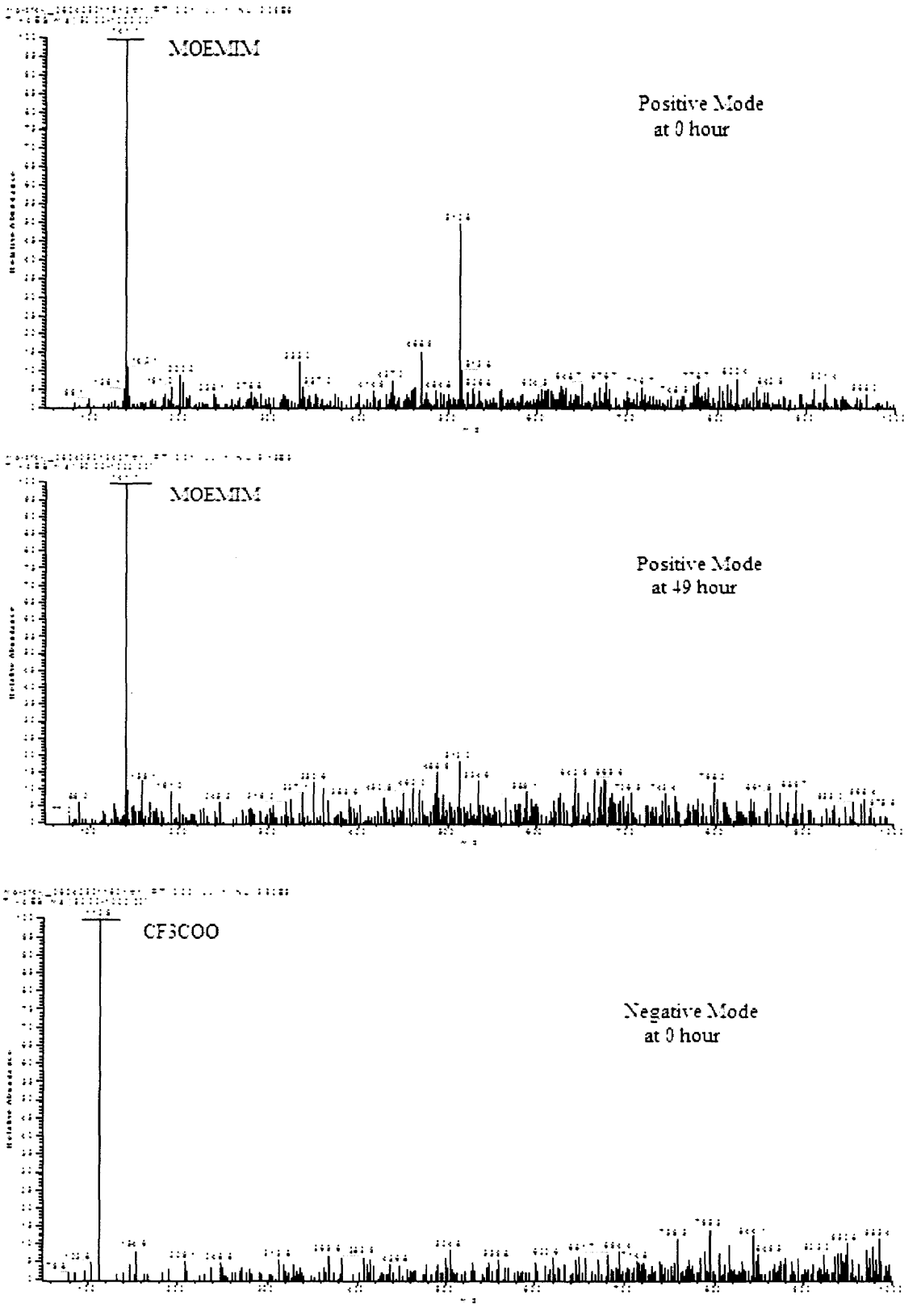

Figure 5.16 MS of medium containing [MOEMIM][CF_3COO] (0.1%).

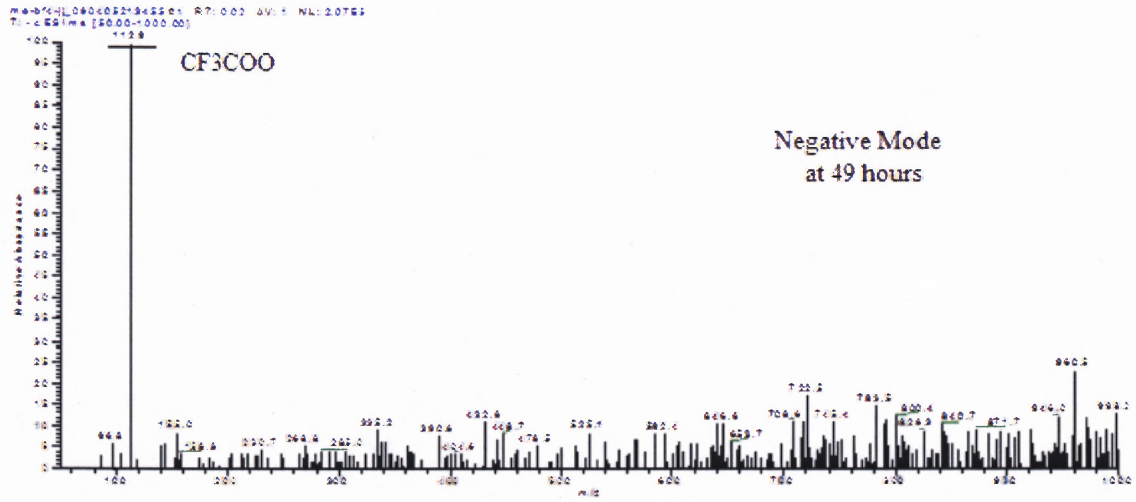

Figure 5.16 MS of medium containing [MOEMIM][CF_3COO] (0.1%)(Continued).

5.3.5 Effects of [MOEMIM][PF_6] on *Clostridium* sp.

5.3.5.1 OD. [MOEMIM][PF_6] showed high inhibition to bacteria. With 0.1% of [MOEMIM][PF_6] in the medium, the OD value only reached 0.2, (0.48 less than the OD of the control). There was almost no growth observed in 1% medium.

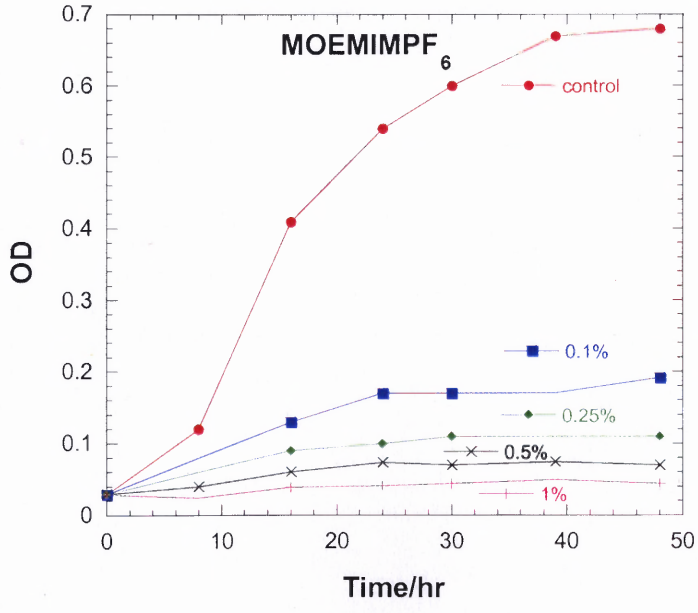

Figure 5.17 Bacteria growth in presence of [MOEMIM][PF_6].

5.3.5.2 pH. Compared with the control, after 48 hours, the pH in 1% medium only decreased to 4.7, much higher the pH 2.9 in the control This is contributed to the high toxicity of the [MOEMIM][PF_6].

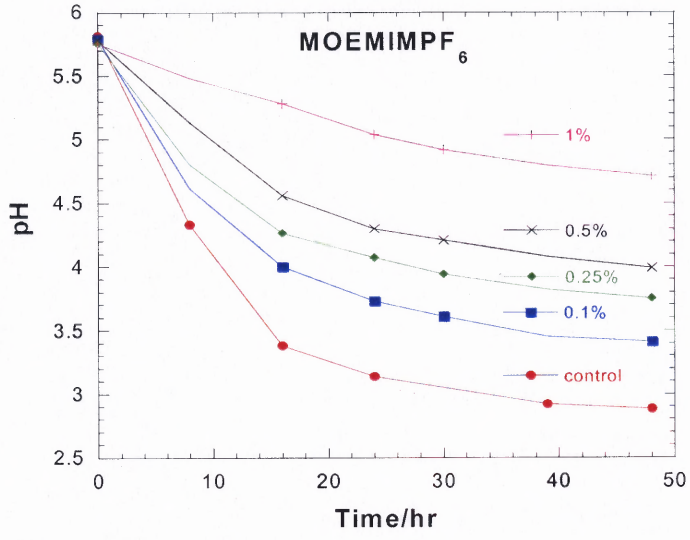

Figure 5.18 Effects of [MOEMIM][PF_6] on pH change during incubation.

5.3.5.3 Gas Production. Figure 5.19 displays the gas volume generated by bacteria. The volume of gas generated by bacteria decreased drastically. When the concentration reached 1%, there was no measurable gas production further showing the strong toxicity.

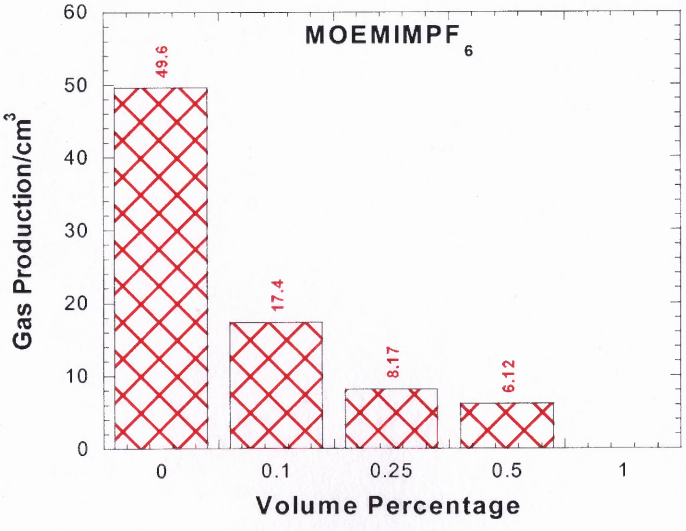

Figure 5.19 Effects of [MOEMIM][PF_6] on gas production during incubation.

5.3.5.4 MS. MS was displayed in Figure 5.20.

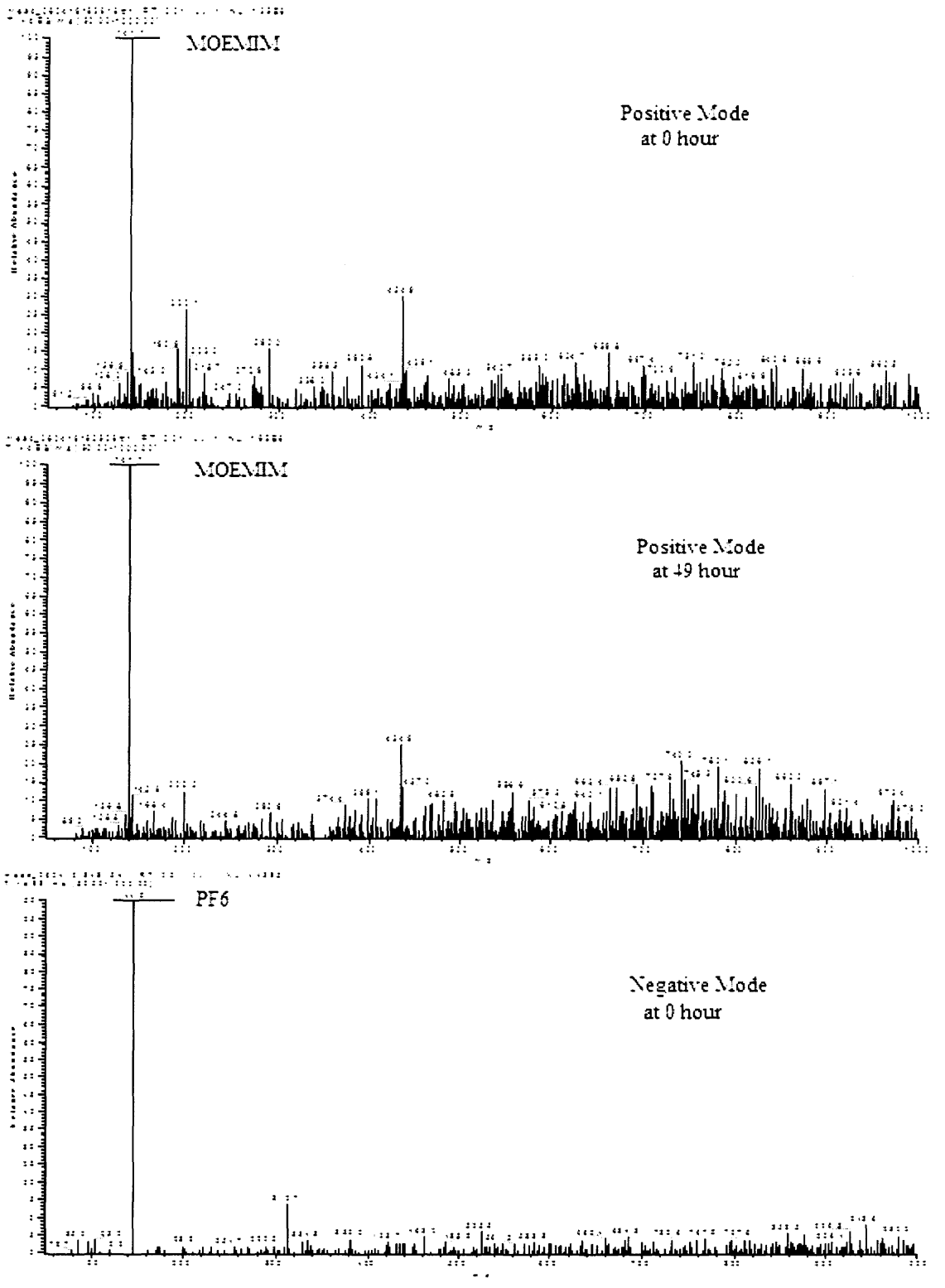

Figure 5.20 MS of medium containing [MOEMIM][PF_6] (0.1%).

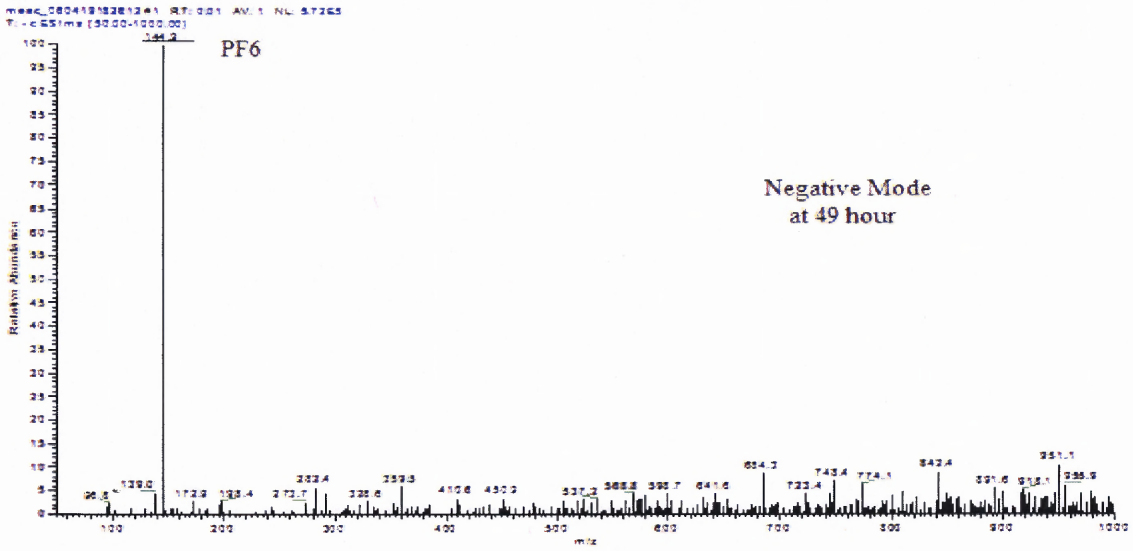

Figure 5.20 MS of medium containing [MOEMIM][PF_6] (0.1%)(Continued).

In positive mode, [MOEMIM] achieved base peak after 49 hours. In negative mode, [PF_6] was still the base peak after 49 hours. No biodegradation occurred.

5.3.6 Effect of [MOEMIM][Tf_2N] on *Clostridium* sp.

5.3.6.1 OD.

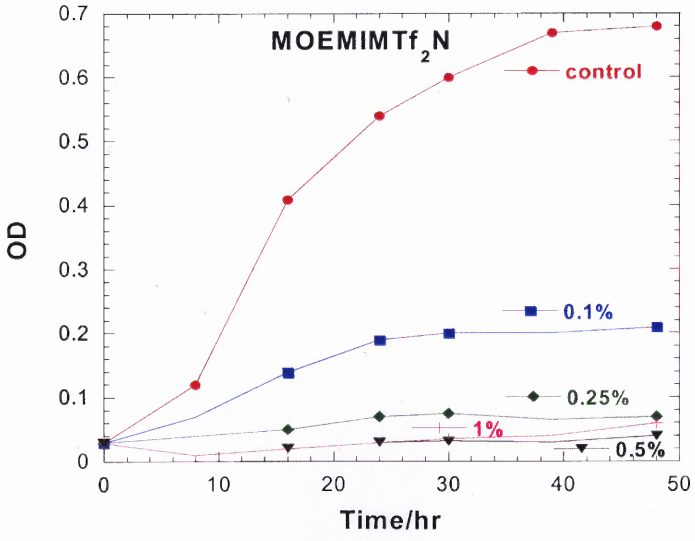

Figure 5.21 Bacteria growth in presence of [MOEMIM][Tf_2N].

Compared with other ILs studied here, [MOEMIM][Tf_2N] exerted the highest inhibition to bacteria. No bacteria growth was observed in 0.5% medium.

5.3.6.2 pH. The pH change (and duration) were shown in Figure 5.22. In 0.5% and 1% media, almost no pH change occurred, indicating the metabolism of bacteria was completely inhibited. It proved [MOEMIM][Tf_2N] is more toxic to the bacteria.

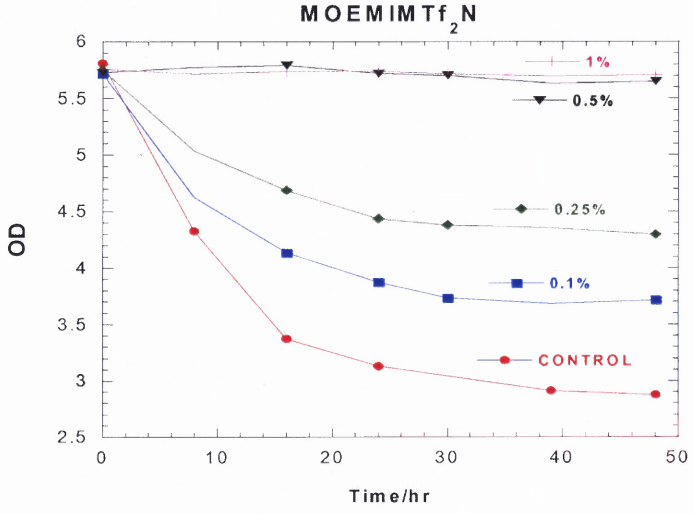

Figure 5.22 Effects of [MOEMIM][Tf2N] on pH change during incubation.

5.3.6.3 Gas Production. Figure 5.23 displays the gas production in presence of [MOEMIM][TF_2N].

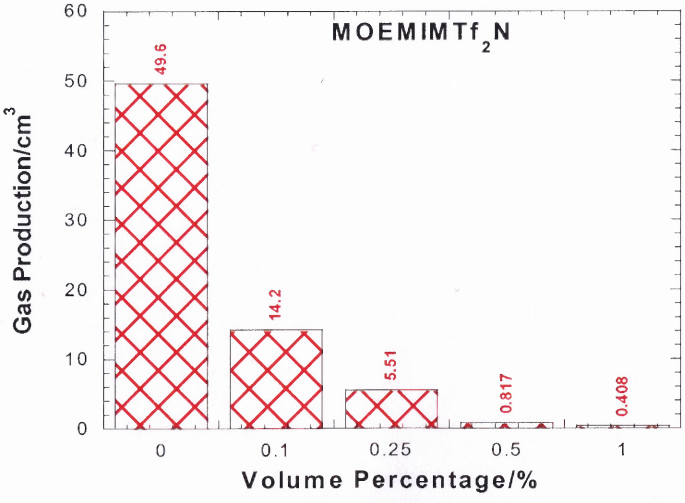

Figure 5.23 Effects of [MOEMIM][Tf_2N] on gas production during incubation.

Gas production also decreased drastically with increase of the concentration, indicating the strong toxicity.

5.3.6.4 MS. Mass spectra data was given in Figure 5.24, which revealed that [MOEMIM][Tf_2N] was not degraded by *Clostridium* sp.

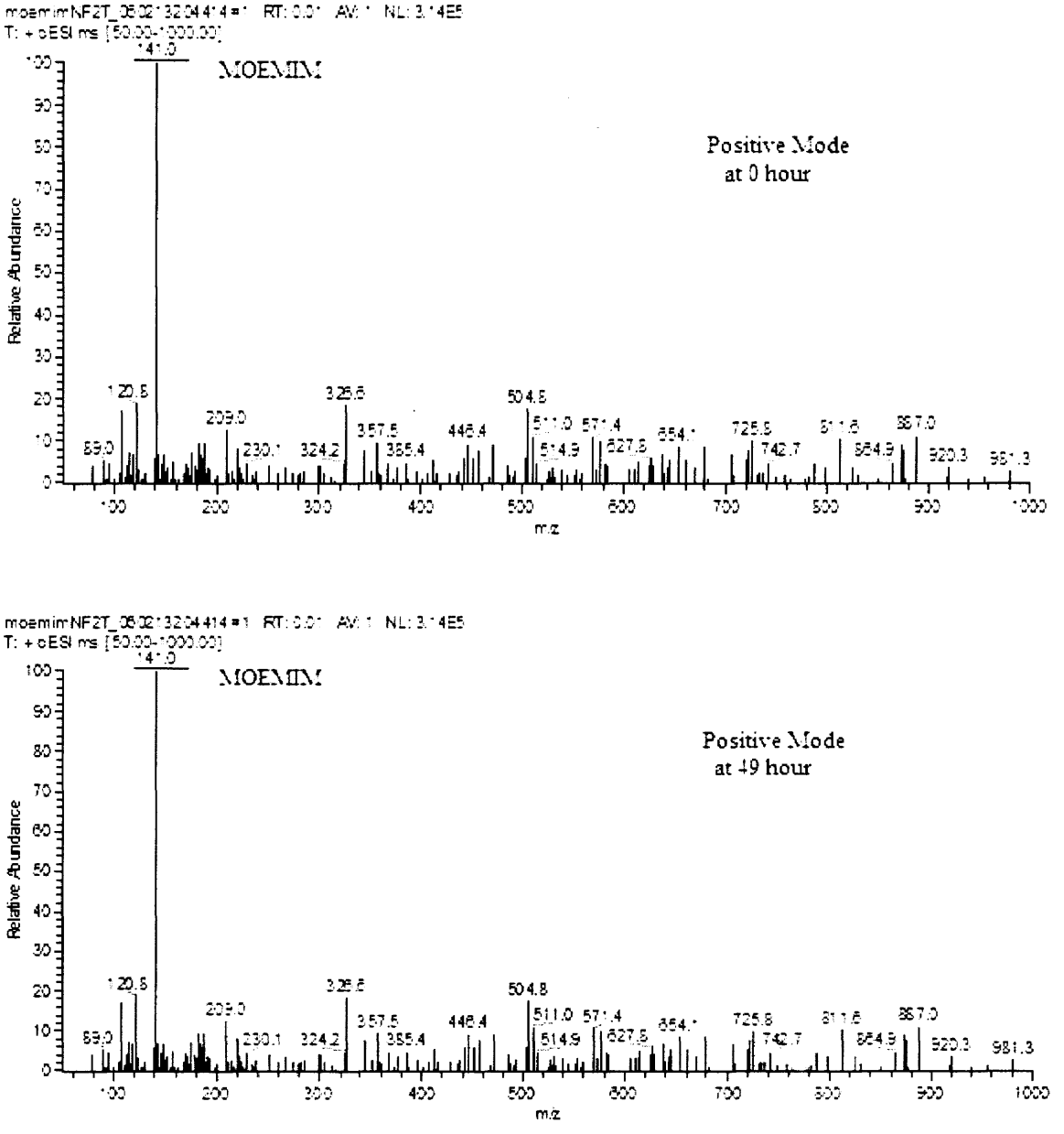

Figure 5.24 Mass spectra of medium containing [MOEMIM][Tf_2N] (0.1%).

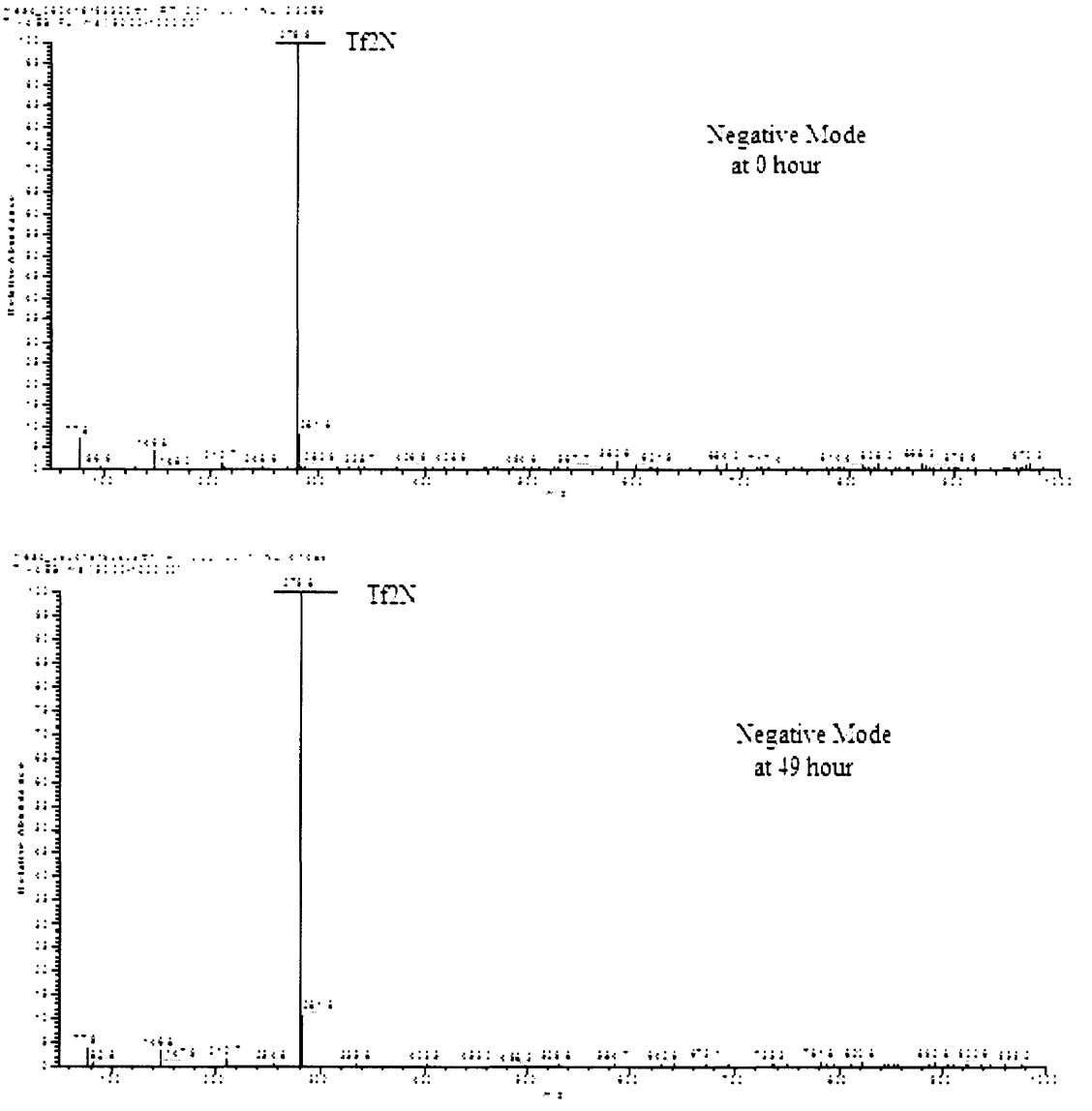

Figure 5.24 Mass spectra of medium containing [MOEMIM][Tf_2N] (0.1%)(Continued).

5.3.7 Summary

To varying extents, all ILs studied here negatively affected the growth of *Clostridium* sp. Throughout, both OD and gas production decreased with an increased concentration of ILs. However, different ILs showed different inhibitory effects on bacteria. For [BMIM][BF_4], at 0.5% concentration, the bacteria were hard to grow. For [MOEMIM][BF_4], part of bacteria grew at 0.5% while fewer bacteria grew at 1%. As for

[MOEMIM][CF_3COO], more inhibition was found. At 0.1% concentration, OD was just 0.28 after a 48-hour incubation. The [MOEMIM][PF_6] was even more toxic than [MOEMIM][CF_3COO]. Compared with the all above, [MOEMIM][Tf_2N] showed itself to be the most prohibitive to bacteria growth. At 0.25% concentration, OD was less than 0.1. [MOEMIM][OMS], however, distinguished itself as the least inhibitive to bacteria. Even at 1%, after 48 hours, the OD can reach 0.48.

5.4 Comparison of toxicity of different ILs

In order to compare the toxicity of still different ionic liquids, one control (without ILs) and 20mM of each ionic liquid was prepared. The same experiment was repeated, and OD, gas production were determined and displayed in figure 5.25 and 5.26.

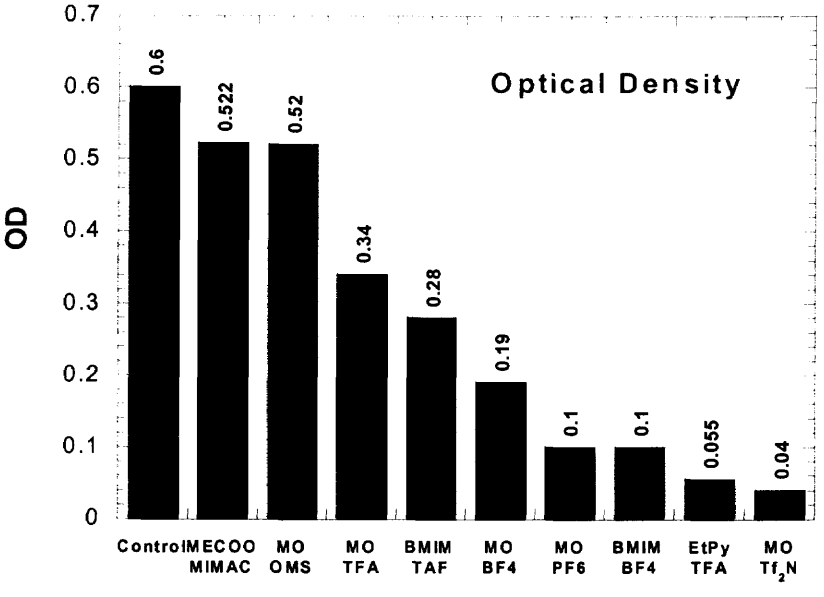

Figure 5.25 Comparison of optical density in media with different ILs.

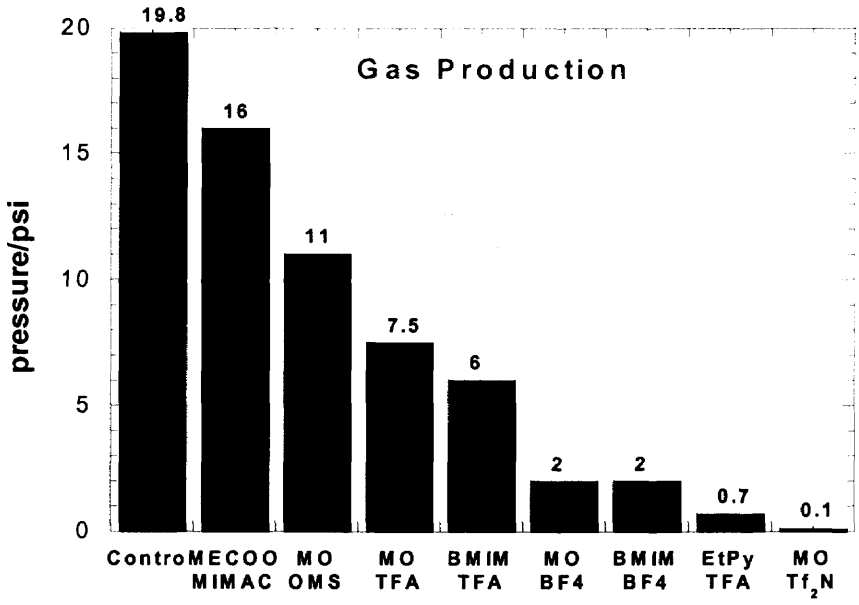

Figure 5.26 Comparison of gas production in media with different ILs.

Both the OD and gas production displayed the same trend of toxicity in ILs. The toxicity order of ILs from highest to lowest is as below:

[MOEMIM][Tf2N] > [BMIMB][F_4] > [MOEMIM][PF_6] > [MOEMIM][BF_4] > [BMIM][CF_3COO] > [MOEMIM][CF_3COO] > [MOEMIM][CH3COO] > [MOEMIM][OMS] > Control

Based on the data shown above, it may be concluded that:

- The Anion has an important effect on toxicity. With the same cation, $[MOEMIM]^+$, different anions show different inhibitory capabilities. The order of inhibition from highest to lowest was:

$$\mathbf{[Nf_2T]^- > [PF_6]^- > [BF_4]^- > [CF_3COO]^- > [OMS]^-}$$

- It is noteable that the more fluoric atoms the anion contains, the higher the ionic liquid's toxicity. The linear regression of the number of F atoms and toxicity is shown in Figure 5.27 ($LogEC_{50\text{-}48hour}$ was obtained in Chapter 6). As shown, the R^2 is 0.996, indicating the good linear relationship between them.

- The side chain of the cation also plays an important role in toxicity. For example, with the same anion, $[BF_4]^-$, toxicity of [MOEMIM][BF4] is less than that of

[BMIM][BF_4]. Also, with the same anion [CF_3COO]$^-$, [MOEMIM]$^+$ shows less toxicity than [BMIM]$^+$. As we mentioned before, the length of the alky chain plays an important part. The longer the side chain, the higher the toxicity of the ILs. In addition, the functionized side chain can also render toxicity. In this study, compared with BMIM$^+$ whose side chain is butyl, we found the toxicity decreases when a methoxyl ethyl group is added to the cation side chain. It may be due to the increase of hydrophilic property of the cation and hence the decrease of its lipophilic character.

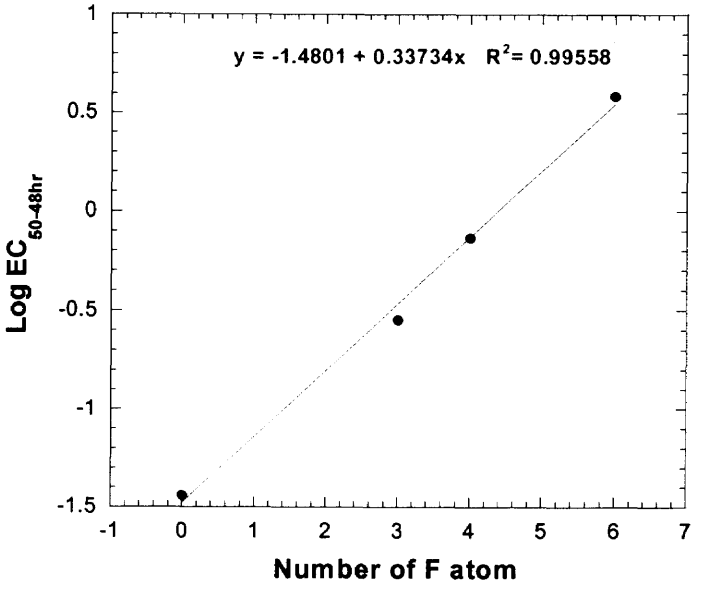

Figure 5.27 Regression of number of F atoms of ILs and toxicity.

CHAPTER 6

QUANTITATIVE STRUCTURE-ACTIVITY RELATIONSHIP (QSAR) FOR PREDICTION OF THE TOXICITY OF IONIC LIQUIDS

6.1 Introduction

For the past decade, Ionic liquids (ILs) have been studied to uncover their unique properties. They are known to be nonvolatile, have high chemical and thermal stability, have good solubility for both organic and inorganic compounds, and so on. Therefore, they are regarded as promising 'green' replacements for conventional organic solvents. It is believed, moreover, that ILs will be widely used by both the chemical and pharmaceutical industries in the future (Wasserscheid, P. and Welton, T., 2003). So far, however, little is known about the toxicity of ILs and research has not been extensive. As a result, with the rapid development of application of ILs, it is important and necessary to study the toxicity of ILs.

While experimentation on each chemical is the most reliable way to obtain toxicity data, such testing is time consuming, demanding of resources, and unsuitable for the screening of large numbers of chemicals. Alternatively, the toxicity of chemicals can be predicted with an understanding of the relationship between their structure and activity (Cronin et al., 2003). In fact, the quantitative structure-activity relationship (QSAR) model has proven to be a reliable tool for the toxicity assessment of organic chemicals (Huang, et al., 2003; Wang, et al., 2006; Papa, et al., 2004). QSAR relates the toxicity of chemicals to their molecular structures and physical chemical properties, and offers the advantage of higher speed and lower costs. In recent years, QSAR has been applied to

study the toxicity of certain chemicals to environmentally important microorganisms (Lu, et al., 2001; Netzeva, et al., 2005).

Presently, however, there is little reported about using the QSAR model to predict the toxicity of ILs. As we know, ILs are new solvents that differ from organic compounds. The former consists of only ions, while the latter consists of molecules. Since the study of ILs is fairly recent, there is very little physical or chemical information available in literature. For example, there is not much information about the partition coefficient of ILs. This makes it difficult to study its toxicity. According to our knowledge, only one paper is available in literature for the QSAR of ILs toxicity. Ranke et al. (2004) investigated the biological effects of imidazolium ionic liquids with varying chain lengths in acute *Vivrio fischeri* and WST-1 cell viability assays, in which the clear influence of the alkyl chain length on toxicity was quantified by linear regression analysis. In our study, we determined the partition coefficient of ILs (K_{ow}), the electrophilicity of cations and anions of ILs (E_{LUMO}), as well as the 50% effective inhibition concentration in 48 hours ($EC_{50\text{-}48hr}$). Based on this limited data, we built a QSAR model to predict the toxicity of ILs, and causally have an insight into the relationship of toxicity and ions. This is the first trial to use QSAR modeling to predict toxicity of ILs.

6.2 Materials and Methods

6.2.1 Chemicals

The ILs used in this study include two series: one is 1-methoxyethyl-3-methyl imidazolium ($[MOEMIM]^+$) based ILs; the other is 3-methy-1-butyl imidazolium

($[BMIM]^+$) based ILs. Both have with a variety of anions, including $[BF_4]^-$, $[PF_6]^-$, $[CF_3COO]^-$, $[OMS]^-$ and $[Tf_2N]^-$. All of the ILs were synthesized and purified in our lab. The synthesis methods have been illustrated in Chapter 2.

6.2.2 Bacterium

Toxicity data ($EC_{50\text{-}48hr}$) was obtained from the bacterium *clostridium* sp.

6.2.3 Descriptors used in QSAR modeling

6.2.3.1 Partition coefficients of ILs in 1-octanol/water (K_{ow}). The octanol-water partitioning coefficient is a physicochemical descriptor that is widely used in QSARs. Octanol is used to mimic properties of the cell membrane. K_{ow} indicates the ability of a chemical to partition between the aqueous phase and the cell membrane. K_{ow} is the most important parameter related to biological activity. The higher the K_{ow} value, the stronger the hydrophobicity, and therefore the easier a compound is bioconcentrated in an organism.

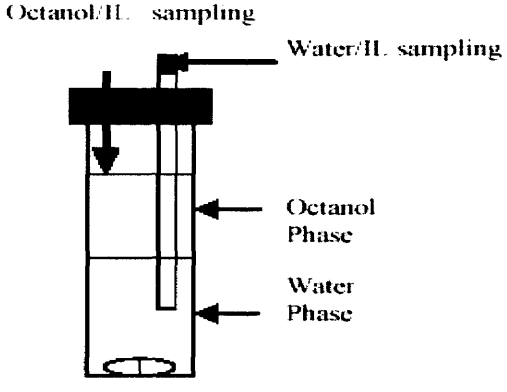

Figure 6.1. Apparatus for K_{ow} measurement.

K_{ow} is determined by slow-stirring method, which is a direct method for measuring K_{ow}. This method yields accurate results over a wide range of values (without the need for complex equipment). The experiment apparatus was configured as shown in Figure 1. 10μl of the IL was added to 5ml of water saturated with octanol in a 40ml vial.

After the ionic liquid was completely dissolved, 5ml of octanol saturated with water was slowly added to this vial in order to minimize the stagnant diffusion layer between the phases while preventing emulsification. Then the vial was sealed tightly to prevent the evaporation of water and octanol. The vials were shaken slowly in a shaker to prevent emulsification and were maintained at room temperature. Samples were taken from the octanol phase by penetrating the septum with a syringe. Samples were withdrawn from the water phase using a syringe inserted directly through the tubing into the aqueous phase in order to prevent octanol contamination (see Figure 6.1.). Sampling ceased when the concentrations in both phases stabilized. The concentrations of IL in each phase were measured by UV-vis spectrometry at 212nm wavelength. To ensure that the measured absorbance was below 1, samples taken from the vials were diluted if necessary. The K_{ow} value was obtained by dividing the concentration of IL in octanol by the concentration of IL in water.

6.2.3.2 The lowest unoccupied molecular orbital (E_{LUMO}). E_{LUMO} is indicative of the electrophilicity of chemicals. It appears as directly proportionate to the electronic affinity of the compound. This may play an important role in the re-ox reaction between the chemical and the cell membranes. The lower the E_{LUMO} values, the stronger the electrophilicity (Wang et al., 1981). All E_{LUMO} values were calculated by quantum

chemical software, Spartan '02, using equilibrium geometry at ground state with the semi-empirical AM1 molecular orbital method.

As we mentioned before, ionic liquids differ from molecular solvents in that they consist only of ions. We cannot calculate the E_{LUMO} of the ionic compounds as we calculate the E_{LUMO} of whole organic molecules. In order to use QSAR modeling, the E_{LUMO} of the cation and anion has to be calculated separately.

6.2.3.3 Toxicity data ($EC_{50\text{-}48hr}$). For each IL, five concentration gradients were carried. The space in the concentrations between the gradients was variable, depending on the toxicity. Two replicates were used for each concentration and control. An aliquot of IL was added to culture the medium and reach equilibrium. 2ml of bacterium culture in a logarithmic growing period was inoculated into a 40ml culture medium in a glove box under anaerobic conditions. This was then incubated in the incubator. The temperature was 25±2°C. After 48 hours, the optical density of each sample was measured by UV-vis at 600nm.

In order to calculate the $EC_{50\text{-}48h}$ of each IL, a regression equation of the cell number as a function of the IL concentration must be obtained. The cell number can be found by directly counting the cells under a fluorescent microscope. To simplify the task of cell counting, a regression equation of the cell number as a function of the optical density is determined. In this way the number of cells can be calculated indirectly.

A BC1 medium without ILs was used to determine the relationship between the optical density and cell number. After inoculation, about 3ml of the sample were withdrawn at different intervals until 48 hours. After the optical density for each sample was determined, 0.5ml of aldehyde was added to kill the bacteria and prevent further

growth. Then bacteria was filtered onto a 0.25um film and dyed with a fluorescent chemical. The cell number was counted and calculated by direct counting method under fluorescent microscopy.

The regression curve and equation were both obtained by excel and shown in Figure6.2. The R^2 was 0.969, indicating the fitting is good. With this regression equation, we could then easily obtain the cell number by simply measuring the optical density and calculating.

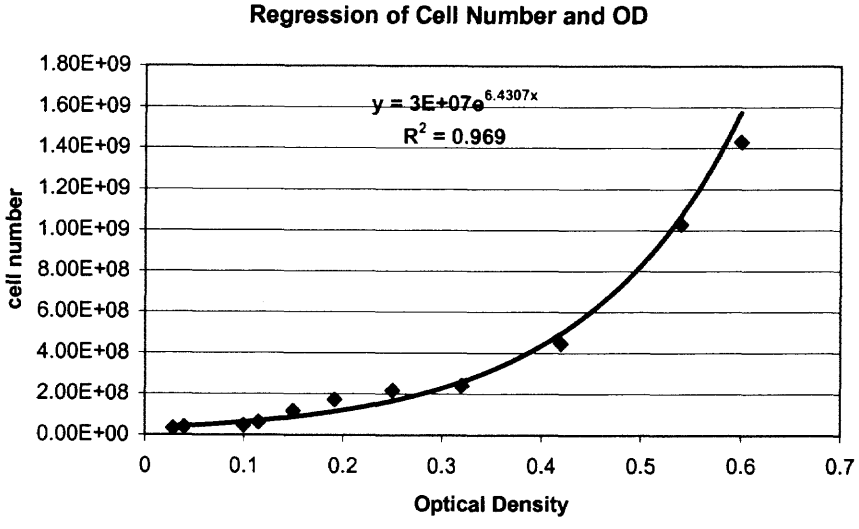

Figure 6.2. Regression analysis of cell number and optical density.

6.2.3.4 Statistic Analysis. Multiple linear regression models were gained using MINITAB 15. Log($1/EC_{50\text{-}48hr}$) values reported as mill moles were used as the dependent variable, while log(K_{ow}) and E_{LUMO} acted as independent variables.

$$\log(\frac{1}{EC_{50}}) = a\log K_{ow} + bE_{LUMO} + c$$

6.3 Results and Discussion

6.3.1 K_{ow} values

K_{ow} values were shown in Table 1 above. Different ionic liquids possess different K_{ow} values. Basically they can be classified into two groups: hydrophobic ILs and hydrophilic ILs. Of all the ILs studied here, ILs with $[PF_6]^-$ or $[Tf_2N]^-$ anion are hydrophobic, while ILs with $[BF_4]^-$, $[CF_3COO]^-$ and $[OMS]^-$ are hydrophilic. It is obvious that the hydrophobic ILs have a larger K_{ow} than hydrophilic ILs. For instance, the K_{ow} of BMIMTfN is as large as 0.667, while the K_{ow} of [MOEMIM][OMS] is only 0.0406.

Table 6.1. Partition Coefficient of Ionic Liquids

[MOEMIM][BF_4]	[MOEMIM][PF_6]	[MOEMIM][CF_3COO]	[MOEMIM][OMS]	[MOEMIM][Tf_2N]
0.066	0.218	0.067	0.052	0.284
$BMIMBF_4$	$BMIMCF_3COO$	BMIMOMS	$BMIMPF_6$	$BMIMTf_2N$
0.08	0.095	0.0406	0.4	0.667

6.3.2. E_{LUMO}

E_{LUMO} values of cation and anion of ILs were calculated by Spartan'02 (Wavefunction Inc.), and the results are exhibited in Table 6.2.

Table 6.2. Energy of Lowest Unoccupied Molecular Orbital of Ionic Liquids/ev

$[BMIM]^+$	$[MOEMIM]^+$	$[BF_4]^-$	$[PF_6]^-$	$[CF_3COO]^-$	$[OMS]^-$	$[Tf_2N]^-$
-4.53	-4.29	10.3	7.9	6.87	6.32	0.76

It is noted that E_{LUMO} was negative for cation while positive for anion.

6.3.3 $EC_{50\text{-}48hr}$

The regression curve for each ILs was exhibited in Figure 6.3.

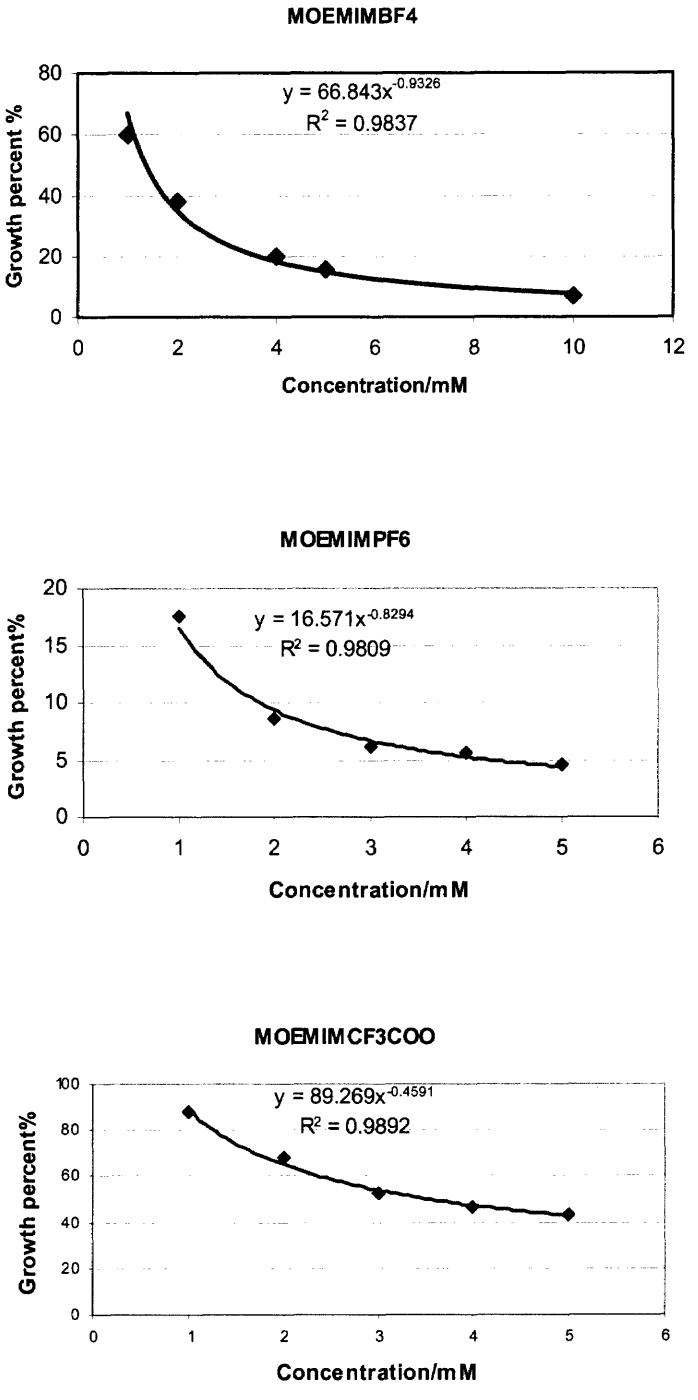

Figure 6.3 Regression curve of growth percentage against IL concentration.

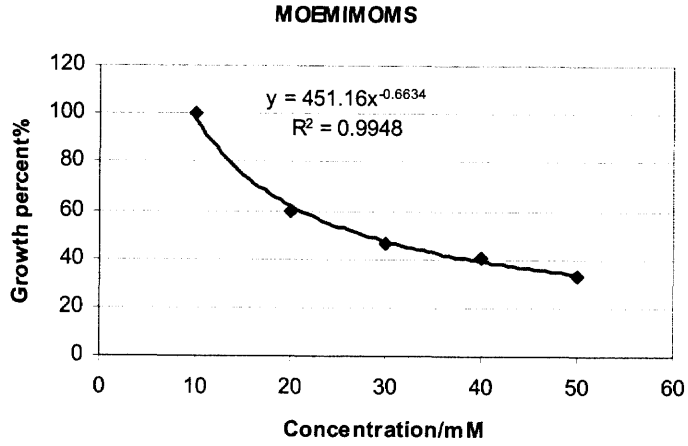

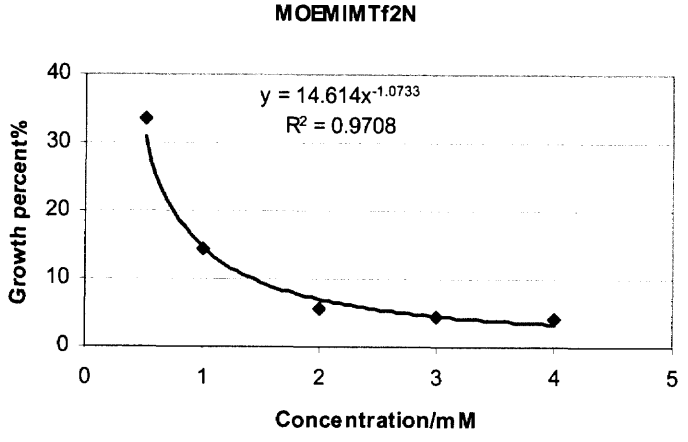

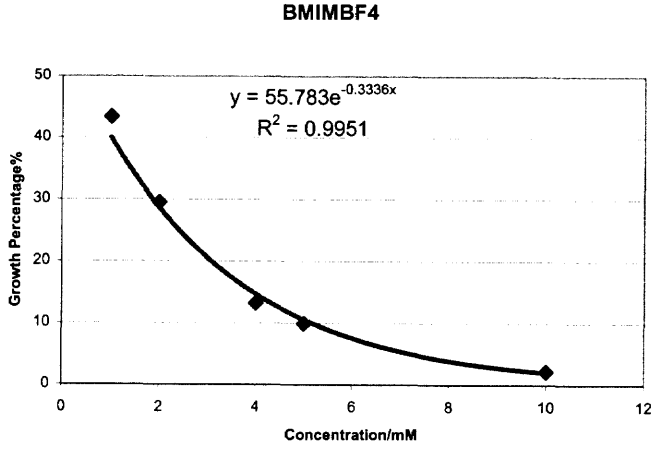

Figure 6.3 Regression curve of growth percentage against IL concentration (continued).

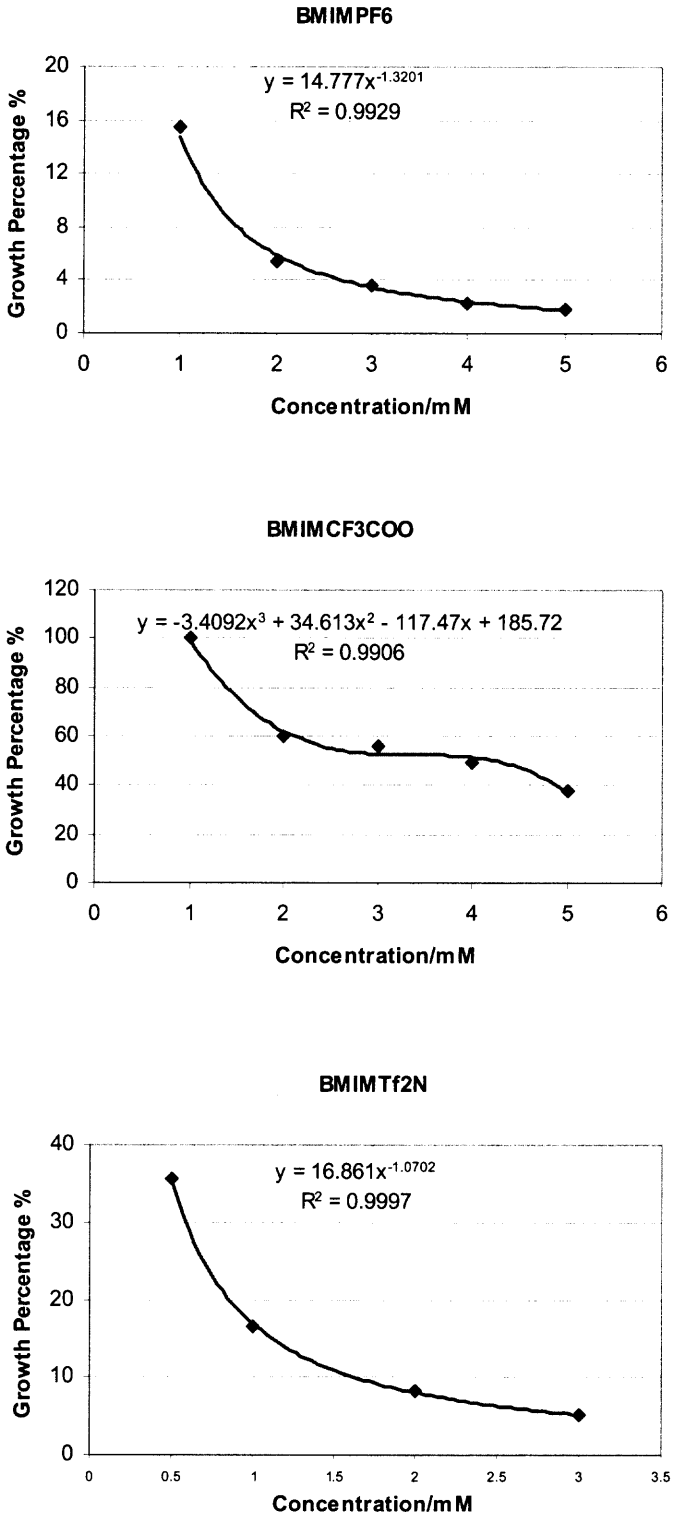

Figure 6.3 Regression curve of growth percentage against IL concentration (continued).

$EC_{50\text{-}48h}$ of each ILs is given in Table 6.3.

Table 6.3 $EC_{50\text{-}48h}$ of Ionic Liquids (mM)

[MOEMIM][BF_4]	[MOEMIM][PF_6]	[MOEMIM][CF_3COO]	[MOEMIM][OMS]	[MOEMIM][Tf_2N]
1.36	0.26	3.52	27.54	0.312
$BMIMBF_4$	$BMIMPF_6$	$BMIMCF_3COO$	BMIMOMS	$BMIMTf_2N$
0.328	0.397	4	20.45	0.36

6.3.4 QSAR Modeling of [MOEMIM]-Based ILs

The correlation between toxicity and hydrophobicity was examined and described in equation (6.1):

$$\text{Log}(1/\text{EC}_{50\text{-}48h}) = 1.88 + 2.15\log(K_{ow}) \qquad (6.1)$$

$$n = 5, \quad R^2 = 76.5\%, \quad s = 0.467, \quad F = 9.75, \quad P = 0.05$$

- n: the number of samples.
- R^2: Percentage of response variable variation that is explained by its relationship with one or more predictor variables. In general, the higher the R^2, the better the model fits your data. R^2 is always between 0 and 100%.
- s: The square root of the mean square of error that indicates the uncertainty in QSAR. It is the standard deviation of the data about the regression line.
- F: Mean square ratio
- P-value: Determines the appropriateness of rejecting the null hypothesis in a hypothesis test. P-values range from 0 to 1. The smaller the p-value, the smaller the probability that rejecting the null hypothesis is a mistake. Before conducting any analyses, determine your alpha (α) level. A commonly used value is 0.05. If the p-value of a test statistic is less than your alpha, you reject the null hypothesis.

In regression equation (6.1), R^2 is 76.5%, which indicates the predictor ($\log(K_{ow})$) explains 76.5% of the variance in toxicity. The P-value is 0.05, indicating the model is significant at a α-level of 0.05. In another words, the K_{ow} value plays an important role in toxicity of ILs.

The linear relationship between toxicity and electrophilicity was also examined and described in equation (6.2).

$$\text{Log}(1/\text{EC}_{50\text{-}48h}) = -0.149 - 0.009\, E_{\text{LUMO-ANION}} \quad (6.2)$$

$$n = 5,\ R^2 = 0.2\%,\ s = 0.961,\ F = 0.00,\ P = 0.949$$

Since all the ILs included in this model have the same cation, the E_{LUMO} of cation was skipped, and only E_{LUMO} of anion was included in modeling. In this model, R^2 is only 0.2%, and P is 0.949, indicating poor fitting of the data. This shows there is no linear relationship between toxicity and electrophilicity. As compared with E_{LUMO}, the K_{ow} contributes much more in the determination of the toxicity of ILs.

In addition, the linear relationship between toxicity and hydrophobicity as well as electrophilicity was examined and described in equation (6.3).

$$\text{Log}(1/\text{EC}_{50\text{-}48h}) = 1.83 + 2.81\ \log(K_{\text{ow}}) + 0.107\, E_{\text{LUMO-ANION}} \quad (6.3)$$

$$n = 5,\ R^2 = 89.8\%,\ S = 0.376,\ P = 0.102$$

As we can see, after taking both K_{ow} and E_{LUMO} into consideration in modeling, the R^2 increased to 89.8% compared with 76.5% in equation 1, indicating a better fitting of data.

6.3.5 QSAR Modeling of [BMIM]-Based ILs

The linear relationship between toxicity and hydrophobicity was examined. It is described in equation (6.4). R^2 is only 52.6%, indicating the fitting model is not so fitting.

$$\text{Log}(1/\text{EC}_{50\text{-}48h}) = 0.792 + 1.13\ \log(K_{\text{ow}}) \quad (6.4)$$

$$n = 5,\ R^2 = 52.6\%,\ S = 0.641\ ,\ F = 3.33,\ P = 0.165$$

Also the linear relationship between toxicity and electrophilicity was determined. It is shown here in equation (6.5).

$$\text{Log}(1/\text{EC}_{50\text{-}48h}) = -0.094 - 0.003\, E_{\text{LUMO-ANION}} \quad (6.5)$$

$n = 5,\ R^2 = 0.0\%,\ S = 0.931,\ F = 0.00,\ P = 0.981$

R^2 is 0.0%, showing the modeling doesn't fit the data at all, which means the linear relationship doesn't exist at all.

Finally, the linear relationship among the toxicity, hydrophobicity and electrophilicity was examined as shown in equation (6.6).

$$\text{Log}(1/\text{EC}_{50\text{-}48h}) = 0.356 + 1.61\ \log(K_{ow}) + 0.129\, E_{\text{LUMO-ANION}} \quad (6.6)$$

$n = 5,\ R^2 = 74.4\ \%,\ S = 0.577,\ F = 2.90,\ P = 0.256$

As compared with R^2 in equation (6.4), R^2 increased from 52.6% to 74.4%, This indicats that the model fit better after the two predictors were included.

6.3.6 QSAR Modeling of both [MOEMIM]-Based ILs and [BMIM]-Based ILs

In this part, MOEMIM based ILs and BMIM based ILs were put together to do the modeling.

Initially, the linear relationship between toxicity and hydrophobicity was examined.

$$\text{Log}(1/\text{EC}_{50\text{-}48h} = 1.08 + 1.40\ \log(K_{ow}) \quad (6.7)$$

$n = 10,\ s = 0.533\ \ R^2 = 57.9\%\ \ ,\ F = 11,\ P = 0.011$

Then, the correlation between toxicity and electrophilicity of anions was examined.

$$\text{Log}(1/\text{EC50}_{\text{-}48h}) = 0.019 - 0.0281\ \text{E}_{\text{LUMO-ANIION}} \quad (6.8)$$

$n = 10,\ s = 0.816\ \ R^2 = 1.4\%\ \ F = 0.12,\ P = 0.741$

Finally, both hydrophobicity and electrophilicity were considered to yield a linear regression equation (This included both $E_{LUMO\text{-}ANION}$ and $E_{LUMO\text{-}CATION}$).

$$\log(1/EC50_{-48h}) = 16.8 + 1.90\log(K_{ow}) + 0.104\ E_{LUMO\text{-}ANION} + 3.69\ E_{LUMO\text{-}CATION} \quad (6.9)$$

$n = 10,\ s = 0.498\ \ R^2 = 72.4\%,\ F = 5.24,\ \ P = 0.041$

Based on equation 6.7, 6.8 and 6.9, it can be concluded: (1) K_{ow} alone shows somewhat the linear relationship with toxicity. The R^2 and P-value are 57.9% and 0.011 respectively; (2) E_{LUMO} alone does not have a linear relationship with toxicity. Its R^2 value is only 1.4%; (3) The model fitting improves when both K_{ow} and E_{LUMO} are included in the model, in which the R^2 increases to 72.4% and P-value is 0.041.

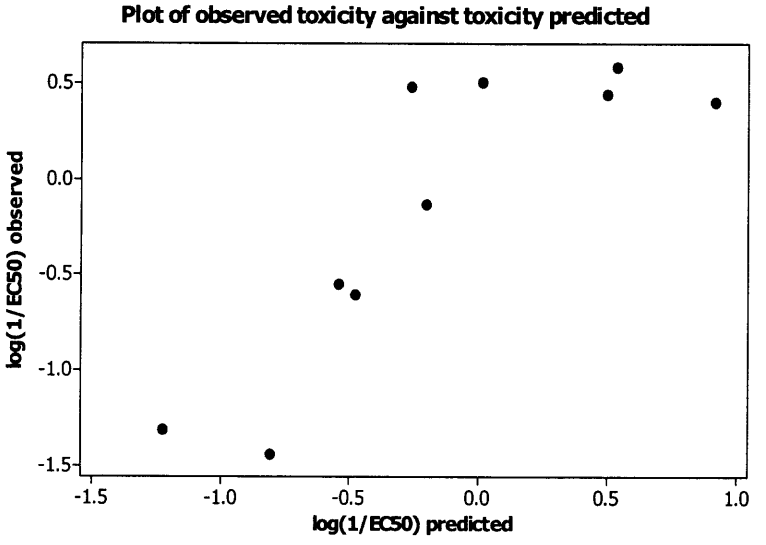

Figure 6.4 Plot of observed toxicity against toxicity predicted from equation 6.9.

The regression of both observed toxicity and predicted toxicity were calculated by equation 6.9. They are described in equation 6.10. The plot was shown in Figure 6.4 above.

$$\log(1/EC_{50\text{-}obs.}) = -0.003 + 0.999\log(1/EC_{50\text{-}pred.}) \quad (6.10)$$

$n = 10, s = 0.432 \quad R^2 = 72.4\%, F = 20.98, \quad P = 0.002$

R^2 is 72.4% and P is 0.002, indicating a good fitting between the observed and predicted toxicity.

6.4 Conclusion

A series of QSAR models are formed to predict toxicity ($EC_{50\text{-}48h}$), hydrophobicity (K_{ow}), and electrophilicity (E_{LUMO}). The results show that: 1) The K_{ow} values of ILs play an essential role in toxicity. These always show a linear correlation to $EC_{50\text{-}48h}$; 2) The E_{LUMO} alone doesn't have a linear relationship with toxicity since the R^2 is very low; 3) Better modeling can be obtained when the both K_{ow} and E_{LUMO} values are considered.

Since we only have a very limited resource of different kinds of ILs, we feel that these samples are not enough for an accurate fitting. If a greater number of varying ILs could be added to this kind of modeling, we feel a broader (and better) result would be obtained.

CHAPTER 7

BIODEGRADATION OF ETPYBF$_4$ IN PRESENCE OF URANIUM

7.1 Introduction

Ionic liquids are considered 'green' solvents because they possess many environmentally-friendly qualities. Most importantly they are said to be benign, non-volatile and recyclable. Therefore, ILs are potentially good alternatives for conventional organic solvents that are volatile and hazardous. The application of ILs in industry is promising. However, little is known about their toxicity, biodegradability, or their persistence and fate in the environment. Only a few studies on their biodegradation have been reported. Kumar et al. (2006) studied the biodegradation of BMIMBF$_4$ by soil microorganisms, waste water microorganisms and *E.coli*. They verified that BMIMBF$_4$ is biodegradable and identified the biodegradation products. Gathergood et al. (2004) designed new ILs containing ester or amide groups in the alkyl side chain, and studied their biodegradability. They demonstrated that the introduction of a group susceptible to enzymatic hydrolysis greatly improves the biodegradation as compared with the commonly used dialkylimidazolium ILs.

Zhang et al. (2006) in our lab studied the biodegradation of ethyl pyridium tetrafluoroborate (EtPyBF$_4$). She cultured a new bacterium from garden soil that displays an excellent ability to degrade this ionic liquid. EtPyBF$_4$ can be decomposed completely in 24 hours. The new cultured bacterium consists of gram positive rods, and has been identified as urealyticum by Accugen Laboratories, Inc. In this study, we are interested in how the biodegradation of EtPyBF$_4$ will be influenced in presence of uranium in solution.

7.2 Materials and Methods

7.2.1 Bacterium

The bacterium used in this study was cultured and isolated from garden soil. It is a rod-shaped, gram positive, aerobic bacterium, identified as corynebacterium urealyticum.

7.2.2 Culture Medium

A mineral salt medium (MSM) was utilized for the culture. It contained: K_2HPO_4, 1g/L; KCl, 0.25g/L; $MgSO_4 \cdot 7H_2O$, 0.25g/L; trace element solution, 1ml (Houghton et al.,1972). The trace element solution contained (per liter): $FeSO_4 \cdot 7H_2O$, 40mg; $MnSO_4 \cdot 4H_2O$, 40mg; $ZnSO_4 \cdot 7H_2O$, 20mg; $CuSO_4 \cdot 5H_2O$, 5mg; $CoCl_2 \cdot 7H_2O$, 4mg; $Na_2MoO_4 \cdot 2H_2O$, 5mg; $CaCl_2 \cdot 6H_2O$, 0.5mg; NaCl, 1g. Several drops of concentrated HCl were added to the solution to prevent precipitation. The final pH was adjusted to 6.5 with HCl or NaOH. 1L of MSM was dispensed to 25 125ml flasks with cotton plugs, and then autoclaved at 250F° for 30 minutes.

7.2.3 Ionic Liquid

$EtPyBF_4$ was synthesized in our lab according to the method afore described. It is a colorless liquid at room temperature and a portion of it crystallizes. In this study, it is used as the sole carbon and nitrogen source for growing bacteria.

7.2.4 Uranium

1,000ug/l uranyl nitrate standard solution was used as stock solution. The concentration studied here is 3.8ppm (0.016mM).

7.2.5 Methods

7.2.5.1 Sample preparation. Controls and samples are listed in the Table 7.1. Each control and sample was carried out in triplicate.

Table 7.1 Composition of Control and Sample

Control 1(**C1**)	Control 2(**C2**)	Control 3(**C3**)	Control 4(**C4**)	Sample(**S**)
U + MSM	U + MSM + EtPyBF4	U + MSM + Bacteria	MSM + $EtPyBF_4$ + Bacteria	U+MSM + $EtPyBF_4$ + Bacteria

A certain amount Uranium and an aliquot of 20ul of $EtPyBF_4$ were added to an elementary flask containing 40ml MSM. The final concentration of EtPyBF4 was 3.2mM and the concentration of U was 0.016mM. After equilibration, a 2ml culture at logarithm phase was transferred to the medium, and inoculated at 26.5 °C. 3ml of sample was withdrawn at intervals, and the optical density, UV-Vis absorbance, pH, HPLC and uranium concentrations in solution were measured.

7.2.5.2 Parameters to be determined.

- Optical density (OD) --- It is proportional to the amount of cells, measured at 600nm by UV-Vis spectrometer.
- pH --- pH change indicates the metabolism of bacteria.
- UV-Vis Spectrometry --- Degradation can be monitored by UV-Vis analysis. (The Pyridium ring has a characteristic absorbance at 259nm. After biodegradation, the ring will be broken down, due to the absorption's completion.).
- Electronic Spray Ionization Mass Spectrometry (ESI-MS) --- It can be used to identify the biodegradation products.
- High performance liquid chromatography (HPLC) --- Biodegradation products can be separated and monitored by HPLC. A Bio-rad organic acid analysis column was used here (300mm×7.8mm), with 0.003M sulfuric acid, there was flow rate of 0.7ml/min in mobile phase. Biodegradation products were monitored by UV detector at 210nm.

- Kinetic Phosphorescence Analysis (KPA) --- KPA was used to determine the U(VI) concentration in solution. KPA is a proven technique for rapid, precise, and accurate determination of uranium in aqueous solutions. 0.1ng/l determination limit can be reached by KPA.

7.3 Results and Discussion

7.3.1 Optical Density

Figure 7.1 displays the growth of bacteria along with the duration. The OD of C4 reached 0.25 after 70 hours. Bacteria in S also grew well, and OD reached 0.22, indicating that, at this concentration, uranium did not limit the bacterium's activity very much.

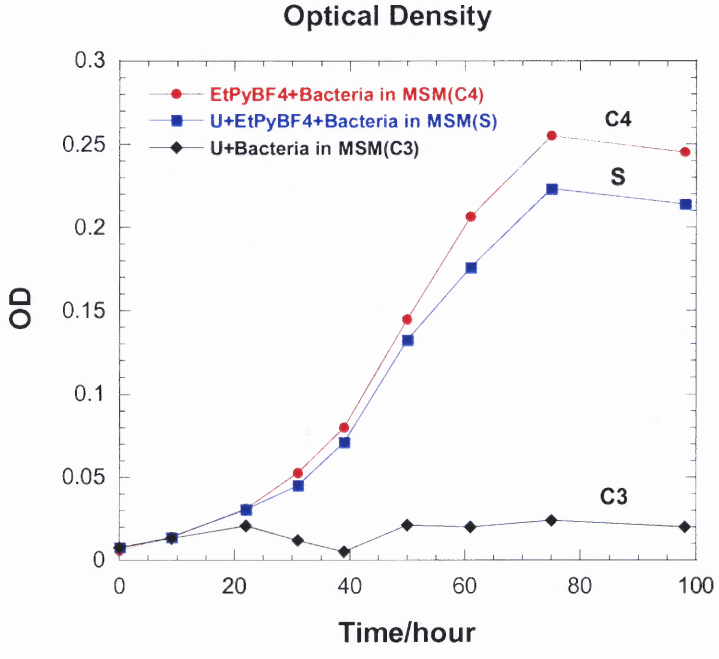

Figure 7.1 Optical density of bacteria growth.

It is noted that bacteria in C3 (without IL) also had a little growth and OD reached 0.02. This was because the 2ml culture transferred from previous culture contained a little bit of the carbon source; the carbon source was used by the bacteria for growth. However, because of the limited amount of the source carbon, a high OD was not reached.

7.3.2 UV-vis Absorption

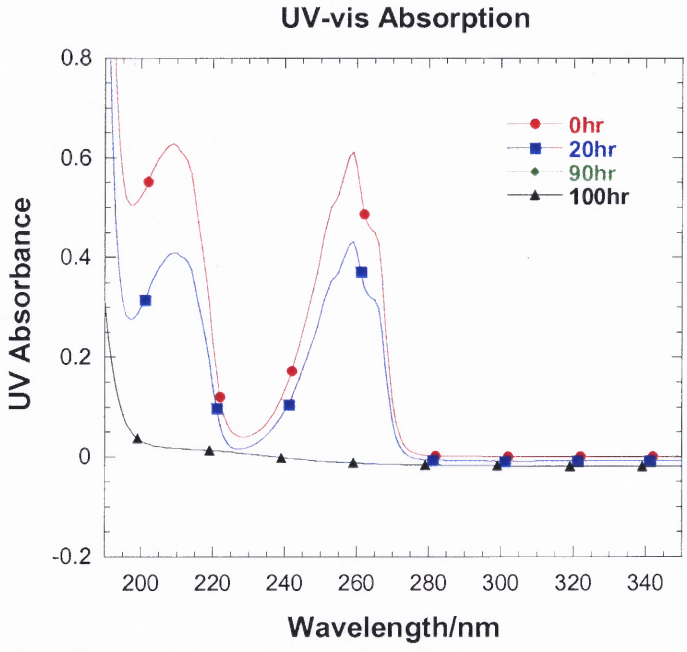

Figure 7.2 UV-vis spectroscopy of [EtPy][BF_4] at different times.

Figure 7.2 displays the UV absorption between 190-350nm during biodegradation. There are two characteristic absorptions, one at 210nm and the other at 259nm, resulting from the pyridium ring. The absorption was strong at the beginning, and then started decreasing. After 90 hours, the two absorptions disappeared, indicating the complete biodegradation of $EtPyBF_4$. Figure 7.3 shows the UV absorption at 259nm along with the time. It is clear that, without bacteria present, degradation did not take place. This was proved by the absence of UV absorbance changes in C2. The UV absorbance of S and C4 decreased in time, dropping to 0.05 after 98 hours. In addition, the UV absorption in S was almost the same as that in C4, indicating that bacteria activity in the presence of uranium was not affected much.

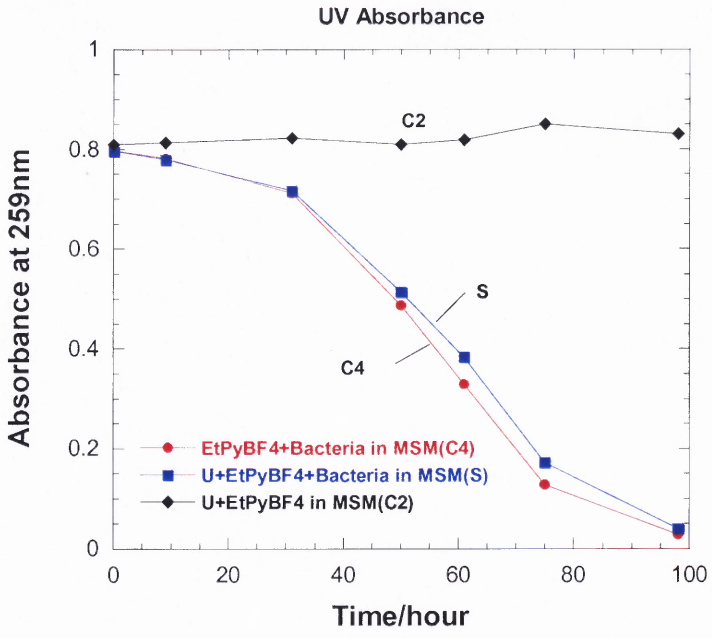

Figure 7.3 UV-vis absorbance of $EtPyBF_4$ at 259nm.

A Biodegradation percentage was calculated based on UV absorbance, and shown along with the OD in Figure 7.4. It is obvious that the OD increased with the disappearance of $EtPyBF_4$. At around 98 hours, the biodegradation reached 98%.

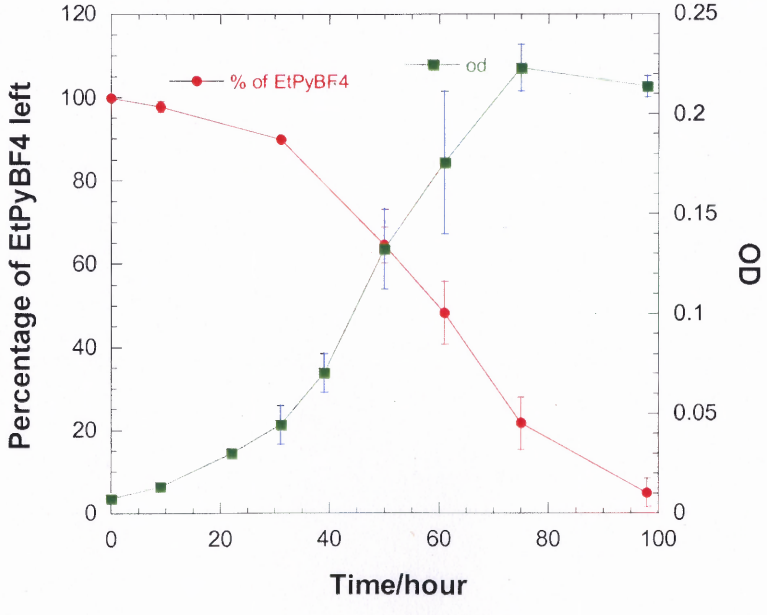

Figure 7.4 Degradation of EtPyBF4 and bacteria growth.

7.3.3 pH

Figure 7.5 shows the pH change during bacteria growth. A significant pH drop in both S and C4 was observed, from 6.5 to 4.6 after 100 hours, which indicated acids were released during biodegradation. Therefore the majority of the biodegradation products should be acids. No pH drop was found in C1 and/or C3 because no bacteria grew. A small pH change took place in C2, due to a small amount of bacteria growth, as described in 3.1.

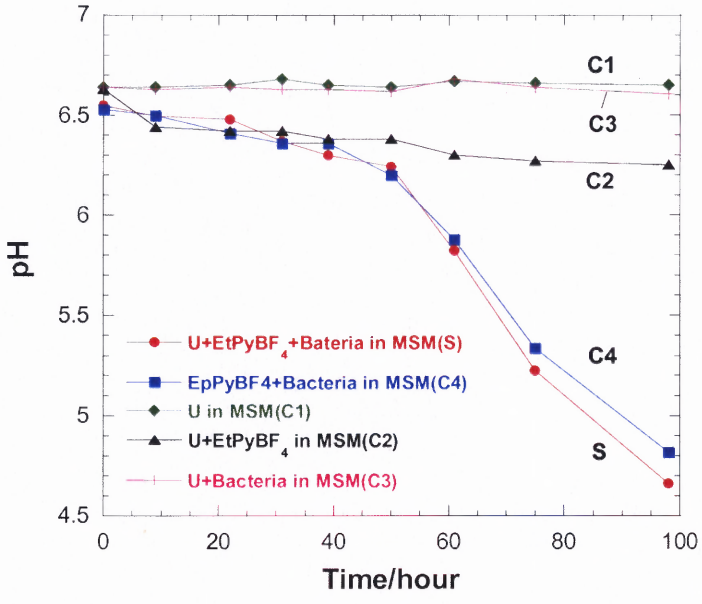

Figure 7.5 pH change during bacteria growth.

7.3.4 HPLC

After filtering by 0.45um filter paper, an aliquot of sample was injected to HPLC to determine the biodegradation products. The products that eluted out of the column at different retention times were plotted along with the inoculation times in Figure 7.6. The

pH change was also plotted. The Y1 represents the area account of peak. Y2 represents the pH.

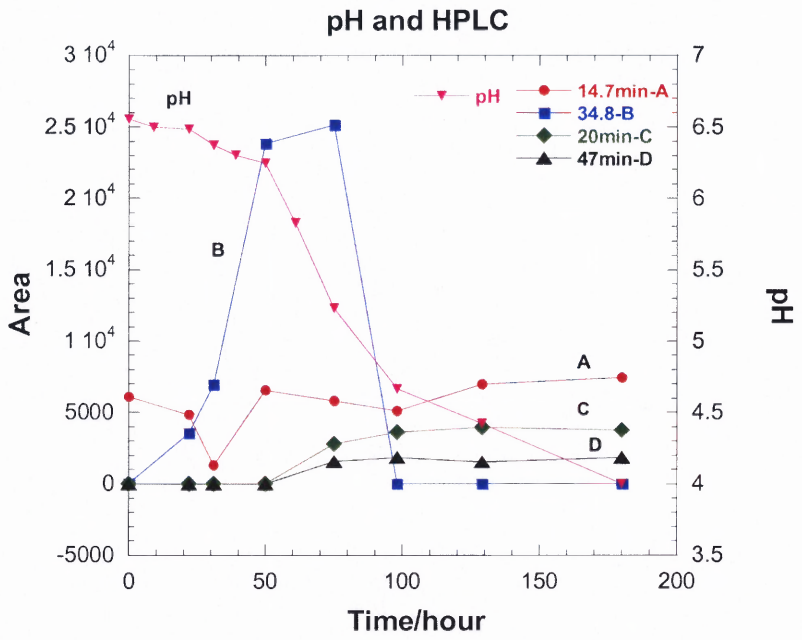

Figure 7.6 Peak area of biodegradation products and pH change as function of time.

At the beginning, there is only one peak showing at 5 min in HPLC, which is the peak of EtPyBF4 and some inorganic salts. These did not interact with the column and eluted out quickly.

After 20 hours, a peak at 34 min appeared, and the area increased gradually, reaching its maximum at around 50 hours. Soon thereafter, however, the 34-min peak started to drop, and in about 75 hours disappeared completely. Throughout, new peaks appeared and increased gradually (20.5min, 24min, 48min and 19min respectively).

We hypothesize that the 34-min peak was a major intermediate resulting from first-step biodegradation. The bacteria first used $[EtPy]^+$ as their carbon and nitrogen sources to produce this intermediate. After all the $[EtPy]^+$ was consumed, the bacteria then started to utilize the intermediate as their carbon and nitrogen sources, further

degrading it into the other smaller molecules. The final products are supposed acids since the pH decreased substantially.

7.3.5 Uranium in Solution

The U concentration added to the medium was 0.016mM (3.8ppm), while the concentration of $EtPyBF_4$ was 3.2mM. The ratio of U to EtPyBF4 was 1:200. However, after reaching equilibrium but before adding bacteria, the uranium concentration in S was just about 7.5ppb, and no concentration for C1, C2 and C3 was detectable.

As we know, the mineral salt medium contained high levels of concentrated phosphate with a pH of 6.5. Under these circumstances, most of the uranyl nitrate formed uranyl phosphate and hydroxide. These precipitated out or suspended in solution, due to the very low solubility of the uranium salts.

Uranium speciation in this condition was determined by **PHREEQC.** The result revealed part of U precipitated out as $(UO_2)_2(PO_4)_3 \cdot 4H_2O$ and $Mg(UO_2)_2(PO_4)_2$. In the solution, the major uranium species were $UO_2PO_4^-$ and UO_2HPO_4.

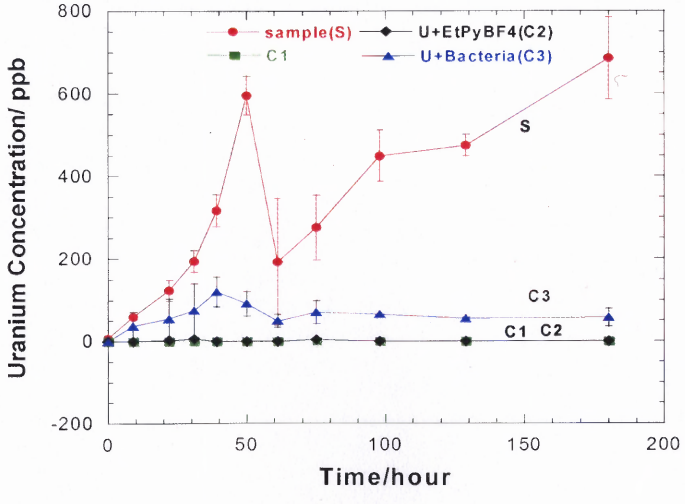

Figure 7.7 Uranium concentration in solution.

Figure 7.7 displays the change of U concentration in time. The error bar is also shown. Throughout the duration of the experiment, there was no detectable uranium in C1 and C2, indicating the concentration was below 0.1ppb (the detect limitation for KPA).

In C3, there was no uranium detected by KPA at 0 hour. However, after some time, part of the uranium came back to the solution, and the concentration stayed almost constant all the time. This was because some bacteria still grew here, drawing on the trace amount of carbon sources from the transferred culture. Due to bacteria activity, a small amount of acid may be produced during metabolism, leading to the increased solubility of the uranium.

However, in the S, from 0 to 50 hours, the U concentration first increased (from 7.5ppb to 600ppb), and then dropped quickly (to 200ppb) in the next 10 hours. After that, it started to gradually increase again, reaching around 700ppb after 180 hours.

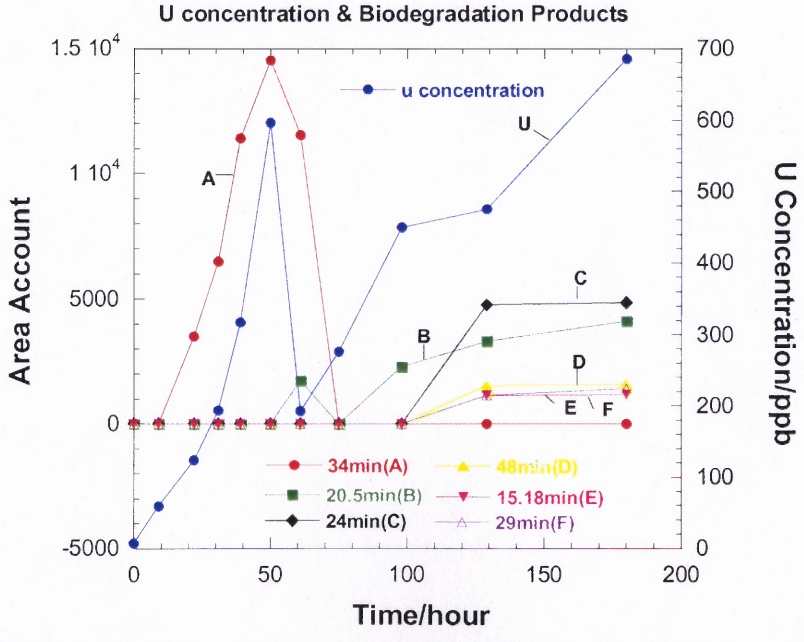

Figure 7.8 Biodegradation products determined by HPLC and the U concentration in solution.

HPLC and U concentrations were plotted together in Figure 7.8. It is noteworthy that during the first 70 hours, the increase and decrease of U concentration coincided with the appearance and disappearance of the 34-min peak in HPLC. Before 50 hours, both increased, while after 50 hours, both decreased and finally disappeared. We hypothesize that the increase of U in solution resulted from the 34-min intermediate. The mechanism could be explained by the formation of a complex. As we know, many organic compounds can form a complex with uranium, leading to a solubility change in an aqueous phase.

At the beginning, most of the U existed in precipitate in the form of phosphate and hydroxide. After 34-min, the intermediate was generated; it could form a strong complex with uranium, and attract the U from the phosphate and hydroxide salts, causing the re-dissolution of U into the solution.

In order to determine a possible complex formed between U and the intermediate, LC-ESI/MS was used to identify the intermediate that eluted out at 34 min from HPLC. The mass spectrum was shown in Figure 7.9.

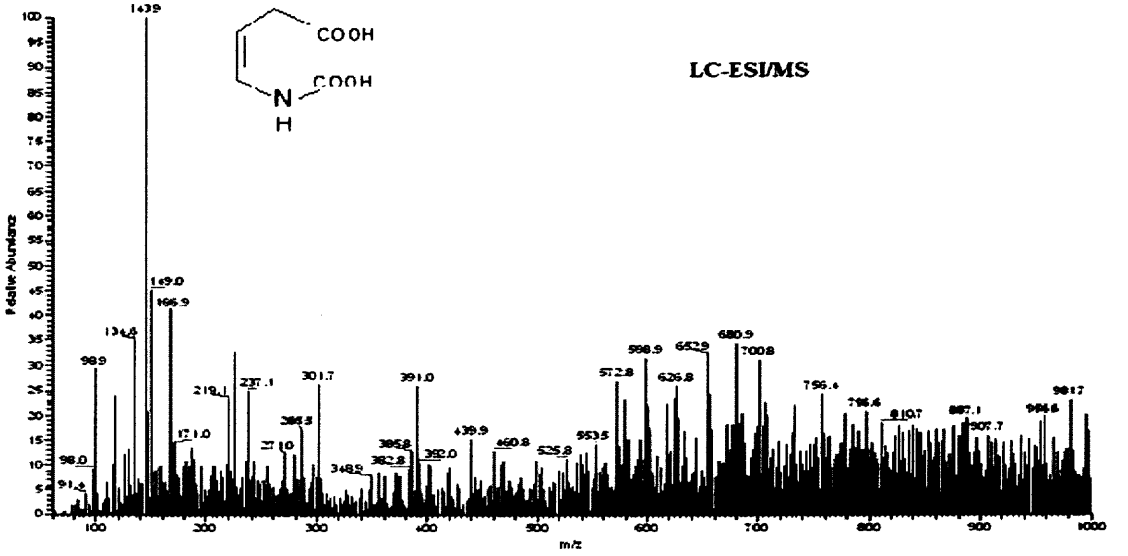

Figure 7.9 LC-MS analysis of intermediate.

The intermediate was identified to be 4-(carboxyamino)butyl-3 enoic acid, whose molecular weight was 145. It has to be mentioned that normally, in the ESI-MS, the m/z value is ± 1 of the actual molecule weight because of the gaining or losing of one H^+. An MS sample at 50 hours was completed to see if any complex molecule formed.

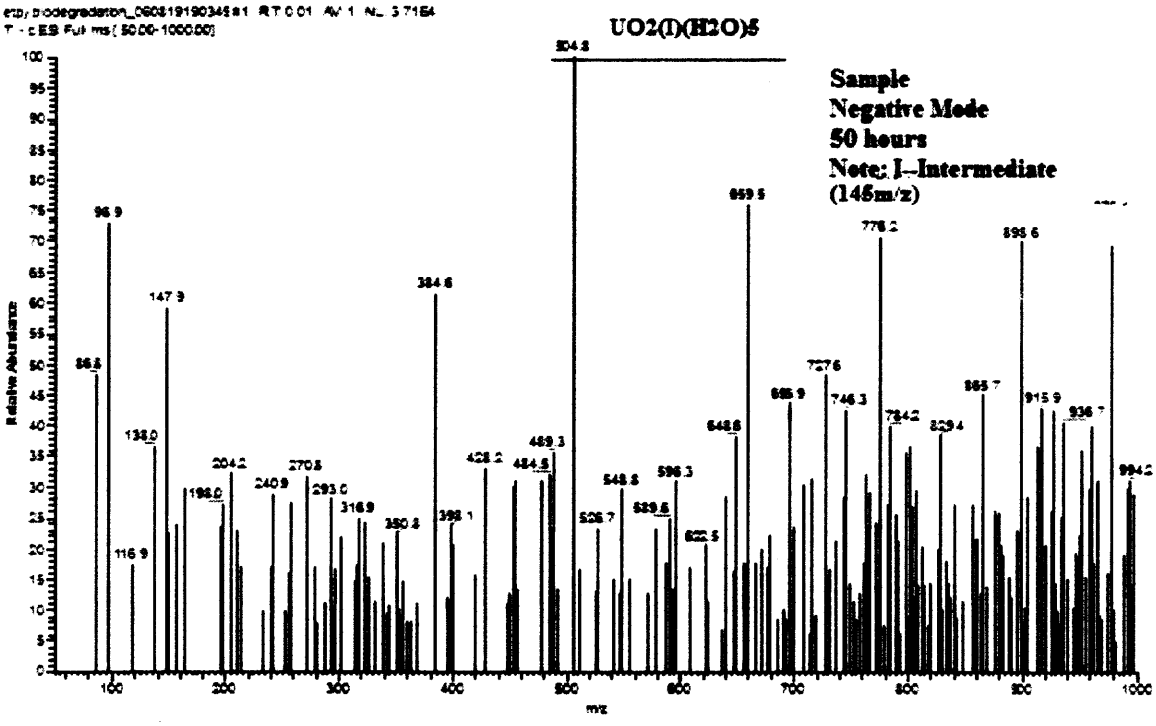

Figure 7.10 Mass spectrum of 50-hour degradation products in negative mode.

The base peak at 505(m/e) was found in mass spectrum, corresponding to complex molecule UO_2(Intermeidate)$(H_2O)_5$, proving the complexation between UO_2^+ and the 34-min intermediate.

In Figure 7.8, after 50 hours, the 34-min intermediate peak started decreasing due to the further degradation by bacteria and disappeared completely at 75 hours. As a result, the uranium complexed with the intermediate was released again. However, this time, the pH was still as high as 6, therefore, this released uranium then reformed uranium

phosphate and hydroxide which again precipitated out of the solution, leading to the decrease of uranium concentration.

Additionally, some new peaks appeared such as 20.5-min, 24-min and 48-min peaks, following the disappearance of the 34-min peak, and increased gradually. With the generation of new biodegradation products, the U in solution started increasing again, reaching 700ppb after 180 hours. Also, the pH dropped to about 4.5. This re-increase of U in solution could be due to the pH decrease resulting from the production of acidic molecules from biodegradation. As a result, the solubility of uranium salts increased with the pH decrease.

7.3.6 Effects of BF_4^- anion on U Solubility

The ratio of U to BF_4^- in solution was 1:200. The concentration of BF_4^- was much higher than the concentration of U. U could form a complex with $EtPyBF_4$, and maintain more uranium in solution. This has been illustrated by prior studies.

In this study, however, in the presence of a phosphate with a pH under 6.5, a complex with uranium was more apt to form precipitate due to the very low solubility. This is why there was no detectable uranium in the solution at the beginning (even if there was much BF_4^- present). In addition, the increase of U in solution was contributed to the organic acids produced by bacteria instead of the complexation with BF_4^-, thus indicating the organic acids generated here have a stronger affinity to uranium than to BF_4^-.

7.3.7 Mass Spectrometry

Mass spectra of the sample at different times are displayed in Figure 7.11. At the beginning, in positive mode, the two major peaks were 108(m/e) and 80(m/e), corresponding to $[EtPy]^+$ and pryidium cation after losing the ethyl group, respectively.

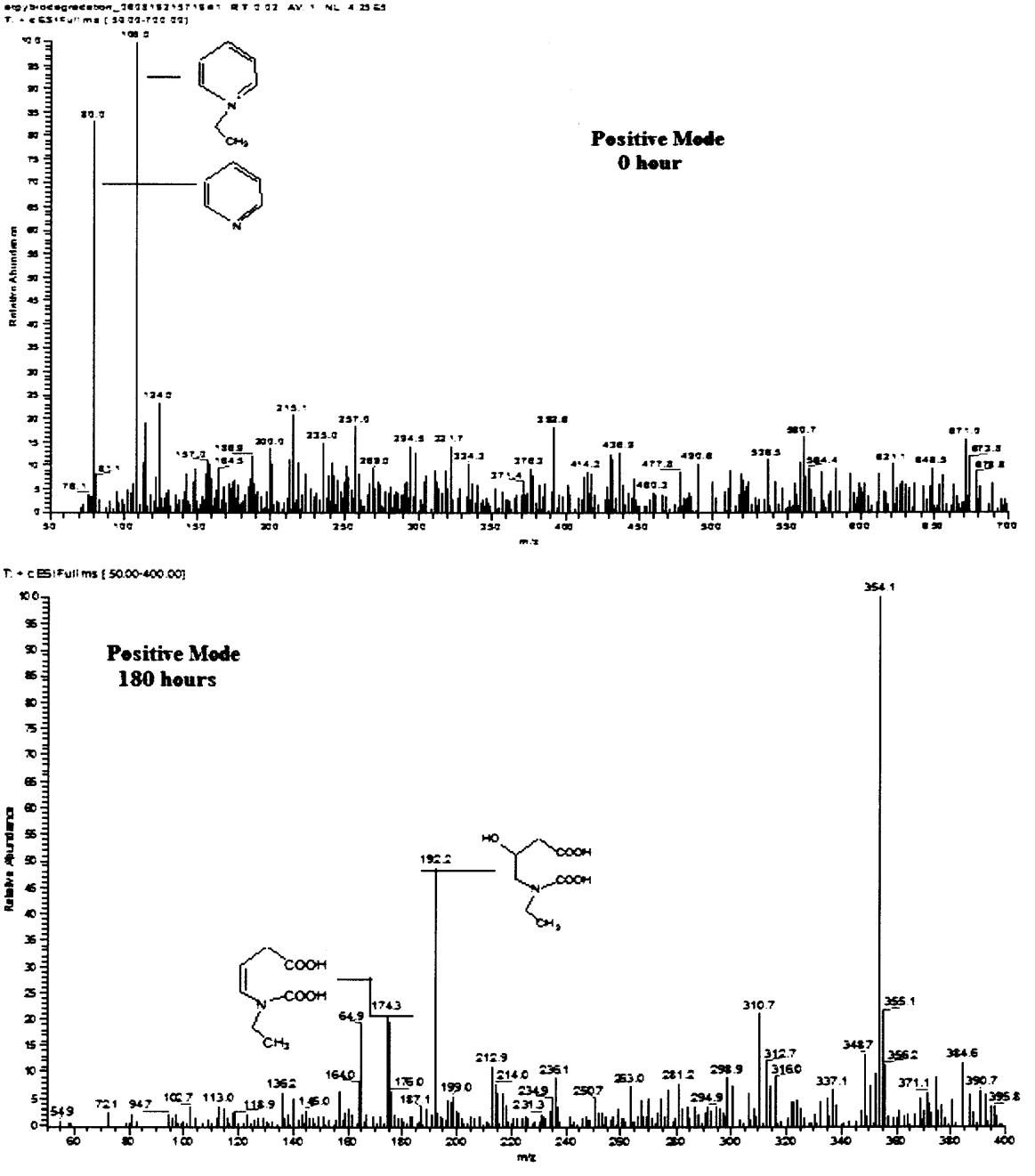

Figure 7.11 Mass spectroscopy of degradation products in positive mode.

Peak 108(m/e) and 80(m/e) disappeared after 180 hours; while a new peak at 354(m/e) then became the base peak. This peak couldn't arise from the complex between uranium and biodegradation products since it had also appeared in the control that didn't contain uranium. It may have resulted from the products associated with the bacteria's metabolism. Furthermore, it was not one of the biodegradation products because its molecular weight exceeded too far beyond 108. Another two major peaks were 192(m/e) and 174(m/e). They were the biodegradation products from $[EtPy]^+$, shown in Figure 7.11.

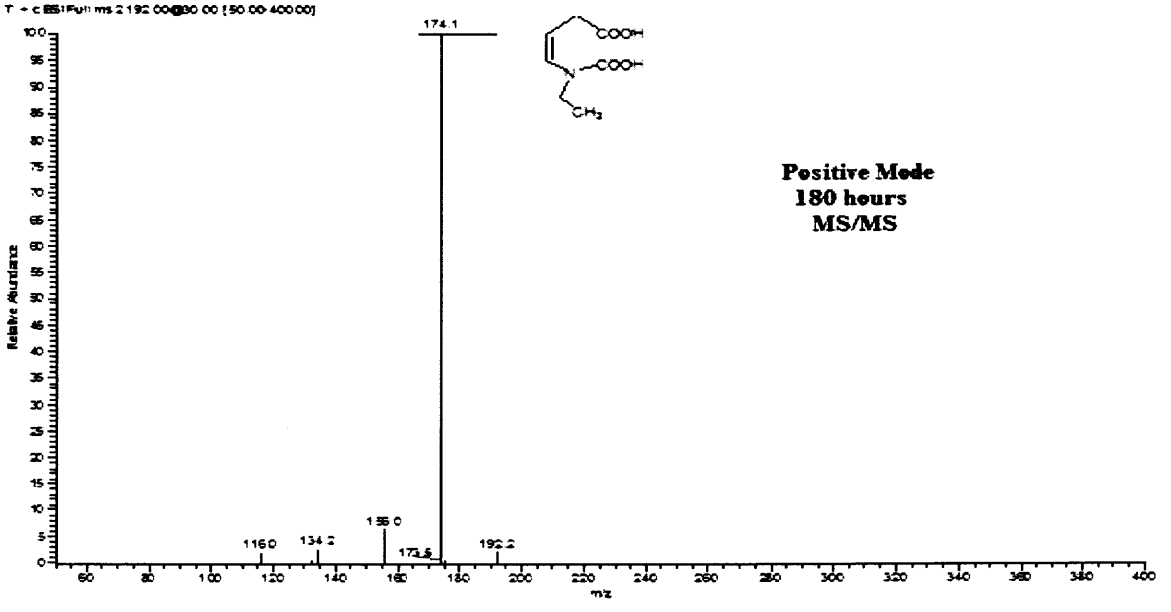

Figure 7.12. MS/MS analysis of 192 (m/e) at 30% collision energy.

MS/MS of peak at 192(m/e) at 30ev is displayed in Figure 7.12. Obviously, the peak at 174(m/e) came from 192(m/e) with an OH group lost.

Figure 7.13 displays the MS range of 50-200(m/z) after 180 hours. Many acids with small molecular weight were found, confirming that the major final biodegradation products were acids.

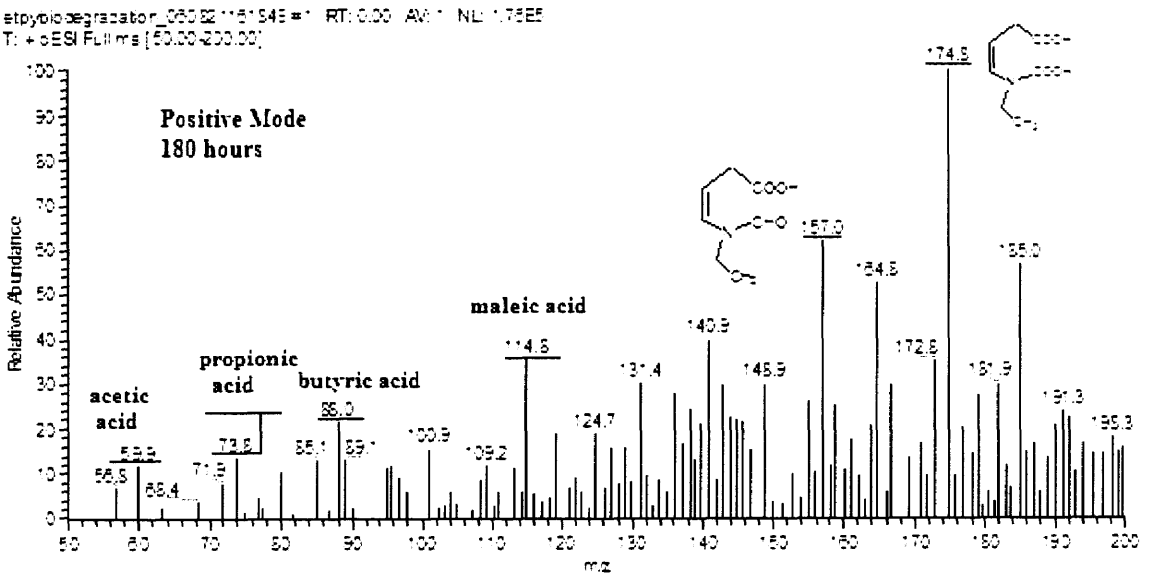

Figure 7.13 Mass spectrum of degradation products between 50-200(m/e) in positive mode after 180 hours.

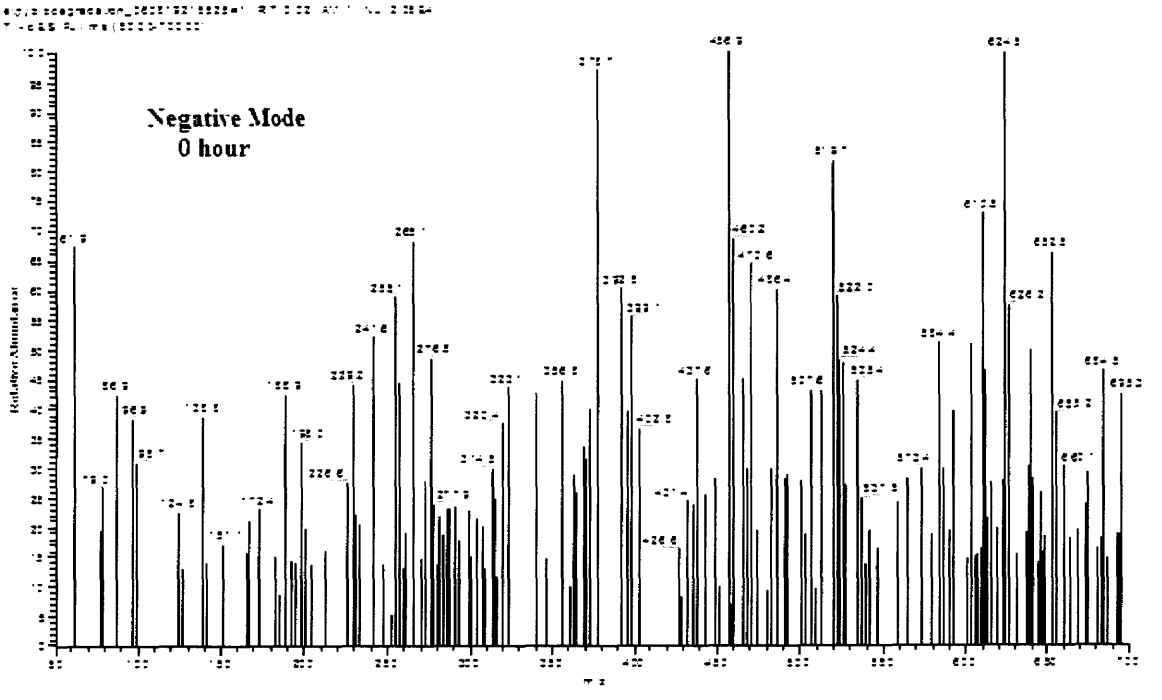

Figure 7.14 Mass spectra of degradation products in negative mode.

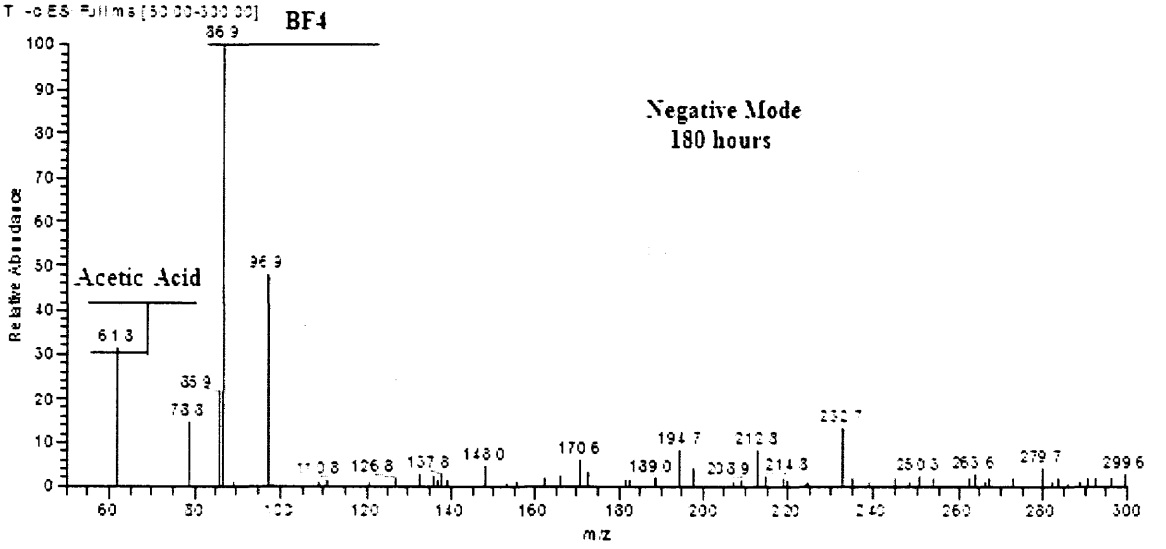

Figure 7.14 Mass spectra of degradation products in negative mode (Continuted).

At the beginning, there were many peaks present due to the salts in the medium. After 180 hours, $BF4^-$ (which can not be degraded) was prevalent in negative mode. However, acetic acid was found at peak 61.8(m/e), indicating it was one of the final biodegradation products formed.

7.3.8 Degradation Pathway

Based on the MS, a possible degradation pathway has been suggested in Figure7.15 (b).The initial degradation started by the opening of the ring between C2 and C3 during oxidation. This step happened quickly. Then one ethyl group connected to the heterocyclic nitrogen was lost, forming the intermediate product. This also happened fast. The next step, however, carried out very slowly. The intermediate first accumulated in the medium reaching its maximum. It then started to further degrade by losing NH_3 and HCOOH to produce maleic acid. The maleic acid continued to degrade generating other smaller acidic molecules like acetic acid, propionic acid and butyric acid.

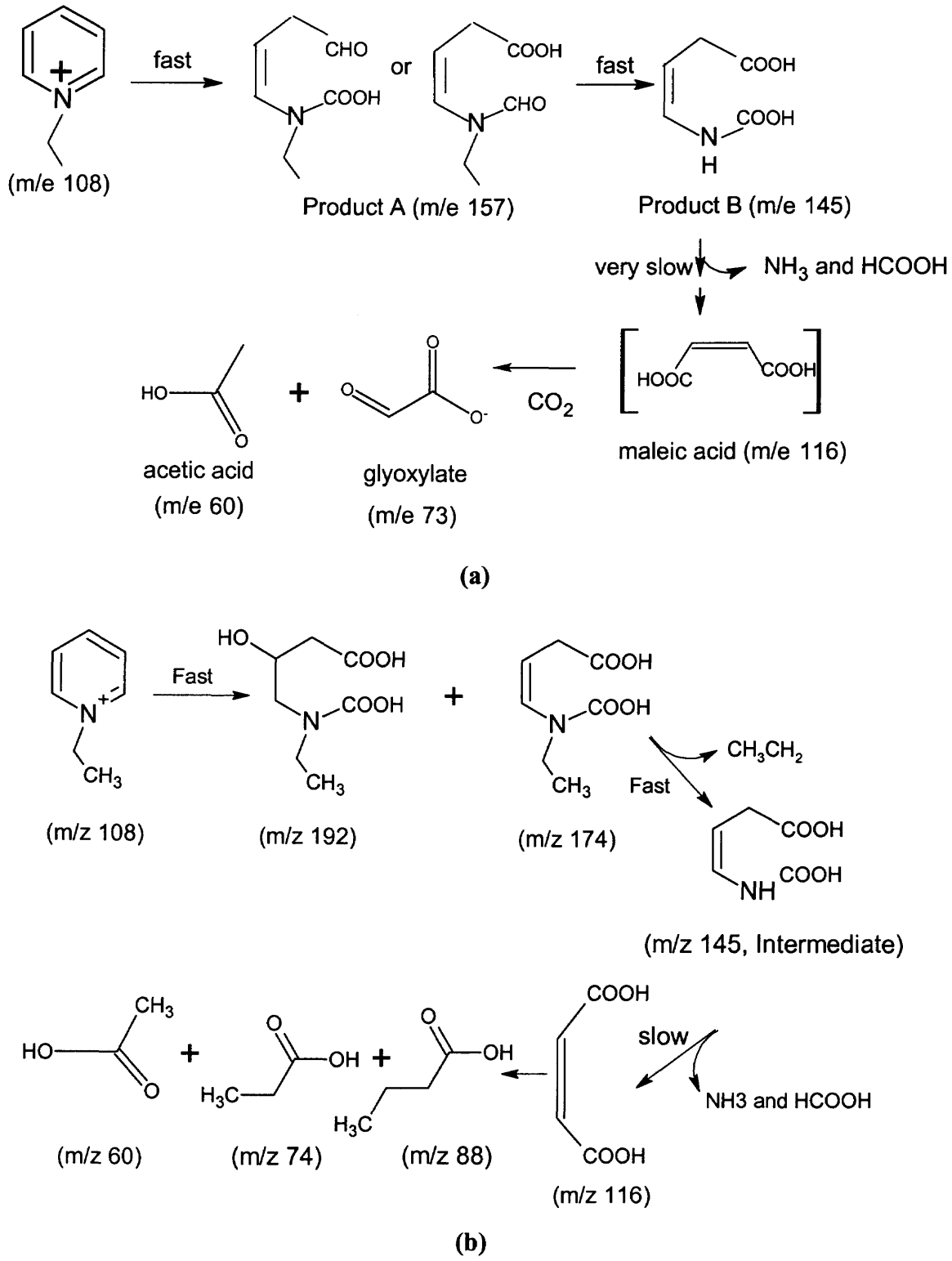

Figure 7.15. Suggested Degradation Pathway: (a) citied from Zhang (2006); (b) from this study.

In another research, Zhang (2006) has studied the biodegradation pathway of [EtPy][BF_4] in the absence of uranium, and proposed very similar pathway (Figure7.15(a)). Therefore, it can be concluded that the presence of uranium at this concentration level does not influence the biodegradation pathway.

7.4 Summary

[EtPy][BF_4] can be completely decomposed by urealyticum cultured from soil. Compared with the control containing no uranium, the presence of 0.016mM uranium doesn't exert much toxicity on bacteria; it still grows very well. At the beginning, there is no detectable uranium in solution as almost all the uranium exists in precipitate in the form of phosphate and hydroxide salts. During biodegradation, an intermediate is produced, which can form a strong complex with uranium, leading to the increase of uranium in solution. Once the intermediate is degraded, the uranium in the solution decreases and precipitates out again. With the production of other acids, the pH drops, and the uranium in solution increases again. The final biodegradation products are all organic acids including butyric acid, propionic acid and acetic acid. Moreover, the biodegradation path in presence of uranium is the same that Zhang (2006) has disclosed in the absence of uranium, indicating that uranium does not affect the pathway of biodegradation.

CHAPTER 8

CONCLUSIONS AND RECOMMENDATIONS

8.1 Conclusion

1. Six different ionic liquids were synthesized in this study, including 1-methoxyethyl-3-methyl imidazolium tetrafluoroborate ([MOEMIM][BF_4]), 1-methoxyethyl-3-methylimidazolium hexafluorophosphate ([MOEMIM][PF_6]), 1-methoxyethyl-3-methyl imidazolium trifluoro acetate ([MOEMIM][CF_3COO]), 1-methoxyethyl-3-methyl imidazolium bis-trifluoromethane sulfonamide ([MOEMIM][Tf_2N]), 1-methoxyethyl-3-methyl imidazolium mthane sulfonate ([MOEMIM][OMS]), and 3-methyl-1-(ethoxycarbonylmethyl) imidazolium acetate [MECOOMIM][CH_3COO]. They were characterized by UV-vis (UV-visible spectroscopy), FTIR (Fourier transform infrared spectroscopy), MS (mass spectroscopy) and NMR (nuclear magnetic resonance).
2. The interaction between uranium and ILs was characterized by UV-vis, titration, MS, EXANES (X-ray near edge spectroscopy), as well as EXAFS (extended X-ray absorption fine structure analysis). Of all these ILs, [MOEMIM][BF_4] demonstrates strong complexation with uranium, while others show weak or no complexation. The proposed uranyl complex associated with [MOEMIM][BF_4] is a monodentate.
3. Complexation of uranium with [MOEMIM][BF_4] enhanced the solubility of U(VI) and U(IV), and maintained most of the uranium in aqueous phase.

4. Complexation of uranium with [MOEMIM][BF_4] decreased the bioavailability of uranium, which resulted in the lower bioreduction of U(VI) to U(IV) by *clostridium* sp.
5. Comparison of the toxicity of various ILs disclosed that both the cation and anion play an important role. In the case of the same cation, the toxicity increases along with the increase of F atoms in the anion. That is to say, the more F atoms an anion contains, the more toxic it is. On the other hand, with the same anion, if a hydrophilic function group is present on the side chain (e.g. ether, ester, or a carboxylic group), the toxicity could be rendered less.
6. QSAR modeling was used for the first time to predict the toxicity of ILs. The linear regression equation was obtained as $\log(1/ LC_{50\text{-}48h}) = 16.8 + 1.90 \log(K_{ow}) + 0.104\ E_{LUMO\text{-}ANION} + 3.69\ E_{LUMO\text{-}CATION}$, in which $n = 10$, $s = 0.5$ $R^2 = 72.4\%$, $F = 5.24$, $P = 0.041$.
7. The biodegradation of [EtPy][BF_4] experiment results showed that in the presence of uranium, a complex could be formed with an intermediate, thus leading to the increase of uranium solubility. The [EtPy][BF_4] can still be completely degraded by the bacteria, however. The degradation pathway is the same as that in absence of uranium.

8.2 Recommendation

1. The interaction between ILs and other actinides, such as plutonium, could be explored. In addition, the bioreduction of plutonium in the presence of ILs should be examined.

2. Only the interactions between uranium and low concentrated IL/water solutions were examined in this study. It is also important to investigate the interaction of uranium with high concentrated IL/water solutions (or even pure ILs), because ILs may behave differently in higher concentrations.
3. Since [MEOMEIM][BF_4] can enhance the solubility of both U(VI) and reduced U(IV), its potential applications in bioseparation in the presence of U, other actinides, or heavy metals could be useful.
4. Imidazolium-based ionic liquids are resistant to complete biodegradation. Since they have been widely used in most ionic liquids, their potential environmental risk now becomes a major concern. Their toxicity and biodegradability should be explored through further investigation.

REFERENCES

Abbott, A.G., Capper, Davies, D., Rasheed, R., & Shikotra, P. (2005). Selective extraction of metals from mixed oxide matrixes using choline-based ionic liquids. Inorganic Chemistry, 44, 6497-6499.

Allen, D., Baston, A.E., Bradley, Gorman, T., Haile, A., Hamblett, J.E., Hatter, M.J.F., Healey, Hodgson, B., Lewin, R., Lovell, K.V., Newton, W.R., Pitnere, W.R., Rooney, D.W., Sanders, D., Seddon, K.R., Sims, H.E., Thied, R.C (2005). An investigation of the radiochemical stability of ionic liquids. Green Chemistry, 4, 152.

Allen, P.G., Bucher, J.J., Shuh, D.K., Edelstein, N.M., & Reich, T. (1997). Investigation of aquo and chloro complexes of UO_2^{2+}, NpO^{2+}, Np^{4+}, and Pu^{3+} by X-ray absorption fine structure spectroscopy. Inorganic Chemistry, 36, 4676-4683.

Anbar, M. & Guttmann, S. (1960). The isotopic exchange of fluoroboric acid with hydrofluoric acid. Journal of Physical Chemistry, 64, 1896

Antonio, M.R., Soderholm, L., Williams, C.W., Blaudeau, J.P., & Bursten, B.E. (2001). Neptunium redox speciation. Radiochimica Acta, 89, 17-25.

Boethling, R.S. (1996). A.C.S. Symposium Serials, 640, 156.

Bonhôte, P., Dias, A.P., Papageorgiou, N., Kalyanasundaram, K., & Gratzel, M. (1996). Hydrophobic, highly conductive ambient temperature ionic liquids. Inorganic Chemistry, 35, 1168-1178.

Boon, J.A., Lander, S.W., Levisky, J.A., Pflug, J.L., Skrznecki-Cooke, L.M., & Wilkes, J. S. (1987). Proceedings of the Joint International Symposium on Molten Salts, 6th Ed., 979-990.

Cronin, M.T.D., Walker, J.D., Jaworska, J.S., Comber, M.H.I., Watts, C.D., & Worth, A.P. (2003). Use of QSARs in international decision-making frameworks to predict ecologic effects and environmental fate of chemical substances. Environ. Health Perspect. 111 (10), 1376-1390.

Definition of ionic liquids, Retrieved February 20, 2007 from the World Wide Web: http://en.wikipedia.org/wiki/Ionic_liquid.

Docherty, K.M., & Kulpa, C.F.J. (2005). Toxicity and antimicrobial activity of imidazolium and pyridinium ionic liquids. Green Chemistry, 7, 185-189.

Dodge, C.J., & Francis, A.J. (1994). Photodegradation of uranium-citrate complex with uranium recovery. Environmental Science and Technology, 28(7), 1300-1306.

Dodge, C.J., & Francis, A.J. (2002) Photodegradation of a ternary Iron (III)-Uranium (VI)-Citric Acid complex. Environmental Science and Technology, 36(9), 2094-2100.

Dodge, C.J., Francis A.J., Gillow, J.B., Halada G.P., Eng, C., & Clayton, C.R. (2002). Association of uranium with ion oxides typically formed on corroding steel surface. Environmental Science and Technology, 36(16), 3504-3511.

Electrorefining of Metals. Retrieved March 10, 2007 from the World Wide Web: http://www.wikipedia.com.

Erbeldinger, M., Mesiano, A.J., & Russel, A.J. (2000). Enzymatic Catalysis of Formation of *Z*-Aspartame in Ionic Liquid - An Alternative to Enzymatic Catalysis in Organic Solvents. Biotechnol. Prog., 16, 1129.

Fisher, T., Sethi, A., & Welton, T. (1999). Diels-Alder reactions in room-temperature ionic liquids. Tetrahedron Letter, 40, 793-795

Francis, A.J., Dodge, C.J., Halada, G.P., & Clayton, C.R. (1994). XPS and XANES studies of uranium reduction by *Clostridium sp.* Environmental Science & Technology, 25, 636-639.

Francis, A.J. (1994). Microbial transformations of radioactive wastes and environmental restoration through bioremediation. Journal of Alloys and Compounds, 213-214, 226-231.

Francis, A.J. (1998). Biotransformation of uranium and other actinides in radioactive wastes. Journal of Alloys and Compounds, 271-273, 78-84.

Francis, A.J. (1999). Bioremediation of radionuclide and toxic metal contaminated soils and wastes. Bioremediation of Contaminated Soils, Agronomy Monograph, No. 37, p239-271.

Francis, A.J., & Dodge, C.J. (1998). Remediation of soils and wastes contaminated with uranium and toxic metals. Environmental Science and Technology, 32, 3993-3998.

Francis, A.J., Dodge, C.J., Gillow, J.B., & Papenguth, H.W. (2000). Biotransformation of uranium compounds in high ionic strength brine by a halophilic bacterium under denitrifying condition. Environmental Science and Technology, 34(11), 2311-2317.

Francis, A.J., Gillow, J.B., Dodge, C.J., Dunn, M., Mantione, K., Strietelmeier, B.A., Pansoy-Hjelvik, M. E., & Papenguth, H. W. (1998). Role of bacteria as biocolloids in the transports of actinides from a deep understanding radioactive waste repository. Radiochimica Acta, 82, 347-354.

Francis, A.J., Gillow, J.B., Dodge, C.J., Harris, R., Beveridge, T.J., & Papenguth, H.W. (2004). Uranium association with halophilic and non-halophilic bacteria and archaea. Radiochimica Acta, 92, 481-488.

Francis, A.J., Joshi-tope, G.A., Dodge, C.J., & Gillow, J.B. (2002). Biotransformation of uranium and transition metal citrate complexes by Clostridia. Journal of Nuclear Science and Technology, supplement 3, 935-938.

Gaillion, L., Bedioui, F. (2001). First example of electroassisted biomimetic activation of molecular oxygen by a (salen)Mn epoxidation catalyst in a room-temperature ionic liquid. Chem. Commun, 1458-1459.

Gaillard, C., Azzi, A.E., Billard, I., Bolvin, H., & Hennig, C. (2005). Uranyl complexation in fluorinated acids (HF, HBF4, HPF6, HTf2N): a combined experimental and theoretical study. Inorganic Chemistry, 44, 852-86.

Ganesh, R., Robinson, K.G., Reed, G.D., & Sayler, G.S. (1997). Reduction of hexavalent uranium from organic complexes by sulfate and iron-reduction bacteria. Applied and Environmental Microbiology, 63, 4385-4391.

Ganesh, R., Robinson, K.G., Chu, L., Kucsmas, D., & Reed, G.D. (1999). Reductive precipitation of uranium by *Desulfovibrio desulfuricans*: evaluation of co-contamination effects and selective removal. Water Research, 33(16), 3447-3458.

Garcia, M.T., Gathergood, N., & Scammells, P.J. (2005). Biodegradable ionic liquids Part II. Effect of the anion and toxicology. Green Chemistry, 7, 9-14.

Gathergood, N., Garcia, M.T., & Scammells, P.J. (2004). Biodegradable ionic liquids: part I. Concept, preliminary targets and evaluation. Green chemistry, 6,166-175.

Gu, B., Ku, Y.K., & Brown, G.M. (2005). Sorption and desorption of perchlorate and U (VI) by strong-Base Anion-Exchange Resins. Environmental Science and Technology , 39(3), 901-907.

Hirayama, N., Deguchi, M., Kawasumi, H., & Honjo, T. (2005). Use of 1-alky-3-methylimidazolium hexafluorophosphate room temperature ionic liquids as chelate extraction solvent with 4,4,4-trifluoro-1-(2-thienyl)-1,3-butanedione. Talanta, 65, 255-260.

Houghton, C., & Cain, R.B. (1972). Microbial metabolism of the pyridine ring. Biochemistry Journal, 130, 879-893.

Huang, J.F., Chen, P.Y., Sun, W., & Wang, S.P. (2001). NMR evidence of hydrogen bonding in 1-ethyl-3-methylimidazolium tetrafluoroborate room temperature ionic liquids. Spectroscopy Letters, 34(5), 591-603.

Huang, H., Wang, X.D., Ou, W.H., Zhao, J.S., Shao, Y., & Wang, L.S. (2003). Acute toxicity of benzene derivatives to the tadpoles (*Rana japonica*) and QSAR analyses. Chemosphere, 53, 963-970.

Hussey, C.L. (1983). Room temperature molten salt systems. Adv. Molten Salt Chem., 5, 185.

Lozano, P., De Diego, T., Guegan, J.-P., Vaultier, M., & Iborra, J.L. (2001). Stabilization of u-chymotrypsin by ionic liquids in transesterification reactions. Biotechnol. Bioeng.,75, 563.

Jeon, B.H., Dempsey, B.A., Burgos, W.D., Barnett, M.O., & Roden, E.E. (2005). Chemical reduction of U(VI) by Fe(II) at the solid-water interface using natural and synthetic Fe(III) oxides. Environmental Science and Technology, 39(15), 5642-5649.

Kelly, S.D., Kemner, K.M., Fein, J.B., Fowle, D.A., Boyanov, M.I., Bunker, B.A., & Yee, N. (2002). X-ray absorption fine structure determination of pH-dependent U-bacterial cell wall interactions. Geochimica et Cosmochimica Acta, 66(22), 3855-3871.

Kragl, U., Kaftzik, N., Schofer, S.H., Eckstein, M., Wasserscheid, P., & Hilgers, C. (2001). Enzyme catalysis in the presence of ionic liquids. Chimica Oggi, 19(7/8), 22-24.

Kumar, S., Ruth, W., Sprenger, B., & Kragl. U. (2006). On the biodegradation of ionic liquid 1-butyl-3-methylimidazolium tetrafluoroborate. Chemistry Today, 24(2), 24-26.

Laszlo, J.A., & Compton, D.L. (2001). Chymotrypsin catalysis in imidazolium-based ionic liquids. Biotechnology and Bioengineering, 75(2), 181-186.

Lee, J.K., & Mahn-Joo, Kim. (2001). Ionic liquid-coated enzyme for biocatalysis in organic solvent. Journal of Organic Chemistry, 67, 6845-6847.

Ley, S.V., Ramarao, C., & Smith, M.D.(2001). Tetra-*N*-propylammonium perruthenate: a case study in catalyst recovery and re-use involving tetraalkylammonium salts. Chem. Commun. 2278-2279.

Lloyd, J.R., Chesnes, J., Glasauer, S., Bunker, D.J., Livens, F.R., & Lovley, D.R. (2002). Reduction of actinides and fission products by Fe(III)-reducing bacteria. Geomicrobiology Journal, 19(1), 103-120.

Lozano, P., De Diego, T., Guegan, J.P., Vaultier, M., & Iborra, J.L. (2001). Stabilization of chymotrypsin by ionic liquids in trans-esterification reactions. Biotechnology and Bioengineering, 75(5), 563-569.

Lu, G.H., Yuan, X., & Zhao, Y.H. (2001). QSAR study on the toxicity of substituted benzenes to the algae (*Scenedesmum obliquus*). Chemosphere, 44, 43-440.

Madeira, L.R., Sorgedrager, M.J., Carrea, G., Rantwijk, F.V., Secuundo, F., & Sheldon, R. A.(2004). Dissolution of Candida antarctica lipase B in ionic liquids: effects on structure and activity. Green Chemistry, 6, 483-487.

Magnuson, D.K., Bodley, J.W., Evans, D.F. (1984). The activity and stability of alkaline phosphatase in solution of water and the fused salt, ethyl ammonium nitrate. Journal of Solution Chemistry, 13(8), 583-587.

Mak, T., Yip, W. (1985). Inorg. Chim. Acta, 109, 131

Markich, S.J. (2002). Uranium speciation and bioavailability in aquatic systems: an overview. Scientific World Journal, 15, 707-729.

Molecular Structure of $UO_2(NO_3)_2 \cdot 2H_2O$. Retrieved March 20, 2007 from the World Wide Web: http://*www.3Dchem.com*

Mousa, G., & Mohammad, H.K. (1997). Study of polymerization mechanism and kinetics of DGEBA with BF3-amine complexes using FT-IR and dynamic DSC. Iranian Polmer Journal, 6(1), 1026-1039.

Netzeva, T.I., & Schultz, T.W.(2005). QSARs for the aquatic toxicity of aromatic aldehydes from Tetrahymena data. Chemosphere, 61, 1632-1643.

Papa, E., Battaini, F., & Gramatica, P. (2005). Ranking of aquatic toxicity of esters modeled by QSAR. Chemosphere, 58, 559-570.

Pernak, J., Sobaszkiewicz, K., & Foksowicz-Flaczyk, J. (2004). Ionic liquids with symmetrical dialkoxymethyl substituted imidazolium cations. Chemical European Journal, 10, 3479-3485.

Pietzsch, K., Hard, B.C., & Babel, W. (1999). A Desulfovibrio sp. capable of growing by reducing U(VI). Journal of Basic Microbiology, 39(5-6), 365-372.

Plutonium and Uranium Recovery by Extraction (PUREX). Retrieved March 11, 2007 from the World Wide Web: http://www.wikipedia.com.

Ranke, J., Moelter, K., Stock, F., Bottin-Weber, U., Poczobutt, J., Hoffmann, J., Ondruschka, B., Filser, J., & Jastorff, B. (2004). Biological effects of imidazolium ionic liquids with varying chain lengths in acute *Vibrio fischeri* and WST-1 cell viability assays. Ecotoxicology and Environmental Safety , 58(3), 396-404.

Robinson, K.G., Ganes, R., & Reed, G.D. (1998). Impact of organic ligands on uranium removal during anaerobic biological treatment. Water Science and Technology, 37(8), 73-80.

Robinson, J. & Osteryoung, R.A. (1979). An electrochemical and spectroscopic study of some aromatic hydrocarbons in the room temperature molten salt system aluminum chloride-n-butylpyridinium chloride. J. Am. Chem. Soc., 101, 323

Sar, P., Kazy, S.K., & Souza, S.F. (2004). Radionuclide remediation using a bacteria biosorbent. International Biodeterioration & Biodegradation , 54, 193-202.

Madeira Lau, R., Van Rantwijk, F., Seddon, K.R., & Sheldon, R.A. (2000). Lipase-Catalyzed Reactions in Ionic Liquids. Org. Lett., 2, 4189.

Suarez, P.A.Z., Dullius, J.E.L., & De Souza, R.F. Dupont, J. (1996). The use of new ionic liquids in two-phase catalytic hydrogenation reaction by rhodium complexes. Polyhedron, 15, 1217-1219.

Summary Production Statistics of the U.S. Uranium Industry from 1993 to 2005. Retrieved Februray, 18, 2007 from the World Wide Web: http://www.eia.doe.gov /fuelnuclear.html.

Tucker, M.D., Barton, L.L., & Thomson, B.M. (1998). Removal of U and Mo from water by immobilized *Desulfovibrio desulfuricans* in column reactors. Biotechnology and Bioengineering, 60, 88-96.

Visser, A.E., & Rogers, R.D. (2003). Room-temperature ionic liquids: new solvents for f-element separation and associated solution chemistry. Journal of Solid State Chemistry, 171, 109-113.

Visser, A.E., Jensen, M.P., Laszak, I., Nash, K.L., Choppin, G.R., & Rogers, R.D. (2003). Uranyl coordination environment in hydrophobic ionic liquids: an in situ investigation. Inorganic Chemistry, 42, 2197-2199.

Visser, A.E., Swatloski, R.P., Griffin, S.T., Hartman, D.H., & Roger, R.D. (2001). Liquid/liquid extraction of metal ions in room temperature ionic liquids. Separation Science and Technology, 36(5&6), 785-804.

Visser, A.E., Holbrey, J.D., & Rogers, R.D. (2001). Hydrophobic ionic liquids incorporating N-alkylisoquinolinium cations and their utilization in liquid–liquid separations. Chemical Communication, 23, 2484-2485.

Walden, P., (1914). Bull. Acad. Sci. St. Petersburg, 405-422

Wamser, C.A. (1948). Hydrolysis of Fluoboric Acid in Aqueous Solution. Journal of American Chemical Society, 70, 1209

Wang, Y., Zhao, C., Ma, W., Liu, H., Wang, T., & Liang, G. (2006). Quantitative structure-activity relationship for prediction of the toxicity of polybrominated diphenyl ether (PBDE) congeners. Chemosphere, 64(4), 515-524.

Wang, Z.Z, & Li, X.D.(1981). Semi-experimental molecular orbital theory and practice. Science, Moscow.

Wasserscheid, P., & Welton T. (2003). Ionic Liquids in Synthesis, Weinheim Wiley-VCH publish.

Wei, G.T., Yang, Z., & Chen, C.J. (2003). Room temperature ionic liquid as a novel medium or liquid/liquid extraction of metal ions. Analytica Chimica Acta, 488, 183-192.

Welton, T. (1999). Room-temperature ionic liquids, Solvents Synthesis Catal. Chem. Rev. 99, 2071–2079.

Wilkes, S.J., Levinsky, J.A., Pflug, J.L. & Hussey, C.A. (1982). Dialkylimidazolium chloroaluminate melts: a new class of room-temperature ionic liquids for electrochemistry, spectroscopy and synthesis. Inorg. Chem., 21, 1263.

Wilkes, S.J., Zaworotko, M.J. (1992). Air and water stable 1-ethyl-3-methylimidazolium based ionic liquids. Chemical Communications, 965-967.

Xiao, Y., & Malhotra, S.V. (2005). Friedel-crafts acylation reactions in pyridinium based ionic liquids. Journal of Organometallic Chemistry, 690(15), 3609-3613.

Xu, Y., Zondlo, J.W., Finklea, H.O., & Brennsteiner, A. (2000). Electrosorption of uranium on carbon fibers as a means of environmental remediation. Fuel Processing Technology, 68(3), 189-208.

Yong, P., Rowson, N.A., Farr, J.P., Harris, I.R., Macaskie, L.E. (2002). Bioreduction and biocrystalization of palladium by Desulfovibrio desulfuricans NCIMB 8307. Biotechnology and Bioengineering, 80(4), 369-379.

Zhang, C.D. (2006). Interaction of ionic liquids with uranium and its implications on biotransformation. Doctoral dissertation, May 2006. New Jersey Institute of Technology.